2008

Designing surface chemistries for in situ AFM investigations of biomolecular reactions with proteins at the nanoscale

Johnpeter Ndiangui Ngunjiri
Louisiana State University and Agricultural and Mechanical College, ngunjiripeter@yahoo.com

DESIGNING SURFACE CHEMISTRIES FOR *IN SITU* AFM INVESTIGATIONS OF BIOMOLECULAR REACTIONS WITH PROTEINS AT THE NANOSCALE

A Dissertation

Submitted to the Graduate Faculty of the
Louisiana State University and
Agricultural and Mechanical College
in partial fulfillment of the
requirements for the degree of
Doctor of Philosophy

in

The Department of Chemistry

by
Johnpeter Ngunjiri
B.S., Moi University, 1999
M.S., Moi University, 2003

May 2008

DEDICATION

I dedicate this dissertation to my father Cyrus Ngunjiri, my mother Mary Wanjiru, my wife Lilian Rongoei and my sons Ian Ngunjiri and Ryan Wanyumu. Their love, support, encouragement and enthusiasm have made me reach this level. I wish to thank my advisor, Prof. Jayne Garno, for her intellectual support, encouragement, and for her patience in teaching me both stylistic and scientific concepts. I thank you all for treating me as a son and investing in my goals without hesitation.

ACKNOWLEDGEMENTS

First I would like to thank Lilian, Ian and Ryan for their unshakable faith in me and their willingness to endure with me during many days of absence. My gratitude extends to my sisters Wangeci, Kirigo, Watetu, and Nyambura for helping me morally and financially in my endeavors. Sincere thanks goes to my only brother Patrick Gichuki who has been a role model for hard work, persistence and personal sacrifices, and who instilled in me the inspiration to set high goals and the confidence to achieve them.

I would like to thank my advisor, Dr. Jayne Garno for her guidance, assistance and great mentorship. Especially the thoughtful critics and suggestions she offered during research are appreciated. In her teaching and direction she has modeled lessons that I will gladly carry forward with my career.

Many faculty members in the Chemistry Department at LSU assisted and encouraged me in various ways during my course of studies. I am especially grateful to Dr. Robert Hammer, Dr. Julia Chan, Dr. Robin McCarley, Dr. Jin-Woo Choi and Dr. Masami Yoshimura for serving on my advisory committee. I thank fellow graduate students in the Garno research group, Belle LeJeune, Wilson Serem, Stephanie Daniels, Brian Lewandowski, Kathie Lusker, Jie-Ren Li, and Algernon Kelly whom I was privileged to work with, to teach and from whom I learned much by way of social and academic challenges.

TABLE OF CONTENTS

LIST OF TABLES

LIST OF FIGURES

ABSTRACT

In situ atomic force microscopy (AFM) characterizations and lithography can be applied to investigate the orientation, reactivity and stability of protein molecules adsorbed on nanostructures of self-assembled monolayers at near-physiological conditions. Automated nanografting was used to fabricate regular arrays of nanopatterns of ω-functionalized *n*-alkanethiols with designated terminal chemistries. After writing nanopatterns, protein binding occurs selectively on carboxylate-terminated nanopatterns via covalent bonds that are formed using N-ethyl-N'(dimethylaminoporpyl)-carbodiimide and N-hydroxysuccinimide activation. The amine groups of lysine residues of proteins bond covalently to nanopatterns of carboxylate-terminated alkanethiol self-assembled monolayers, to form a robust surface attachment for sustained contact-mode AFM imaging during biochemical reactions. Staphylococcal protein A (SpA) furnishes a generic foundation for binding immunoglobulins for nanometer scale sandwich assays.

The self-assembly of α,ω-alkanedithiols onto Au(111) was investigated using AFM. When SAMs of 1,8-octanedithiol or 1,9-nonanedithiol are grown naturally from solution, different surface orientations are observed in comparison to methyl-terminated *n*-alkanethiols. Local views from AFM images reveal a layer of mixed orientations in which the majority of α,ω-alkanedithiol molecules adopt an orientation parallel to the surface with both thiol endgroups bound to Au(111). Results from AFM studies reveal that the chemisorption of thiol endgroups of dithiols inhibits the phase transition from a lying-down to a standing orientation during natural self-assembly.

Another method for producing protein nanostructures is particle lithography. Monodisperse mesospheres can be applied to rapidly prepare millions of exquisitely uniform nanometer-sized structures of proteins on flat surfaces using conventional benchtop

chemistry steps of mixing, centrifuging, evaporation and drying. The natural self-assembly of monodisperse spheres provides a high throughput and efficient route to prepare circular geometries over millimeter scale areas. The spontaneous assembly of silica or latex mesospheres into organized crystalline layers on flat substrates supplies a structural frame to direct the placement of proteins. Nanopatterns of ferritin, apoferritin, immunoglobulin G and bovine serum albumin were produced with particle lithography. The applicability of particle lithography to generate arrays of protein nanostructures on surfaces such as mica(0001), glass and Au(111) was demonstrated. The morphology and diameter of the protein nanostructures can be tailored by selecting the ratios of protein-to-particles and the diameters of spheres.

CHAPTER 1. INTRODUCTION

Methods of atomic force microscopy (AFM) and particle lithography can be applied to engineer protein surfaces for nanoscale surface investigations. Specific reactions with protein can be accomplished on nanografted patterns using surface activation chemistry to provide new approaches for *in situ* investigations of protein binding at the molecular level. Natural assemblies of template mesospheres combined with solution based deposition can be employed to produce nanostructured protein films over large surface areas.

Scanning probe lithography (SPL) provides a way to design the chemistry of surfaces at the nanoscale to furnish nondestructive conditions for *in situ* studies of biomolecules. The best choice for an SPL method for patterning should be chosen according to the type of binding chemistry desired for linking proteins to surfaces. Chapter two provides a contemporary review of scanning probe investigations with protein nanopatterning, with an emphasis on reports which use nanopatterns of self-assembled monolayers (SAMs) for protein adsorption. Chapter two summarizes the key differences in the mechanisms for writing nanopatterns of self-assembled monolayers (SAMs), the type of molecules to be written and the nature of the substrate. The writing mechanisms for bias-induced nanolithography, catalytic probe lithography, dip pen nanolithography and nanografting with SAMs are described, reviewing examples from literature reports. Examples are provided for applications of SPL that have been used for protein investigations, with a comprehensive discussion of nanografting; the method chosen for studies in this dissertation. An AFM tip can be applied as a tool for both fabrication and characterization, to create highly controllable test structures for protein binding studies. The capabilities for superb control of writing parameters with piezoscanners (such as force, speed, density and direction) enable reproducible fabrication of arrays of SAM nanopatterns

with well-defined shapes, sizes and spatial arrangement. Nanostructures of SAMs with reactive head groups establish the surface sites for protein adsorption. Molecular scale views of structural changes when proteins bind to surfaces can be achieved using *in situ* AFM in liquids.

A critical requirement for investigations of biochemical activities of proteins at the molecular level is the ability to position and interrogate biological molecules with high spatial precision. Chapter three addresses the mechanics of automated nanografting with SAMs and demonstrates results for various writing strategies when using an AFM tip to write patterns of *n*-alkanethiol SAMs. Strategies are described for programming the tip translation to improve the uniformity, alignment and geometries when writing SAM nanopatterns.

Unlike *n*-alkanethiols, molecules of α,ω-alkanedithiols spontaneously self assemble on Au(111) in a lying down configuration with both thiol groups attached to the substrate. Thiol-terminated surfaces with α,ω-alkanedithiol molecules are important because the free thiol group can be used for further chemical reactions. Nanografting can produce nanostructures of standing-up α,ω-alkanedithiol molecules. For nanografted dithiols, molecules self-assemble on very small areas of freshly exposed gold produced by a scanning AFM tip, with one sulfur group attaching to the gold substrate. The other thiol end group is presented at the surface of the patterns. The spatial confinement assembly mechanism of nanografting prevents the molecules from assembling in a lying-down position, to produce an upright configuration. In chapter four, AFM investigations are used to derive an assembly model for 1,8-octanedithiol and 1,9-nonanedithiol during natural self assembly and compared to spatially-constrained assembly of nanografting.

Nanoscale protein assays can be designed and monitored using *in situ* AFM. Physical adsorption of receptor proteins on biochip surfaces is not sufficiently robust to enable

continuous contact-mode AFM imaging. Strategies for covalent attachment of proteins on surfaces hold promise for more efficient biosensor surfaces as described in chapter five. Chemical activation of reactive head groups of SAMs such as carboxylates (using EDC and NHS reagents) enables mild conditions for tethering proteins to nanopatterns via covalent bonds. Further steps of biochemical reactions can be accomplished in an AFM liquid cell after nanografting, for *in situ* experiments. The selectivity of nanopatterns of SAMs and the coupling chemistry are important for adhesion of proteins to biochip or sensor surfaces. Successive AFM images of surface changes for the nanopatterns were captured after each step of a protein binding assay. Chapter five demonstrates and extends the *in situ* capabilities of AFM for detecting and visualizing biomolecular interactions on surfaces.

The potential for high-throughput protein analysis lies in designing high-density arrays of proteins. Particle lithography holds promise for reproducibly generating nano-sized features over large surface areas for high-throughput applications. Particle lithography provides a rapid method for preparing millions of exquisitely uniform nanostructures of proteins on flat surfaces as demonstrated in chapter six. High throughput production of nanopatterns can be achieved using conventional benchtop chemistry steps of mixing, centrifuging, drying and rinsing.

A number of advancements were achieved for applying AFM for molecular-scale studies of surface reactions with proteins and SAMs. Parameters of AFM-based nanografting were improved to achieve better control of pattern shape, size, spacing and chemistry. Chemical methods for activating SAMs using EDC and NHS coupling were extended and tested for molecular-level surface investigations. Nanografting and chemical activation methods were integrated with SPL, to develop nanoscale protein assays. The nanometer scale protocols provide insight into protein binding and protein-protein interactions. New methods for

producing nanopatterns of ferritin, apoferritin, BSA and IgG molecules using particle lithography were developed using both conductive and insulating surfaces. The new SPL methods provide groundwork which can be generally applied for studies with new systems of proteins and other biomolecules.

CHAPTER 2. NANOLITHOGRAPHY: TOWARDS FABRICATION OF NANODEVICES FOR LIFE SCIENCES

2.1 Introduction: Engineering Surfaces at the Nanoscale

Tools for nanofabrication have begun to provide important contributions for life sciences investigations, for developing biochip and biosensing technologies, as well as in supplying basic research in protein-protein interactions and protein function. Scanning probe microscopes (SPMs) supply tools for visualization, physical measurements, and precise manipulation of atoms and molecules at the nanometer scale. Nanoscale studies can facilitate the development of new and better approaches for immobilization and bioconjugation chemistries, which are key technologies in manufacturing biochip and biosensing surfaces.

Protein patterning is essential for the integration of biological molecules into miniature bioelectronic and sensing devices. To fabricate nanodevices for the life sciences it is often necessary to attach biomolecules to surfaces with retention of structure and function. For example, controlling the interaction of proteins, biomolecules, and cells with surfaces is important for the development of new biocompatible materials. Precisely engineered surfaces can be used for the exploration of biochemical reactions in controlled environments. Spatially well-defined regions of surfaces can be constructed with reactive or adhesive terminal groups for the attachment of biomolecules. Micropatterning of proteins has been applied for biosensors and biochips.[2-5] Direct applications of protein patterning include biosensing, medical implants, control of cell adhesion and growth, and fundamental studies of cell biology.[6-8] Protein patterning has been accomplished at the micrometer level using microcontact printing,[9-14] photolithography,[15-17] and microfluidic channels.[18, 19] Thus, capabilities for micrometer scale

---

Reproduced with permission from Wiley-VCH: Ngunjiri, J. N.; Li, J.-R.; Garno, J. C., Chapter 3, Nanodevices for the Life Sciences. Wiley-VCH: Weinheim, **2006**.

methods for controlling the spatial arrangements of biomolecules have been well-established and offer valuable new research capabilities for life science investigations. Collectively, these techniques provide a means for assembling proteins at a size scale of hundreds of nanometers or larger.

To progress to even smaller size scales, AFM-based lithography can be applied to pattern surfaces at nanometer dimensions. Scanning probe lithography (SPL) provides versatile approaches for designing the chemistry of surfaces at the nanoscale. Figure 2.1 shows the dimensions which can be achieved using various micro and nanopatterning methods. Arrays of SAMs and proteins can be fabricated via SPL, with precise control over chemical functionality, shape, dimension, and spacing on the nanometer length scale. Combined with the capabilities for high-resolution imaging and characterization, scanning probe microscopy (SPM) enables a

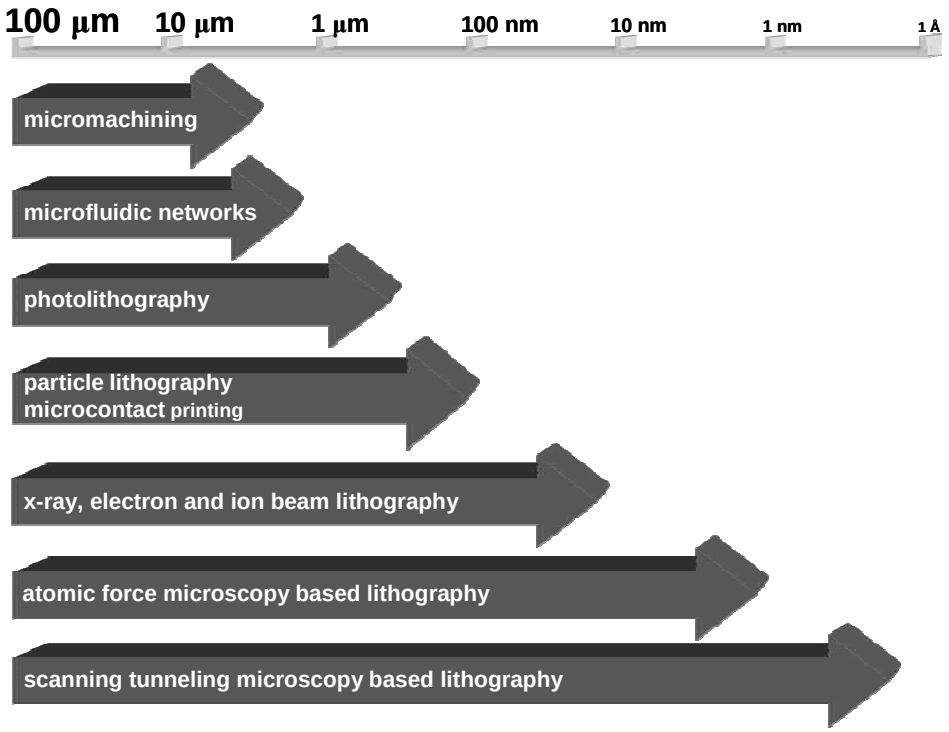

Figure 2.1 Overview of the hierarchy of dimensions which can be achieved using various micro and nanopatterning methods.

molecular level approach for directly investigating changes that occur on surfaces during biochemical reactions. The tools of SPL are accessible to investigators across a broad range of disciplines and do not require costly instrument modifications.

Cutting-edge research has begun to apply nanolithography for studying proteins on surfaces, possibly at the level of single molecule detection. At this time, nanodevices constructed by SPM-based lithography are being conceptualized and to the best of our knowledge, SPL has not yet been applied for making nanodevices. Readers are referred to recent reviews which discuss potential nanoscale devices.[20, 21] Although there are also many studies which investigate peptides, DNA and cells we will limit the focus of this chapter to studies which apply nanoscale lithography to proteins, and applications for nanoscale protein assays. This chapter will provide an overview of advances in the application of nanolithography using scanning probe microscopy and latex particle lithography for protein patterning. Beginning with a general introduction of the chemistry for immobilization of proteins on surfaces, the application of self-assembled monolayers (SAMs) for coupling proteins to surfaces will be presented. Nanolithography methods including bias-induced lithography, AFM-based force-induced nanolithography, "Dip-Pen" nanolithography (DPN) and latex particle lithography will be described, including examples of protein nanopatterning. The chapter will conclude with discussion of nanoscale detection of protein binding and future directions with cantilever array technology.

2.2 Immobilization of Biomolecules for Surface Assays

A number of factors need to be considered for choosing a successful protein immobilization strategy, such as the efficiency and rate of binding, potential side reactions, and the strength and resilience of the attachment. For protein assays, the binding site recognized by

immunoglobulin G (IgG) on an antigen is relatively small; consisting of only 5-6 amino acids or several sugar residues. The recognition element is referred to as an antigenic determinant or epitope. Proteins must be attached in such an orientation that their active sites or binding domains are accessible for binding, and not buried or blocked by the surface. The binding site is only a small part of the total surface area of the protein. Adsorption on a surface may impair or prevent the protein's activity. The eventual orientation of proteins on surfaces is determined by multiple factors such as the type of binding, the positions and composition of external residues on the protein surface, the isoelectric point of the protein, and the pH of buffers used during application.

Proteins have a three-dimensional structure which is critical to their function and activity. Most proteins have both positively and negatively charged regions that interact with surfaces. Upon encountering a surface, intramolecular forces within proteins can be disrupted, causing the proteins to unfold and become denatured. Some proteins are known to lose activity when bound to a solid surface, due to a loss of tertiary structure. For example, the strong polarization forces at metal surfaces along with ionic or covalent interactions on many inorganic metal oxides and semiconductor surfaces may cause denaturation of biomolecules.[22] For retention of activity, chemistries for protein arrays should permit the immobilization of proteins on surfaces such that perturbation to the native 3-D structure is minimized. Using a spacer or linker molecule on the sensor surface often enables biomolecules to retain their functionality and 3-D structure. The tools of organic chemistry provide a wealth of chemical strategies and binding motifs for conjugating biomolecules such as proteins to solid surfaces.[23, 24]

2.3 Strategies for Linking Proteins to Surfaces

Increasingly, researchers have begun to use the self-assembly of functionalized alkanethiol and alkylsilane molecules as model surfaces for protein binding. The terminal moieties of self-assembled monolayer (SAM) surfaces mediate the type of binding, such as through electrostatic interactions, covalent binding, molecular recognition or via specific interactions (Figure 2.2). The following sections will introduce representative examples of chemical immobilization strategies which have been applied for protein patterning.

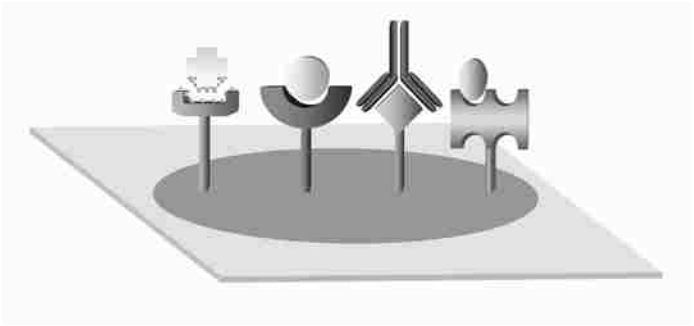

Figure 2.2 Strategies for linking proteins to surfaces include electrostatic interactions, covalent bonding, antigen-antibody recognition, and biotin-streptavidin specific interactions.

2.3.1 Electrostatic Immobilization

The strategy of functionalizing a surface through electrostatic assembly is often used to immobilize biomolecules on surfaces. Electrically charged amino acids are found mostly on the exterior of proteins and can mediate assembly on charged surfaces. Proteins contain both positively and negatively charged domains that interact with surfaces via long-range electrostatic forces. The electrostatic attraction between oppositely charged molecules is nonspecific, and surfaces are negatively or positively charged, depending on the solution pH.

Electrostatic binding is physically mediated and proteins often retain their activity after immobilization. It is a direct, simple method for attaching proteins to surfaces without requiring multiple steps for chemical activation. Binding is reversible, since certain buffers and

detergents can remove proteins from nanopatterns. However, a potential disadvantage of electrostatic immobilization is that the resulting orientation of proteins on surfaces is random, electrostatic-mediated binding does not provide a means for directing the protein assembly in a designed conformation. Representative examples of chemistries for the electrostatic immobilization of proteins which have been applied for nanopatterning proteins are summarized in Table 2.1. For example, alkanethiols or alkylsilanes terminated with functional groups, such as NH_2 or COOH, have been used to immobilize biomolecules through electrostatic interactions.

2.3.2 Covalent Immobilization

Covalent immobilization is important for applications in which displacement or desorption of proteins can be a problem. Covalent bonds occur when two molecules share atoms and form the strongest chemical bonds for surface immobilization. The methods of covalent attachment are boundless, thousands of proteins have been immobilized on hundreds of different solid supports for affinity-capture assays.[23] The best choice for covalent immobilization will depend on the functionalities of both the protein and the surface. Several amino acids provide suitable functional groups for covalent modification. Common functional groups of amino acids used for covalent immobilization include: amino groups from the side chains of lysine and the N-terminus; carboxyl groups from the C-terminus, aspartic and glutamic acids; sulfhydryl groups of cysteine; hydroxyl groups of serine and threonine; and the phenyl groups of phenylalanine and tyrosine. Since proteins typically present a number of these groups, the chemical nature of the solid surface becomes a primary consideration. A specific chemical reaction is chosen to activate the surface, and then proteins are immobilized upon exposure to the active surface groups. Examples of chemistries for covalent immobilization of proteins include activation of surface hydroxyl groups, carboxyl groups and amines. Also,

bifunctional crosslinking reagents such as glutaraldehyde have been used to covalently couple proteins to various surfaces. Further examples of covalent immobilization chemistries are listed in Table 2.1.

Table 2.1 Strategies used to immobilize proteins applied for nanopatterning proteins

Type of Interaction	Surface Derivatization	Proteins Studied	Surface	SPL method	Dimensions	Ref
chemisorption	S-Au attachment of C-terminal thiol groups	bundle metalloproteins	Au(111)	nanografting	100 nm	80
chemisorption	gold surface	thiolated collagen	Au(111)	DPN	30-50 nm	92
covalent	3-mercapto-1-propanal patterns in a decanethiol resist	lysozyme, IgG	Au(111)	nanografting	40 – 350 nm	74
covalent	mercaptohexadecanoic acid passivated with EG_3-SH, then activated to form aldehyde groups	elastin-like polypeptide	Au(111)	DPN	200 nm dots	91
covalent	1,2-diols cleaved to produce aldehydes	acetylcholine esterase - insulin	Au(111)	nanografting	50-200 nm	79
covalent and specific	EDC activation of mixed hydroxyl and carboxyl SAMs, then biotin-streptavidin binding	anti-IgG, protein G	Au(111)	uCP	10 micron	10
electrostatic	mercaptohexadecanoic acid SAM decanethiol resist	lysozyme	Au(111)	nanografting	100-400 nm	74
electrostatic	mercaptohexadecanoic acid and dodecanethiol SAMs	lysozyme	Au(111)	natural assembly	< 1 micron	[1]
electrostatic	mercaptohexadecanoic acid passivated with ethylene glycol SAM	rabbit IgG, lysozyme	Au(111)	DPN	100 - 350 nm	86
electrostatic	mercaptohexadecanoic acid	mouse anti-p24 IgG HIV-1 p24 antigen	Au(111)	DPN	60 nm	108
electrostatic	gold surface	cytochrome c	Au(111)	DPN	200 nm dots	87
electrostatic	mercaptoundecanoic acid passivated with octanethiol and glycol SAMs	rabbit IgG anti-rabbit IgG	Au(111)	nanografting	500 nm - 1μm	78
electrostatic	mercaptohexanol, mercaptopropionic acid, N-(mercapto)hexylpyridinimum bromide thiols in matrix terminated with hexa(ethylene glycol) resist	lysozyme, bovine carbonic anhydrase, rabbit IgG	Au(111)	nanografting	200 – 400 nm	77
electrostatic and specific	biotin-streptavidin on mercaptohexadecanoic acid, with oligoethylene glycol SAM passivation	biotinylated BSA	Au(111)	DPN	100 - 230 nm	89
physical adsorption	PDMS stamping onto glass surfaces	rabbit IgGs, BSA, Avidin	glass	uCP	40-100 nm	138
physical adsorption	nickel oxide surface	ubiquitin and thioredoxin	nickel oxide	DPN	80 nm	95
physical adsorption	direct writing on bare gold; passivation with PEG	lysozyme, rabbit IgG	Au(111)	DPN	45 - 200 nm	94
physical adsorption	direct writing on modified SiO_2	IgG, anti-rabbit IgG	SiO_2	DPN	55-550 nm	93
specific avidin-biotin	oligo-(ethylene glycol) SAM	avidin – biotin-BSA	Si(111)	bias-induced SPL	90 nm	66
specific avidin-biotin	oxidized regions of poly(methyl methacrylate) layer spin-coated onto p-doped silicon wafer	biotin IgG - avidin	Si wafer	bias-induced SPL	0.5 - 1.5 μm	61
specific maleimide-cysteine	maleimide substituted SAM as ink for specific immobilization of cysteine-labelled biomolecules	virus capsid particles	Au(111)	DPN	150 nm	90

An important factor to be considered in covalent attachment of proteins is the possibility of chemically altering the protein in such a way that its reactivity is reduced. For example, covalent approaches may be hindered by competing side reactions. It is possible that groups associated with the active site or binding site of a protein could be involved in the reaction. In addition, chemical cross-linking within protein domains could occur, causing damage to the protein's tertiary structure.

2.3.3 Molecular Recognition and Specific Interactions

Highly specific interactions between binding pairs can be used effectively for protein immobilization. Examples include affinity capture ligands such as biotin-streptavidin binding and molecular recognition through antigen-antibody binding. Such affinity ligands require either physical or covalent immobilization of one moiety of the affinity pair onto the surface. Small-molecule receptors such as biotin offer viable strategies for the immobilization of proteins. Further examples are listed in Table 2.1. A strong advantage of specific immobilization is to provide a means for directing the protein assembly in a designed conformation. The orientation of proteins on surfaces can be designated by selectively targeting certain amino acid residues of the protein for specific coupling.

2.3.4 Nonspecific Physical Adsorption to Surfaces

By far, the most widely used method of protein immobilization for protein arrays uses nonspecific adsorption of proteins dried on solid supports. Forces which nonspecifically influence the binding of proteins to almost any substrate includes ion bridging, hydration forces, hydrophobic forces, and short range attractive or repulsive forces. This approach produces randomly oriented proteins, some of which may be denatured. Surface assays typically include a blocking step, such as with the adsorption of bovine serum albumin (BSA) to prevent

nonspecific binding of proteins. BSA is a globular serum protein which is often used in bioassays to backfill uncovered areas of surfaces where proteins did not attach.

2.4 Self-assembled Monolayer Chemistry

Self-assembled monolayers (SAMs) provide a chemical method for creating well-defined surfaces with controllable surface functionality.[25] Due to their stability, ease of preparation and well-ordered surface structures, SAMs of alkanethiols and alkylsilanes provide excellent models for studying protein binding, since layers of defined thickness and designed properties can be generated.[26, 27] Thiol endgroups of *n*-alkanethiols bond via chemisorption to metal surfaces. SAM surface properties can be flexibly controlled by changing the functional (head) groups of the alkyl chain (Figure 2.3), also, these end groups can be used for further chemical reactions. The acidity, adhesion, wetting and structural properties of surfaces can be modified by choosing specific chemical headgroups (such as NH_2, OH, COOH, CH_3, glycol, etc.).[28, 29] For example, surfaces can be made hydrophilic by introducing SAMs with polar moieties such as hydroxyl or carboxyl groups. Non-polar functionalities such as methyl-terminated groups yield hydrophobic surfaces. The preparation, characterization, and properties of SAMs have been described and reviewed previously.[29-33] SAMs have promising applications in biosensing, corrosion inhibition, lubrication, surface modification, and molecular device fabrication. This section will introduce the chemistry and structure of SAMs of alkanethiols and alkylsilanes, (Figure 2.3) which are often applied for nanolithography with proteins.

Close-packed *n*-alkanethiol SAMs can be readily prepared with high reproducibility to present functional groups such as alkyls, amides, esters, alcohols, etc. on surfaces of gold or coinage metals. Typically, alkanethiol SAMs are formed by soaking gold thin films in dilute (0.1 - 1.0 mM) solutions of thiols dissolved in solvents such as 2-butanol, hexane or ethanol.

Typically, substrates can be stored in a thiol solution for 1-7 days at room temperature to ensure the formation of mature monolayers. Alkanethiols on Au(111) form a close packed, commensurate (√3x√3)R30° lattice on Au(111) surfaces.[34-37] In surface assemblies of alkanethiol SAMs, according to studies by IR, near-edge X-ray absorption fine structure (NEXAFS) spectroscopy, and grazing incidence X-ray diffraction (GIXD), the alkyl chains of thiol molecules are tilted approximately 30° from surface normal (Figure 2.3A).[37-39] The sulfur atoms of alkanethiol molecules are considered to bind at the triple hollow sites of Au(111) lattices.[30]

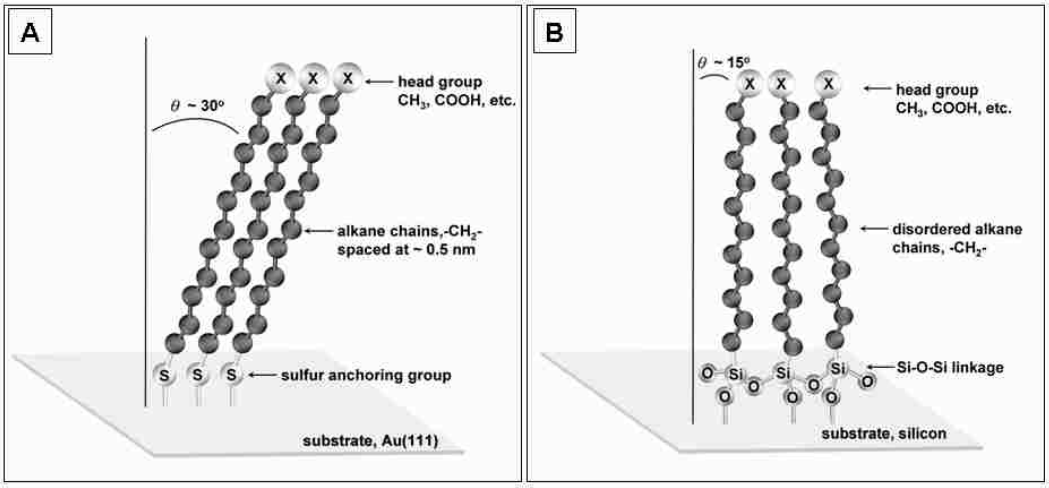

Figure 2.3 General structural features of self-assembled monolayers of [A] *n*-alkanethiols/Au(111) and [B] *n*-alkylsilanes/Si(111).

STM and AFM studies have confirmed the long-range order and periodicity of alkanethiol monolayers and have provided a direct view of defects such as domain boundaries, etch pits, steps and dislocations within SAM films.[30, 40] Scanning probe microscope images visualize the intricate details of the surface topography of SAMs. Figure 2.4 displays a typical topographic view of an octadecanethiol SAM/Au(111) acquired in ethanol by AFM. These molecular landscapes may appear somewhat rough, because at the atomic scale most surfaces are not truly smooth and flat, and contain defects. Considering that the height of gold steps is

~0.25 nm, the overall surface roughness of the underlying gold substrates for these images is less than 1 nm. The monolayer surfaces consist of domains of closely packed thiol molecules decorated with etch pits. Readers are referred to several works using STM for a more detailed discussion of the morphology and packing of *n*-alkanethiol SAMs.[30, 40-42]

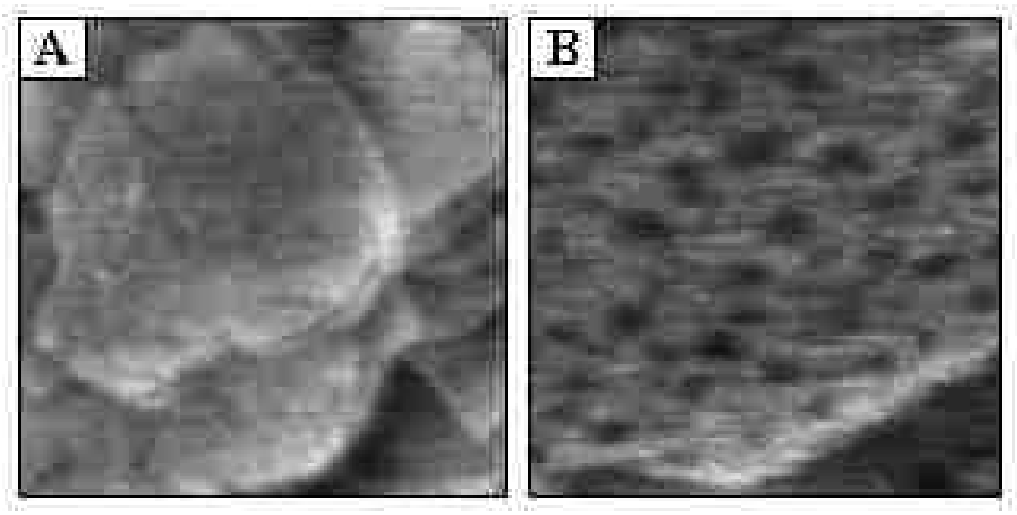

Figure 2.4 Contact mode AFM topographs of an octadecanethiol self-assembled monolayer on Au(111). [A] Terrace arrangement of flat gold steps coated with octadecanethiol SAM (400 x 400 nm^2). [B] Zoom-in view displays etch pits (80 x 80 nm^2).

Similar to alkanethiols, the chain length and terminal moieties of alkylsilane SAMs can be tailored to meet experimental requirements; however the properties of alkylsilane assemblies are quite different from SAMs of alkanethiols. SAMs of alkylchlorosilanes, alkylalkoxysilanes, and alkylaminosilanes require hydroxylated surfaces to form polysiloxane, which is connected to surface silanol groups (-SiOH) through a network of Si-O-Si bonds. Substrates on which silane SAMs have been prepared include silicon oxide, aluminum oxide, quartz, glass, mica, zinc selenide, and germanium oxide.[33] High-quality alkylsilane SAMs are not as simple to produce as thiol SAMs, because of the need to carefully control the presence of water in solutions. Reproducibility can be a problem, since the quality of the monolayers formed is very

sensitive to reaction conditions. Silane monolayers on mica typically consist of domains separated by boundaries. Within domains, silane molecules form structures without long-range order or periodicity.[43-45] The headgroups of silane SAMs cross-link into a Si-O network, and the chains tilt ~ 15° from surface normal (Figure 2.3B).[43, 44]

SAM surfaces can be engineered to avoid non-specific protein adsorption, yet make specific interactions with targeted proteins to be assayed, by choosing the appropriate buffered conditions as well as an effective matrix layer, resistive to protein adsorption (such as glycol-terminated SAMs). Very few surfaces resist protein adsorption, and it remains a challenge to understand the mechanisms that contribute to protein resistance or adhesion to surfaces. To prepare monolayers that resist protein adsorption, Whitesides,[46-49] Mrksich,[50] and Grunze[51] have conducted systematic studies of functionalized SAMs to determine the molecular characteristics that impart resistance to protein adsorption. The factors which determine the resistance to protein adsorption were found to include characteristics such as the hydrophilicity of the terminal group, lateral packing density, the presence of hydrogen bond accepting groups and the absence of hydrogen bond donor groups, and terminal groups with overall electrical neutrality. Approaches which use chemical methods for the activation of SAM surfaces are beginning to gain importance for the surface coupling of biomolecules. Thus far, most reactions for the surface activation of SAMs for protein adsorption have been accomplished after the SAM has been formed with monolayers terminated with carboxyl, amino or hydroxyl groups. Hundreds of synthetic pathways can be applied for *in situ* activation chemistry, including reagents such as N-hydroxysuccinimide (NHS), 1-ethyl-3-(3-dimethylaminopropyl) carbodiimide hydrochloride (EDC) and dithiobis (succinimidyl undecanoate) (DSU).[11, 52]

2.5 Methods for Nanolithography with Proteins

With the invention and continuing development of scanning probe instruments, such as the scanning tunneling microscope (STM) [53] and the atomic force microscope (AFM),[54] surface changes became evident when too much force was applied by an AFM tip, or if the applied bias voltages exceeded certain thresholds using STM or conductive AFM imaging. Researchers began experimenting to deliberately and selectively control these alterations.

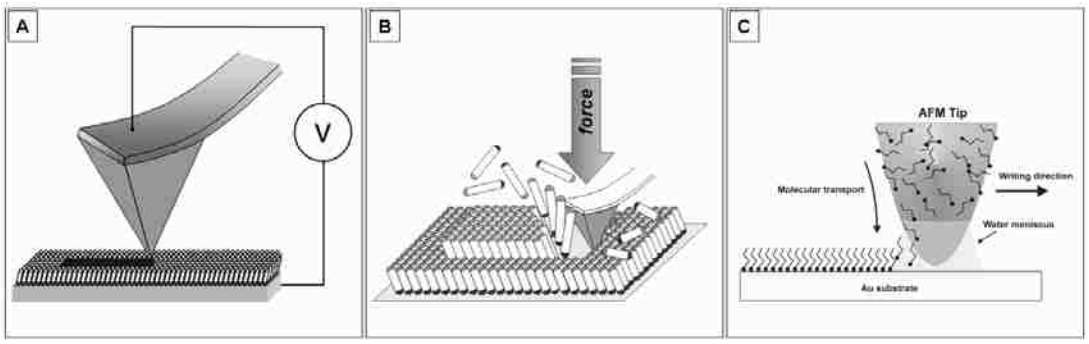

Figure 2.5 Schematic representations of three AFM-based nanofabrication techniques; [A] bias-induced lithography; [B] force-induced nanolithography (nanografting); [C] Dip-Pen Nanolithography (DPN) – Figure C reproduced with permission from *Science*.[55]

Molecules of SAMs can be written precisely on surfaces using a variety of different scanning probe lithography (SPL) methods. Figure 2.5 illustrates the fabrication principles of the three most predominant SPL methods applied for patterning proteins. SPL provides flexible and convenient approaches to construct SAM nanopatterns with designated functionalities in selected nano-sized areas. These nanoengineered surfaces can then be used to selectively immobilize desired proteins through covalent, electrostatic or specific recognition approaches.

A common feature of all SPL methods is that an SPM tip is used as a tool for both nanofabrication and characterization of surfaces. A helpful analogy for describing SPL methods with SAMs is an SPM tip (pen) which writes with molecules (ink) on various surfaces (paper). SPL provides exquisite control of surface chemistry including parameters such as the spatial

arrangement, chemical composition, and the written density of molecular ligands. The shape and dimensions of the tip dictate the detailed resolution of written nanostructures – SAM patterns as small as 5 nm have been reported, and it has become routine to achieve patterns of 20-50 nm (or larger). Since the dimensions of proteins range from tens to hundreds of nanometers, SPL methods are ideally suited for surface studies of protein binding. Particle lithography is another promising method for protein nanopatterning, which can produce arrays of protein nanostructures. Table 2.2 provides a comparison of approaches which have been successfully applied for protein patterning. The next sections of this chapter will present further details of these nanolithography methods, including nanografting,[56] bias-induced lithographies,[57] dip-pen nanolithography,[55] and latex particle lithography.[58]

As a tool for high-resolution characterization, the same SPM tips used to write nanopatterns on surfaces are also used to explore the morphology of nanopatterns after protein adsorption. Both AFM and STM are highly suitable, established methods for visualizing surfaces with high resolution. AFM and STM and have emerged as significant and powerful techniques for imaging surfaces at the molecular scale. Unlike electron microscopy methods which require high vacuum environments and conductive coating of specimens, *in situ* AFM/STM experiments can be accomplished under physiological conditions in aqueous buffered environments. SPM provides exquisite resolution for the detailed characterization of molecular structures, has versatility in imaging modes, and can be used for local modification of surfaces by lithography

Topographic images provide direct visualization of changes on surfaces after proteins bind to nanopatterns. Commercial advances continue to improve SPM resolution by providing consistently higher quality probes at lower cost and by the on-going development of imaging

modes for viewing chemical contrast differences for surfaces. AFM imaging modes can be applied for probing friction, softness, surface charge, polarizability, magnetic domains and viscoelasticity at the atomic scale.

Table 2.2 Comparison of methods applied for nanopatterning proteins.

Nanopatterning Method	Pen	Paper	Mechanism	Surface Chemistry	Citation
bias-induced oxidation	biased tip STM/AFM	conductive or semi-conductive substrate	surface oxidation	oxidization of surfaces or SAM terminal groups	33
bias-induced replacement lithography	biased tip STM/AFM in solution	conductive or semi-conductive substrate with SAM	displacement of SAMs under elevated bias	replace matrix SAM with new molecules	75
nanoshaving	bare tip (AFM)	SAMs including silanes, thiols	force & sweeping motion of tip	uncover areas of substrate for new molecules to attach	62
nanografting	bare AFM tip in a SAM solution	thiol SAMs	force & solution replacement	replace matrix with diverse functional groups of new SAMs	1, 91
Dip-Pen Nanolithography	ink-coated AFM tip in air	clean, uncoated surface	meniscus liquid transfer	write diverse functional groups of SAMs & other nanomaterials	15
latex particle lithography	(not an SPL-based method)	mica(0001) Au(111)	physical adsorption	self-ordering of monodisperse spheres as a structural template	76

2.5.1 Bias-induced Nanolithography of SAMs

When an electric field is applied at elevated bias voltages between a conductive SPM tip and sample, local chemical or physical changes occur in the area under the tip. Depending on the nature of the surface and environmental conditions (ambient vs. UHV), the "bias-induced" changes may result from electrochemistry (oxidation) at either the tip or sample which occurs from electric field effects;[59] or the changes may result from ohmic heating, which induces

evaporation or desorption of organic layers.[60, 61] This section will describe the method of bias-induced lithography and then present an example of bias-induced nanofabrication applied for protein nanopatterning. Figure 2.5A displays the general principle of bias-induced lithography. For bias-induced SPL, short (microsecond to millisecond) pulses of bias voltage are applied between a conductive SPM tip placed very near but not in contact with the surface. The size of the surface features are determined by the duration and magnitude of the electric field, and also by the dimensions of the area probed by the SPM tip. Often, with bias-induced oxidation, the chemical changes produced by an electric field do not manifest height changes, and thus are not detectable by topographic imaging. However, SPM imaging modes which display contrast between different terminal groups, such as force modulation, lateral force imaging, and current/electrical force images can clearly differentiate areas that are modified based on chemical changes.

Bias-induced lithography is emerging as a flexible and convenient means for nanofabrication of designed surface components, using either silane or thiol SAMs. Requirements for bias-induced nanofabrication include a conductive or semi-conductive substrate and a conductive SPM probe. To prepare conductive AFM tips, a thin film of metal (usually gold) is sputter-coated onto the surface of probes pre-coated with a precursor binding layer of chromium or titanium. Conductive tips and cantilevers comprised of doped silicon exhibit sufficient electrical conductivity for bias-induced modification of surfaces without requiring metal coatings. Bias-induced SPL methods are now accessible techniques for most SPM users, as a result of improvements in instruments and in the quality, cost and availability of commercial AFM probes, which now include coatings of cobalt, diamond-like carbon, doped diamond, platinum, platinum/iridium, tungsten carbide, titanium nitride, and nickel.

Researchers have begun to apply biased-induced SPL to pattern proteins. Bias-induced lithography was used directly for protein patterning by attachment of IgG-biotin to an array of 30 dot patterns generated using 1 ms voltage pulses (40V – 80V).[62] The substrate was a poly(methyl methacrylate) PMMA layer spin-coated on polished *p*-doped silicon wafer. Differences in hydrophobicity between the patterned areas and the substrate provided a driving force for the selective electrostatic deposition of proteins on nanopatterns.

After reaction with avidin-FITC, micron-sized patterned regions could then be imaged by fluorescence microscopy. To further extend the capabilities of bias-induced lithography for patterning SAMs with designated surface chemistries, methods which include replacement or addition of new molecules from solution have recently been developed.[57] After voltage pulsing, small areas of the surface were exposed for adsorption of new molecules using bias-induced replacement lithography.[63-65] In another approach, bias conditions which selectively oxidize SAM terminal groups (tip-induced electrooxidation) were used to generate surface oxides of SAMs. Oxidized areas were then used to chemically attach new molecules with desired functional groups.[59, 66] Nanopatterned protein arrays were fabricated by Cai et al. using bias-induced oxidation followed by protein adsorption (Figure 2.6).[67] Bias-induced SPL was applied to oxidize the headgroups of monolayers of α-hepta(ethylene glycol) methyl ω–undecenyl ether on Si(111) substrates. Bursts of 1 microsecond pulses of +17 V were applied to the sample, to generate rows of spots (90 nm diameter) separated by ~ 270 nm. The nanopatterned templates were then used to attach avidin followed by biotinylated bovine serum albumin. Although bias-induced lithography has not yet been widely applied for nanopatterning proteins, the newly introduced capabilities of customizing chemistry by tethering coupling agents to oxidized surfaces holds promise for new applications of bias-induced lithography in future investigations.

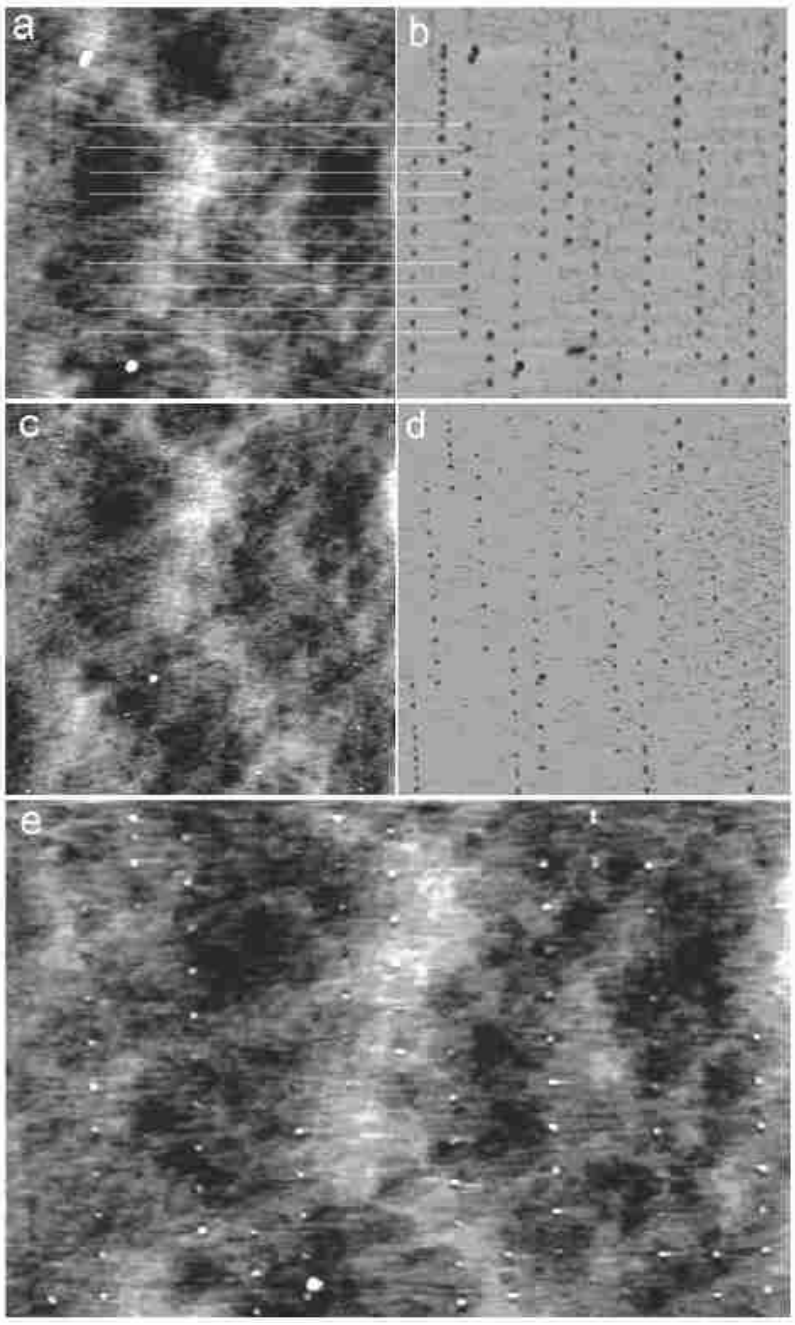

Figure 2.6 More than one hundred protein dot arrays produced by bias-induced nanofabrication. [A] AFM height and [B] friction image of nanoholes produced by bias-induced nanofabrication after treatment with EDAC/avidin (4×4 μm^2). The lines provide a reference for corresponding features. The dots are approximately 90 nm in diameter. [C] Topography and [D] friction images of the same area after incubation with biotinylated-BSA. [E] After the nanopatterns of biotinylated-BSA were reacted with avidin a positive height was observed for the nano-dot arrays. Reproduced with permission from *J. Am. Chem. Soc.*[67]

2.5.2 Force-induced Nanolithography of SAMs

Nanofabrication of SAMs can be accomplished by applying mechanical force to an AFM tip during scans. An intrinsic advantage of AFM instruments is the superb control of forces applied between the tip and sample, ranging from pico to nanonewtons. For high-resolution and faithful imaging of surface topography it is critical to apply minimal, non-destructive forces. When too much force is applied by an AFM tip, areas of the surface can be swept clean or "nanoshaved."[60] Nanografting was first invented in 1997, and combines nanoshaving with the simultaneous replacement of matrix SAM molecules by the self-assembly of new molecules.[56, 68] A broad range of thiolated molecules have been nanografted to provide tremendous flexibility in choosing the desired molecular lengths and terminal groups for experimental designs.[69-73] This section will describe the procedure for nanografting SAMs, present an example using automated nanografting with SAMs, and then review examples which apply force-induced lithography (nanografting) for protein patterning.

Nanografting (Figure 2.5B) is accomplished in dilute SAM solutions containing the selected molecule to be patterned by exerting a high local force on an AFM tip, pushing through the matrix SAM to contact the underlying gold surface. During scanning, pressure between the tip and surface displaces the SAM matrix molecules underneath the tip. As matrix molecules are removed, new thiol molecules from solution immediately adsorb onto the uncovered areas of the substrate to form nanopatterns, following the scanning track of the tip. SPM controllers can be programmed for automated lithography, to rapidly and consistently generate desired surface arrangements of arrays of SAM nanopatterns.[74] Commercial instruments typically include software with capabilities to control the length, direction, speed, bias pulse duration, residence time, and the applied force of the scanning motion of the SPM tip, analogous to a pen-plotter.

Automated SPL offers tremendous advantages for the speed and reproducibility of nanopatterning, and can produce highly sophisticated pattern arrangements and geometries, with superb precision and reproducibility for the alignment, spacing and shapes of nanopatterns. Examples of SAM nanopatterns generated by force-induced AFM-based lithography (nanografting) are shown in Figure 2.7.

The AFM contact-mode topograph (Figure 2.7A) displays sixteen nanopatterns of 11-mercaptoundecanoic acid (11-MUA) written within a resist of octadecanethiol. The corresponding frictional force image (Figure 2.7B) more clearly displays the arrangement and shapes for the nanopatterned array of circular designs.

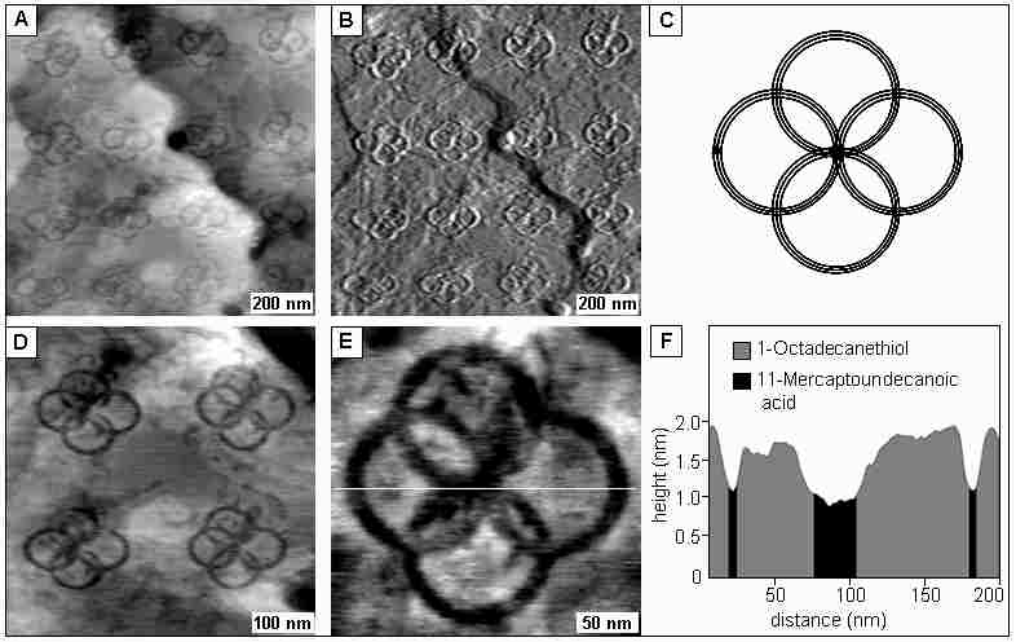

Figure 2.7 Nanopatterned array generated by automated nanografting. [A] Topography and [B] corresponding friction images (1.0 x 1.0 μm^2) of nanopatterns of 11-mercaptoundecanoic acid grafted in octadecanethiol/Au(111). [C] Design of nanopatterned (100 nm) ring elements. [D] Close-up view of four patterns; [E] Zoom-in view of a single pattern (250 x 250 nm^2). [F] Cross section taken along the line in E.

Nanografting was executed using a programmable computer module interfaced to the AFM controller for translating the tip rapidly and uniformly across the surface to create

designed arrangements of nanopatterns. (Controllers from RHK Technology, Troy, MI) A computer script (written in-house) was used to apply a higher load on the tip to inscribe the pretzel-shaped designs. Each design was generated by writing four 100 nm diameter rings as in Figure 2.7C. The rings were inscribed by outlining each circle three times with the AFM tip, beginning with the bottom ring and moving in a clockwise direction around the center intersection. It required approximately three minutes to complete the entire 4 × 4 array, (~ 12 seconds to write each pattern). After nanografting, AFM images were acquired under normal imaging conditions using minimal force. Figure 2.7D displays a close-up view of four nanopatterns, exhibiting nearly perfect alignment and symmetry. The high-resolution topograph of a single nanopattern in Figure 2.7E reveals the exquisite capabilities of AFM-based nanolithography to write and visualize surface details. The height difference between the ODT nanopattern and the 11-MUA matrix SAM is indicated by the cursor profile (Figure 2.7F) to be approximately 0.7 ± 0.1 nm, in close agreement with the theoretical height difference (0.7 nm). The line width of the rings is approximately 10 nm. Commercial silicon nitride cantilevers with an average spring constant of 0.58 N/m were used for both imaging and lithography (Veeco Probes, Santa Barbara, CA). The patterning and imaging experiments for Figure 2.7 were conducted *in situ*, in a liquid environment.

Typically, it requires less than one minute to fabricate individual nanopatterns using force-induced SPL such as nanoshaving and nanografting. Hundreds of nanopatterns can be written during an experiment without evidence of tip damage, provided that a minimal threshold force is applied. The fabrication forces used for force-induced SPL typically range from 2 to 30 nN, depending on the system under investigation and the geometries and spring constants of the cantilevers. Of course, if far too much force is applied the tip or substrate can be damaged, so it

is critical to determine the minimum force for nanofabrication with each experiment. Commercially available soft Si_3N_4 cantilevers have mostly been used for nanofabrication by mechanical force, with force constants ranging from ~ 0.03 N/m to 2.0 N/m. When imaging in liquid, the total force applied typically is less than 1 nN, to prevent damage to substrate layers.

The first studies using nanografting to immobilize proteins were conducted in 1999 by Gang-Yu Liu and co-workers using either electrostatic or covalent interactions to immobilize lysozyme, rabbit immunoglobulin G (IgG) and bovine serum albumin (BSA) on SAM nanopatterns.[75] Since then, a growing number of investigators have taken advantage of the flexibility of nanografting in liquids for surface studies with biomolecules. The typical general steps of an *in situ* protein binding experiment are (1) to fabricate nanopatterns of adhesive tethering molecules, (2) bind proteins to these nanopatterns, and then (3) test the activity of the immobilized proteins by introducing a second antibody or protein which will bind specifically to the surface-bound protein.

An important advantage of nanografting is the capability to conduct experiments *in situ*, viewing the successive changes in surface topography after the steps of nanopatterning SAMs, rinsing, and introducing buffers and proteins. With *in situ* nanografting, the protein patterns are not subjected to air exposure, and remain in a carefully controlled environment by rinsing and exchanging solutions within the liquid cell. As molecules bind to nanopatterns, sequential real time AFM images expose reaction details at a molecular level, uncovering critical details of the adsorption of proteins to nanostructured surfaces. Figure 2.8 illustrates the basic steps of an *in situ* protein adsorption experiment using nanografting. In the initial investigations of protein immobilization on nanografted SAMs, Liu used functionalized alkanethiol SAMs to mediate electrostatic and covalent binding of IgG and lysozyme.[75]

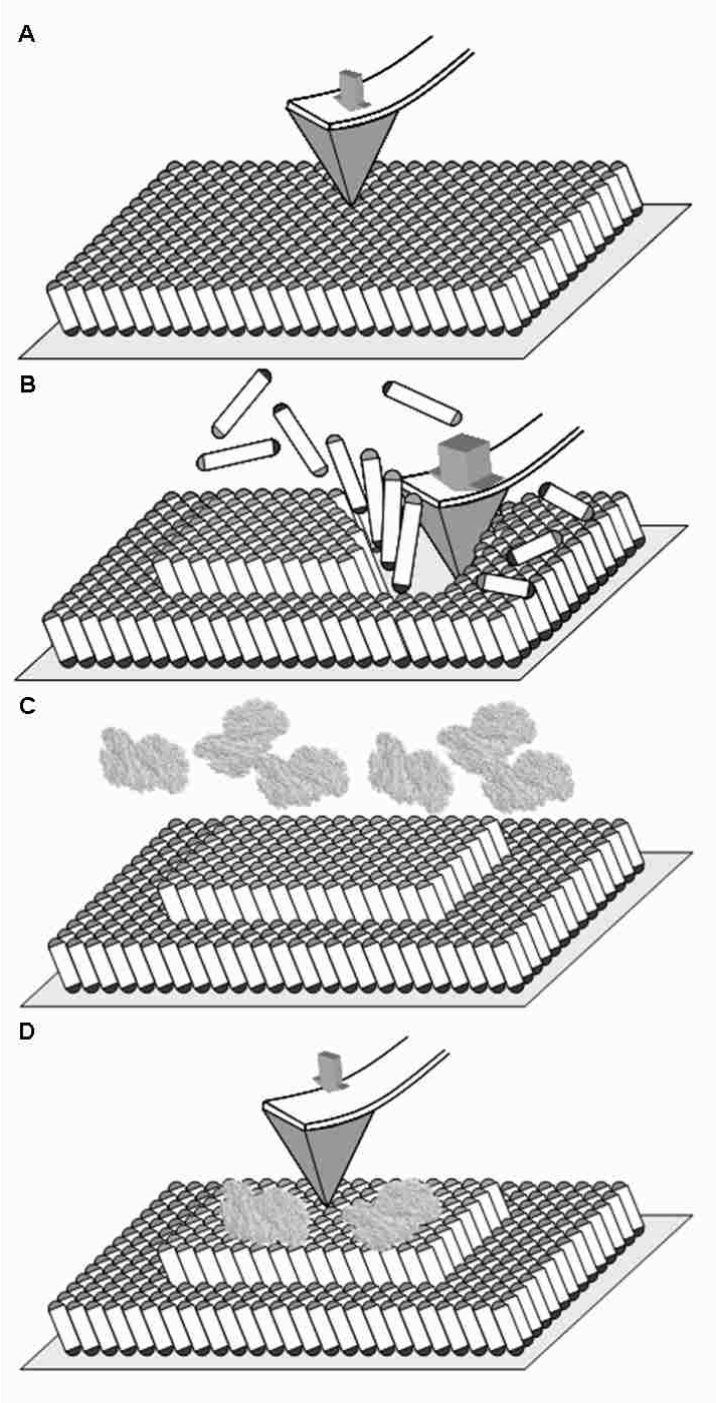

Figure 2.8 Steps for nanopatterning proteins using force-induced lithography. [A] A flat area is chosen for writing nanopatterns, by imaging at low, non-destructive forces. [B] Nanofabrication is accomplished by applying higher force to write new SAM molecules. [C] Proteins are introduced by exchanging liquids. [D] Protein nanostructures can be characterized under low force.

The reactivity and stability of protein nanopatterns was studied in further reports, and included investigation of the retention of specific activity of the immobilized proteins for binding antibodies.[76, 77] Protein patterns sustained washing with buffer and surfactant solutions and were stable for at least 40 hours of AFM imaging. The smallest protein feature yet produced by nanografting is a 10 x 150 nm^2 line containing three proteins.[75, 77]

The first *in situ* antigen-antibody binding AFM experiment with nanofabricated SAMs was conducted using nanografting to direct protein immobilization.[76] The activity of covalently immobilized rabbit IgG was tested by reactivity toward mouse anti-rabbit IgG. AFM topographs of protein binding on nanografted patterns of an aldehyde-terminated SAM are shown in Figure 2.9. Several aldehyde-terminated nanopatterns, a1–a5, were first grafted into a dodecanethiol SAM matrix. The depth of these patterns measured 0.8 ± 0.2 nm, and images display dark contrast where the rectangular patterns were inscribed (Figure 2.9A). After injecting rabbit IgG and rinsing with a surfactant solution, selective adsorption was observed on all six nanopatterns (Figure 2.9B) in which the bright contrast indicates heights taller than the matrix SAM. In the next step, mouse anti-rabbit IgG was introduced (Figure 2.9C) showing further height increases. By comparing the height of nanopatterns before and after secondary IgG binding, it was observed that immobilized IgG may adopt various configurations (Figure 2.9G).

Several investigators have applied nanografting to write nanopatterns for protein immobilization. Abell et al. conducted a side-by-side comparison of protein adsorption on multifunctionalized surfaces at the nanoscale using nanografting. Protein adsorption on three differently charged linkers nanografted within a hexa(ethylene glycol) terminated alkanethiol resist SAM, was monitored *in situ* by AFM at various pH values.[78] The adsorption of proteins

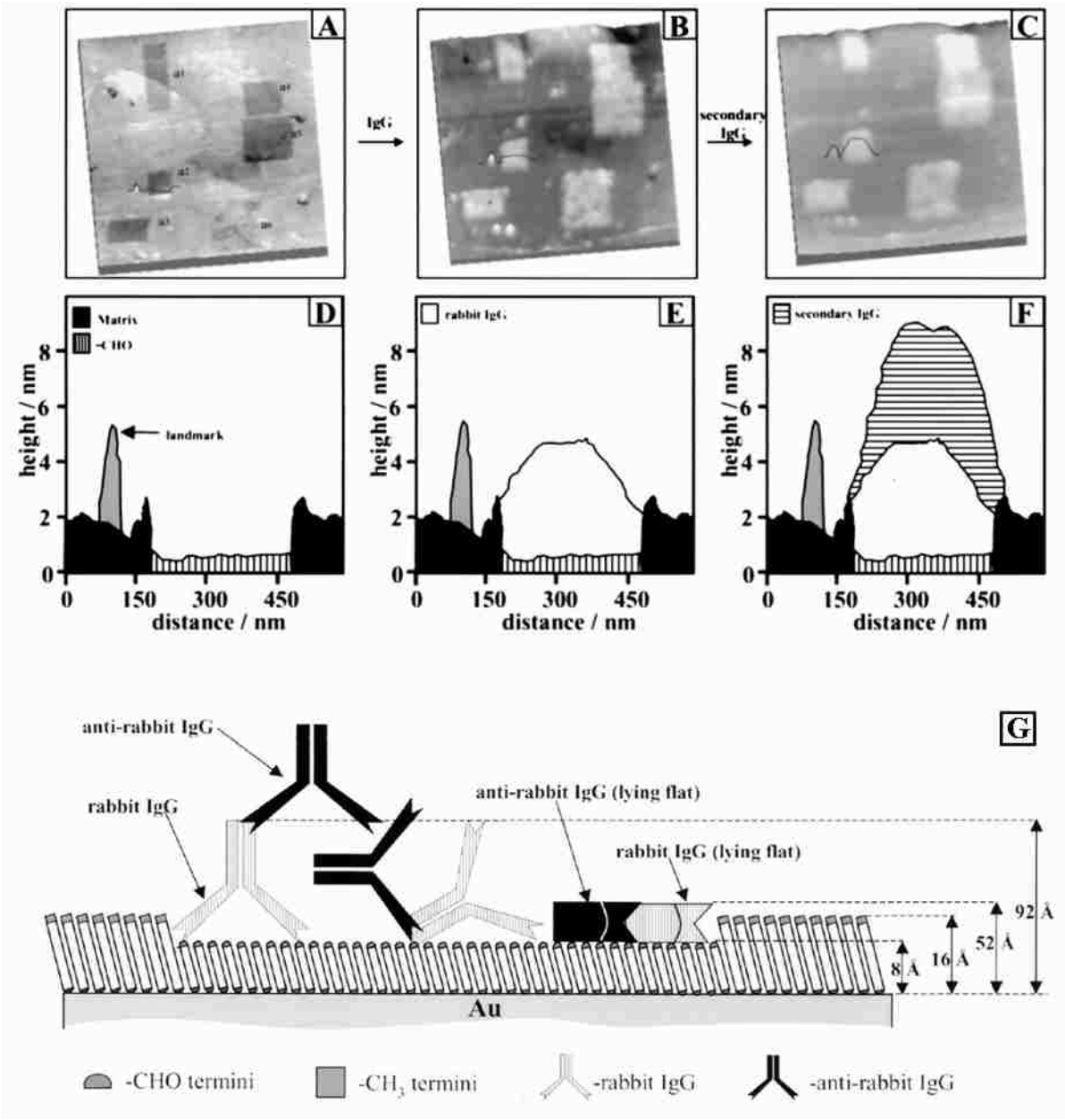

Figure 2.9 The steps of protein binding and molecular recognition with nanografted patterns captured by AFM topographic images. [A] Five nanopatterns of 3-mercapto-1-propanal were written in a dodecanethiol SAM. [B] The image contrast changed after rabbit IgG bound covalently to the aldehyde-terminated nanopatterns. [C] After introducing mouse anti-rabbit IgG, the patterns display further height changes, indicating the antibody binds specifically to the protein nanopatterns. Cursor traces across pattern a2 indicate the height changes [D] after nanografting; [E] after injecting IgG; [F] after introducing anti-rabbit IgG. [G] Map for understanding the evolution of molecular height changes during the steps of this *in situ* experiment. Reproduced with permission from *Biophys J.*[76]

onto nanografted patterns (400 × 400 nm^2) of 6-mercaptohexan-1-ol (MCH), *n*-(6-mercapto hexyl) pyridinium bromide (MHP), and 3-mercaptopropionic acid (MPA), was studied with lysozyme, IgG and carbonic anhydrase II. They conclude that in addition to the overall charge of protein molecules, the charge of local domains of the proteins plays a role in immobilization. In the same paper, Abell used nanografting to assemble multilayered protein G/IgG/anti-IgG nanostructures through electrostatic interactions, as a potential means to orient IgG molecules for antibody-based biosensor surfaces.

Using force-induced SPL methods of nanografting and nanoshaving, Porter et al. compared three approaches for protein patterning.[79] They successfully combined force-induced SPL with immobilization of IgG via EDC activation of 11-mercaptoundecanoic acid; through direct adsorption of Fab'-SH fragments to nanoshaved regions of an EG_3-OMe matrix; and through chemisorption of a disulfide coupling agent, dithiobis(succinimidyl undecanoate). Ducker et al. applied nanografting to immobilize insulin and acetylcholinase esterase on nanografted 1,2-diols which were activated by sodium periodate to produce aldehyde groups.[80] Retention of catalytic activity for demonstrated for nanopatterned enzymes. Nanografting was applied to directly pattern designed metalloproteins by Au-S chemisorption by Scoles et al.[81] The bundle protein structure was designed to present the C-termini of three helices, terminated with D-cysteine residues for assembly in a vertical orientation, normal to the Au(111) substrate. A potential disadvantage for nanografting is that exchange takes place between solution molecules and the surface matrix SAM for some systems of alkanethiols. Natural self-exchange is an issue particularly when nanografting longer chain thiols into a shorter chain matrix layer, thus it is important to use very dilute (< 0.1 mM) solutions for nanografting. Exchange can be

detected within 2-4 hours (depending on the age of the matrix SAM) when molecules from solution adsorb onto defect sites and at step edges.

Although not yet practical for high throughput applications and manufacturing, combining SPL with protein immobilization enables new approaches for directly investigating changes that occur on surfaces during biochemical reactions. Nano-engineered surfaces are useful for viewing antigen-antibody binding at the nanometer scale, to assess the specificity of selective binding, and to evaluate protein orientation and the accessibility of ligands for binding. Advantages of force-induced SPL include the ability to precisely produce nanometer-sized patterns of bioreceptors and to successively image and conduct fabrication *in situ*, within well-controlled environments. For protein nanopatterning, force-induced SPL can be applied to either directly write proteins on surfaces via nanoshaving, or can be applied to write molecules for attaching proteins to surfaces through electrostatic, covalent or specific binding chemistries.

2.5.3 Dip-Pen Nanolithography of SAMs and Proteins

Dip-pen nanolithography (DPN), developed by Chad Mirkin et al. in 1999, has emerged as an important and versatile method for producing multicomponent arrays of SAM nanopatterns, as well as other molecules and nanomaterials.[82] This section will describe the DPN nanofabrication method and then present examples of DPN applied for protein nanopatterning. Protein nanopatterning has been accomplished by several different approaches via DPN. For SAM molecules written directly by DPN, proteins may be attached to nanopatterns through electrostatic, covalent or specific interactions on nanopatterns after surface passivation. Another strategy is to use surface activation of nanopatterned amine, carboxylate or hydroxyl groups for protein immobilization. Direct writing of proteins has also been accomplished by DPN using modified AFM tips. In DPN, an AFM tip (pen) is coated with a

molecular "ink" to write on clean gold substrates or "paper" under ambient conditions in air.[55, 83] Ink molecules migrate from the coated AFM tip through a capillary meniscus to the substrate by diffusion (Figure 2.5C). Capillary transport of molecules from the AFM tip to the substrate can be used to directly write arrays of SAM nanopatterns. Additional mechanical force is not applied to the AFM tip or "pen." When an AFM tip is used in air to image a surface, the narrow gap between the tip and surface forms a tiny capillary meniscus from the condensation of water. Nanopatterns such as individual lines, dots, grids and arrays of alkanethiols have been written on bare gold surfaces.[55, 84, 85] The size of the water meniscus that bridges the tip and substrate depends on the tip shape and the relative humidity.[86] In DPN, the meniscus is used to transport molecules from the tip to the surface. The resolution of DPN depends on several parameters, such as the geometry of the AFM tip, the humidity of the ambient environment, as well as by the duration in which the inked tip is placed in contact with the surface – typically on the order of approximately 1 to 10 seconds. With commercial cantilevers, DPN routinely generates feature sizes down to 15 nm.

Protein arrays were produced with DPN by patterning 16-mercaptohexadecanoic acid (MHA) for immobilizing lysozyme and IgG through electrostatic interactions by Mrksich et al. (Figure 2.10).[87] After writing MHA dots (diameter 100-350 nm) the gold surface was passivated with 11-mercaptoundecyl-tri(ethylene glycol). The MHA patterns were exposed to proteins by immersing substrates in a solution containing the desired protein. The arrays were then rinsed with buffer and imaged in air by tapping mode AFM. Reaction of IgG patterns with rabbit antibody and with mixtures of proteins was also studied, using AFM to investigate and detect nonspecific binding to nanopatterns and to passivate areas of the substrate.

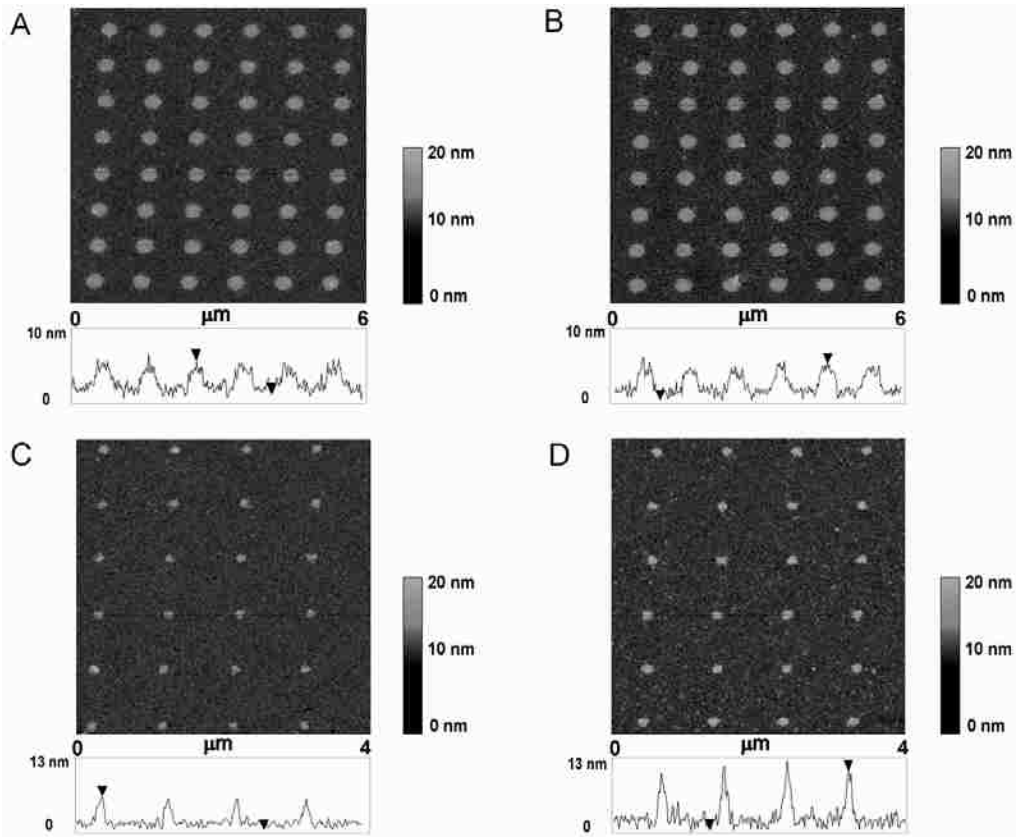

Figure 2.10 Snapshots of protein patterns generated by DPN captured *ex situ* by tapping mode AFM images in air, and corresponding AFM height profiles. [A] MHA dot array written by DPN after rabbit IgG adsorption; [B] Same IgG array after treatment with a mixture of lysozyme, retronectin, goat/sheep anti-IgG, and human IgG. No height change or non-specific adsorption is detected. [C] A rabbit IgG array before and [D] after treatment with a mixture containing lysozyme, goat/sheep anti-IgG, human anti-IgG, and rabbit anti-IgG. The height of the nanopatterns increased from 6.5 ± 0.9 to 12.1 ± 1.3 nm indicating the binding of anti-IgG onto IgG nanopatterns. Reproduced with permission from *Science*.[87]

In another study, Choi et al. immobilized cytochrome C through electrostatic adsorption on nanopatterns of MHA written by DPN.[88] The areas surrounding the MHA nanopatterns were passivated with octadecanethiol. Covalent attachment of synthetic peptides was accomplished by Ivanisevic and Cho using DPN.[89] First, nanopatterns of amine-terminated silane molecules (3-aminopropyl-triethoxysilane) (APTES) were written on SiO_x surfaces by DPN. Next, the heterobifunctional cross-linker N-hydroxysuccinimide ester (SMPB) was conjugated to the

APTES nanopatterns. In the final step, a TAT peptide was covalently linked to SMPB via a cysteine residue in the peptide sequence.

The molecular recognition-mediated, stepwise fabrication of patterned protein nanostructures was accomplished by Zauscher and colleagues using DPN.[90] First, a self-assembled monolayer (SAM) of 16-mercaptohexadecanoic acid (MHA) was patterned on gold by dip-pen nanolithography (DPN), shown in Figure 2.11. Next, the surrounding regions were passivated with a protein-resistant oligoethylene glycol-terminated alkanethiol SAM, (11-mercaptoundecyl-tri(ethylene glycol) (EG_3-SH). Nonspecific adsorption of proteins on the background was prevented by passivation with EG_3-SH. In the third step, an amine-terminated biotin derivative was covalently conjugated with the MHA nanopatterns through a reaction with N-hydroxysuccinimide (NHS) and 1-ethyl-3-(dimethylamino)propyl carbodiimide (EDAC). The surface was then incubated with streptavidin in a fourth step, mediated by molecular recognition between biotin and streptavidin. In the final step, protein nanopatterns were fabricated by molecular recognition-mediated immobilization of biotinylated protein (BSA) in solution. This method provides a generic platform for immobilization of biotin-tagged molecules mediated by biospecific interactions of biotin-streptavidin ligands.

For the specific immobilization of cysteine-labeled cowpea mosaic virus capsid particles, Mirkin and co-workers applied DPN to write a mixture of two dialkyl disulfides as ink.[91] The areas surrounding the nanopatterns were passivated with penta(ethylene glycol) groups. The density of maleimide groups provided efficient thiol capture through Michael addition of the thiol from cysteine residues of engineered CPMV particles to the nanopatterned maleimide groups.

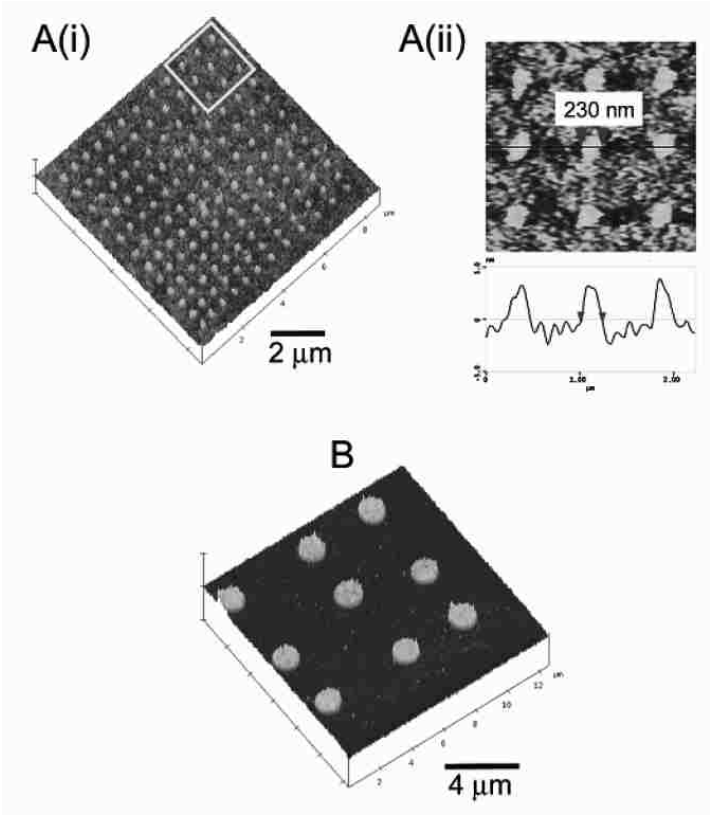

Figure 2.11 Nanopatterns of biotin-BSA imaged by tapping mode AFM. [A(i)] An array of 144 dots written by DPN; [A(ii)] Zoom-in view of the area within the frame, showing the size of the dots. [B] 3D dot array with 1 micron features. Reproduced with permission from *Nano Letters*.[90]

Surface activation of nanopatterns of MHA written by DPN was used by Zauscher and co-workers to fabricate nanostructures of stimulus-responsive elastin-like polypeptide (ELP).[92] First patterns of MHA were written directly using DPN. The surface was then passivated with 11-mercaptoundecyl-tri(ethylene glycol). Next, the COOH groups of the nanopatterned MHA were reacted with N-hydroxysuccinimide (NHS) and 1-ethyl-3-(dimethylamino)propyl carbodiimide (EDAC), to covalently conjugate ELP to the surface. ELP was end-grafted to the surface through an amine group to dictate the surface orientation.

Mirkin and colleagues have presented several studies with direct writing of proteins using DPN. Thiolated collagen was used as ink for direct-writing of collagen nanopatterns on

gold substrates.[93] Using a modified AFM tip, IgG was written directly on either negatively charged SiO_2 or on aldehyde-modified SiO_2 surfaces by DPN.[94] Tips were coated with 2-[methoxypoly(ethyleneoxy)propyl]trimethoxysilane (Si-PEG), which forms a biocompatible and hydrophilic surface layer on AFM tips for protein inking. Protein arrays of IgG and lysozyme were nanopatterned by direct-writing using metallized AFM tips (gold) with a thioctic acid coating, for protein adsorption.[95] Humidity is a critical variable in transporting proteins from tips to a surface, for direct-writing of proteins; optimum results were obtained in a glove box at 80-90% humidity to achieve consistent transport properties. Direct writing of proteins on nickel oxide surfaces also was accomplished using tips modified with nickel. For direct-write DPN, AFM tips were coated with ~ 5 nm of nickel to facilitate transfer of histidine-tagged proteins (ubiquitin and thioredoxin) as inks.[96] High humidity enabled diffusion from the tip to the surface and also served to minimize the denaturation of protein structures on nickel substrates. Oxidized nickel has a high affinity for polyhistidine residues, and patterns could not be generated for protein inks without histidine tags. The binding activity of the nanopatterns was investigated by reaction with fluorescently labeled antibodies, indicating that surface structures remained active for fluorescent labeling.

Another strategy for DPN nanopatterning is accomplished by combining bias-induced electrochemistry and DPN.[97] Electrochemical "Dip-Pen" nanolithography (E-DPN) was used to immobilize histidine-tagged proteins on nickel substrates.[98] Silicon AFM probes were coated with polyhistidine-tagged peptides, proteins and free-base porphyrins for nanopatterning. By applying a negative bias (-2 to -3V) to the coated AFM tips, nanopatterns could be written on nickel surfaces using tapping-mode AFM. Without an applied potential, protein deposition was not observed.

DPN provides methods for directly writing chemical inks on surfaces for complex, multi-step fabrication of nanostructures of proteins. Chemical reagents can be delivered directly to nanosized areas of a surface, and then the surrounding uncovered areas can be passivated with resistive SAMs. The DPN method is amenable to conducting experiments at ambient temperatures in air, and ink transfer is facilitated by controlling humidity. After each reaction step, samples can be characterized *ex situ* by AFM imaging. Different molecules can be deposited by exchanging tips to produce multi-component arrays of nanopatterns. For protein nanopatterning, DPN can be applied to either directly write proteins on surfaces using modified tips or to nanopattern SAM molecules for attaching proteins to surfaces through electrostatic, covalent or specific binding.

2.5.4 Latex Particle Lithography with Proteins

Particle or nanosphere lithography is an approach for nanopatterning which uses physical adsorption of materials to surfaces. Monodisperse latex particles self-assemble into periodic structures on flat surfaces, which have then be used as structural templates or photomasks for defining the deposition of proteins or other materials. The latex particles are removed by various approaches, such as calcination, solvent dissolution, or simple rinsing with water. Particle lithography has been successfully applied for patterning metals, sols, polymers, and inorganic materials.[99-103] Researchers have also applied colloidal lithography with latex beads as photomasks, to construct functional surfaces for selective protein adsorption on lithographically defined regions.[103, 104] This section will describe a method of particle lithography which can be applied directly for controlling the organization of proteins on surfaces through physical adsorption.[58]

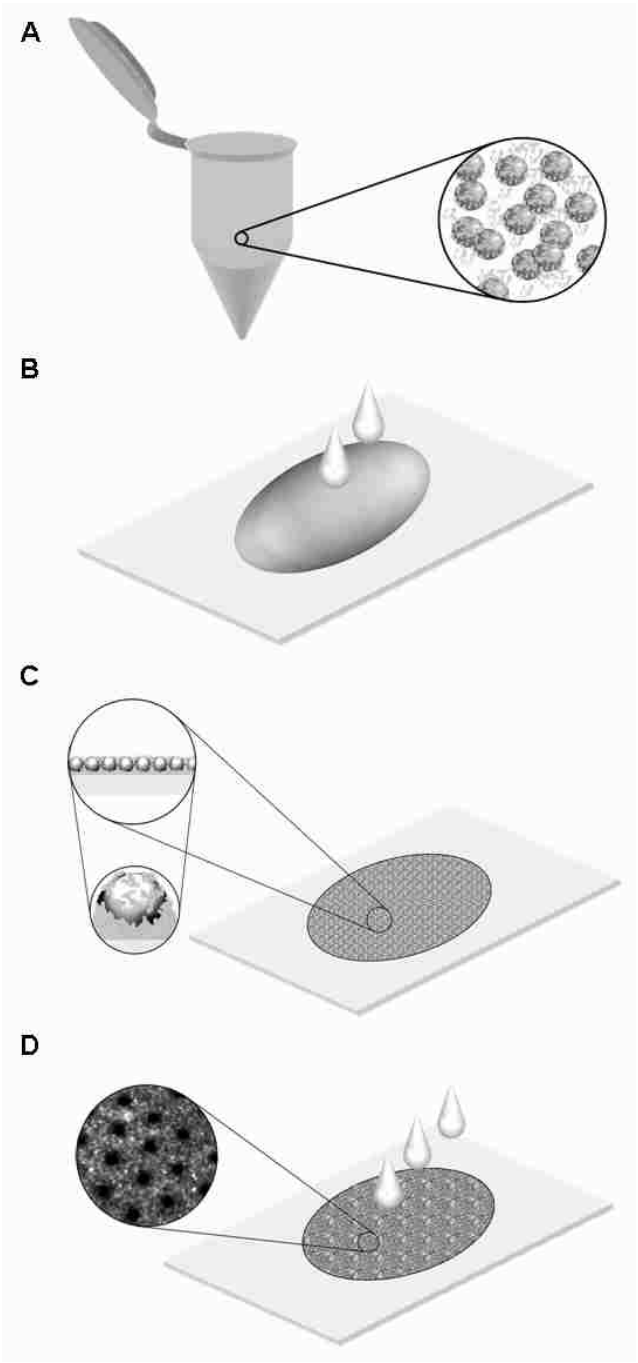

Figure 2.12 Fabrication steps for creating arrays of protein nanostructures via particle lithography. [A] Monodisperse latex particles are mixed with protein; [B] The mixture is deposited on a flat surface such as mica(0001); [C] After the droplet dries, an ordered crystalline layer is formed; [D] Latex are removed by rinsing with deionized water, leaving a layer of protein nanostructures on the surface.

Particle lithography can be used to construct arrays of protein nanostructures on surfaces, with superb control of the distribution of proteins within a single layer over micron-sized areas.[58] An outline of the steps for patterning proteins using latex particle lithography is shown in Figure 2.12. First, the protein and latex are mixed together in an aqueous solution. For best results, the solution containing protein and latex should be allowed to remain at room temperature for time intervals not longer than 4 h. (To maintain protein activity the solutions should be freshly prepared, and to minimize contaminants, the latex particles should be prewashed to ensure that the particles are free of surfactants). In the second step, a small volume (10 microliters/cm^2) of the colloidal suspension is deposited at the center of the substrate surface, using a pipette. The liquid spreads out into a thin layer across the surface as it dries. The protein and latex mixture forms ordered assemblies supported by mica or gold. During drying, the convective motion of water as it evaporates pulls the latex together into close-packed assemblies. After the deposits have dried, the latex is rinsed away with deionized water to leave a single layer of protein nanostructures on the surface. The assembly of latex particles and the protein nanostructures can be characterized using AFM throughout the fabrication process. Example images of BSA arrays formed from 500 nm and 200 nm diameter spheres are shown in Figures 2.13A and 13B, respectively.

The 2-D AFM topographs reveal an organized arrangement of circular dark holes, (uncovered areas of mica) surrounded by clusters of BSA. The periodicity of the resulting nanopatterns depends on the separation of latex spheres, which is observed to be 10-15% smaller than the original latex diameters. This is likely attributable to the shrinking and deformation of latex particles during drying. Using 500 nm particles, the ratio of BSA:latex was 55,000:1 which roughly corresponds to a single layer of proteins encapsulating a sphere. For

the 200 nm particles, the ratio of BSA:latex was 9000:1, also corresponding to a monolayer shell. The ratios for successful lithography have ranged from approximately half of monolayer coverage of spheres to that of two layers, yielding different distributions and surface morphologies. Particle lithography uses mild conditions (ambient temperatures, buffers), yet provides nanometer-level control of the spatial distribution of proteins organized within a single surface layer. Particle lithography was also successfully applied for nanopatterning rabbit IgG.[58] Both IgG and BSA nanopatterns retained the ability to bind corresponding specific antibodies.

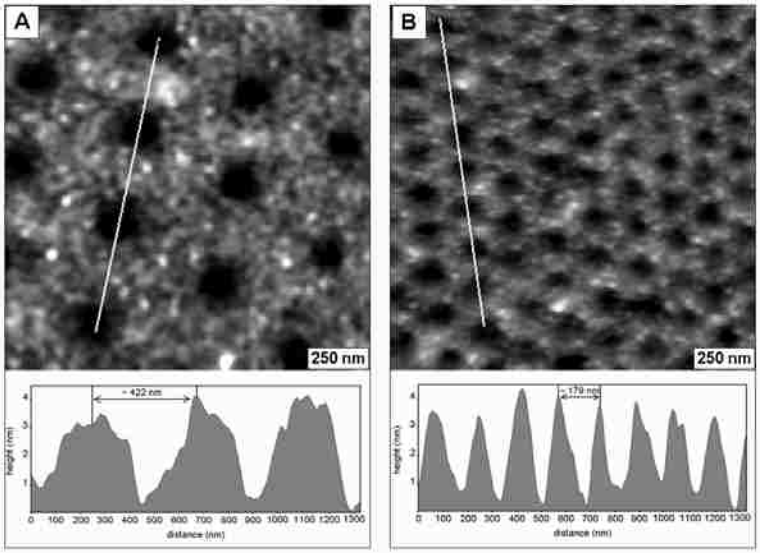

Figure 2.13 Periodic arrays of BSA nanostructures generated with latex nanoparticle lithography. [A] BSA nanopatterns from 500 nm particles, using a BSA-to-latex ratio of 55000:1. The corresponding cursor indicates the periodicity of the BSA nanostructures is 422 ± 33 nm. [B] BSA nanostructures generated using 200 nm particles and a BSA-to-latex ratio of 9000:1. The periodicity of the BSA nanostructures measured 179 ± 21 nm.

Particle lithography is a highly reproducible and robust method for patterning proteins, and serves as an excellent starting point for continuing to develop more complex bioassays with different surfaces and proteins. Using latex particles to control the arrangement of proteins on surfaces is a practical technology which is amenable to microspotting or immersion methods used for protein microarrays and biochips. Latex bead immobilization has been applied in

spotting solutions to create microarrays for detection of antibodies.[105] Particle lithography offers the advantages of nanometer precision and high throughput, since a small vial of solution can produce hundreds of replicate samples. Future investigations will address the suitability of particle lithography to other surfaces and to other proteins, for application in surface-bound immunoassays.

2.6 Detection of Protein Binding at the Nanoscale

Nanoengineering approaches for the development of nanoscale bioassays capitalize on the unique in situ and high-resolution capabilities of SPM. Designed surfaces can be created with precisely placed proteins, which are subsequently monitored during the binding of secondary antibodies. SPM can be applied directly for detection, measuring changes in the heights of nanopatterns with protein binding. The height changes indicate the side-on or end-on orientation of immobilized proteins (Figure 2.14).[75] In some investigations, fluorescent labels were conjugated to antibodies for microscopic examination of samples. Optical microscopy can detect changes in fluorescence after antigen-antibody binding.

An important question to address is whether or not the tagging entity hinders the affinity and efficiency of antigen-antibody binding. Many fluorescent dyes currently used are hydrophobic, which substantially decreases the solubility of protein-dye conjugates. This could adversely influence signal intensity for fluorescent detection.[106] Nanoscale studies can be applied to refine critical parameters used to link and organize proteins on surfaces of biochips and biosensors. SPM images of protein binding can be beneficial for evaluating the effectiveness of different bioconjugation chemistries for biomarkers.

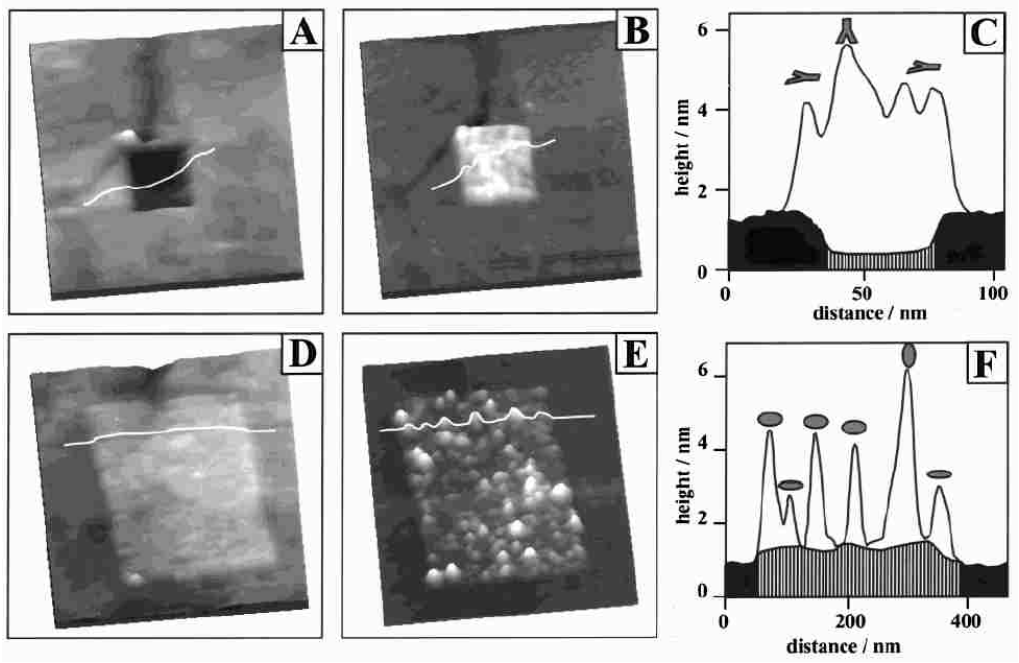

Figure 2.14 Nanografted patterns of aldehyde-terminated SAMs were used to covalently immobilize proteins via imine bonds. [A] Nanopattern of 3-mercapto-1-propanal (150 × 150 nm^2) written in decanethiol; [B] after *in situ* immersion in buffer containing rabbit IgG; [C] combined cursor profiles for lines in A and B. [D] Nanografted rectangle of mercaptodecanal (340 × 300 nm^2) written in hexanethiol; [E] after immersion in lysozyme solution; [F] Corresponding cursor profiles across D and E. The ellipsoidal lysozyme and Y-shaped IgG molecules may adopt various orientations, as shown in the schematics above the cursor plots. Reproduced with permission from *Langmuir*.[75]

At the core of biosensing is detection of biomolecular binding events with high selectivity and sensitivity. Typically, bioassays for surface-bound proteins are not as sensitive as approaches which use solution chemistry, due in part to the accessibility of molecules for binding. Pressing the limits of protein patterning to the nanometer scale will furnish direct views of the differences in immobilization chemistries. Conventionally, biosensors and biochips rely on microspotting or solution deposition to place proteins on various surfaces, without control of the placement and arrangement of target proteins. There is a requirement for efficient yet mild immobilization chemistries which preserve tertiary structure and maximize the activity of fragile biomolecules.

Biomolecules immobilized on a surface serve as the receptor and in some cases as the signal transducer in biosensors. Therefore, the placement of biological ligands in precisely defined locations can increase the density of sensor elements and lead to improved detection limits with molecular-level control of the surface reactivity.[107, 108] As a proof-of-concept, Wolinsky and Mirkin have reported a nanometer-scale antibody array prepared by DPN to test for the presence of the human immunodeficiency virus type 1 (HIV-1) in blood samples.[109] The HIV-1 antibodies were immobilized on the MHA nanopatterns for hybridizing (HIV-1 p24) antigen and bound proteins. With a nanoarray of 100 nm features written by DPN, the three-component sandwich assay exceeded the limit of detection of conventional enzyme-linked immunosorbent assay (ELISA) based immunoassays by 1000-fold.

2.7 Future Directions

It can be anticipated that array-based technologies in proteomics including protein-based biochip and biosensing devices will significantly advance biotechnology, clinical diagnostics, tissue engineering, and targeted drug delivery.[110-112] Ultra small protein patterns can be used in biosensing, control of cell adhesion and growth, and in biochip fabrication.[6, 7, 113] Methods of high-throughput protein analysis offer immense potential for fast, direct and quantitative detection, including the possibility of screening thousands of proteins within a single sample to test for protein, ligand, and drug interactions. Improved binding to surfaces onto which capture proteins are arrayed and improved sensitivity of detection are technical challenges advancing protein microarray technology. The next sections will first discuss the motivation for advancing beyond microtechnology to the nanoscale frontier and then describe new technologies which are being developed for multiplexing AFM systems for parallel processes.

2.8 Advantages of Nanoscale Detection

Tools for nano- and microfabrication will provide important contributions in developing biochip and biosensing technologies, as well as supply basic research in protein-protein interactions. With the rapid progress in development of large sets of characterized antibodies, protein and antibody arrays will provide tremendous advantages for diagnostics and medical science. Miniaturization provides rewards of reduced quantities of analytes and reagents, increased density of sensor and chip elements, and more rapid reaction response.[108, 114-116] Multiplex screening of many interactions in a parallel fashion reduces analysis time and gives insight into the multiplicity of factors involved in diseases. Protein microarrays used in experiments based on AFM detection may soon reach capabilities for routinely achieving single molecule detection.

Nanotechnology offers advantages not only for array production but also for sample detection for bioarrays. In the nanoscale size regime, material properties are different than at macroscopic scales, exhibiting phenomena such as electromagnetic field enhancement, narrow emission band fluorescence, surface plasmon resonance, and conductivity and signal amplification. These properties enable new signaling and recognition capabilities for use in sensor systems. For example, bioconjugates of nanoparticles and quantum dots may provide improved stability and sensitivity for quantitative fluorescence detection with advantages over the conventional approach of fluorescent staining which suffers from the disadvantage of photobleaching.[117] With regard to biomolecule detection, new strategies based on functionalized metal nanoparticles, in combination with magnetic detection have been reported, using superparamagnetic beads coated with antibodies for detection.[118]

2.9 Development of Cantilever Arrays

Using SPM-based nanofabrication, the single pen-and-ink approach is far too slow for cost-effective manufacturing of protein arrays. AFM-based lithography offers the ultimate capabilities for nanometer-scale control of surfaces with extremely high spatial precision, however, it has the limitation of relatively low throughput by fabricating each pattern individually. If higher throughput can be accomplished for nanoscale biochips, such arrays would offer immense capabilities. Miniaturization of protein sensing to nanodimensions will require techniques for rapid, efficient and high-throughput writing of biomolecules and SAMs. New designs for AFM probe arrays are being developed which will provide parallel and multiplexing capabilities for surface characterization and fabrication. Readers are referred to two recent reviews which detail the developments in multiple probe systems.[82, 119]

Successful lithography with probe arrays has been demonstrated by several researchers, and representative examples are summarized in Table 2.3. Initial designs of tip arrays used feedback from a single cantilever for operation. This can sometimes be problematic for lithography because of variations in tip geometries and difficulties for precise alignment.[120] Micromachined arrays of cantilevers operated in parallel (2×1, 5×1, 10×1, 32×1 and 50×1) were used for bias-induced oxidation of silicon as reported by Quate, et al.[120-122] Proof-of-concept experiments were presented for operation of parallel AFM probes for bias-induced lithography using as many as 50 probes. Arrays with integrated z-axis control were found to improve the quality and reproducibility of writing. There are several approaches for control and actuation of individual probes within cantilever arrays, including piezoelectric sensing,[122-124] optical interferometric detection,[125] thermal actuation of bimetallic tips,[126-130] and conductivity sensing of tip-surface contact.[131]

Table 2.3 Examples of AFM probe arrays which have been successfully demonstrated for AFM imaging/lithography applications.

Year	Array size	Tip actuation method	Application	Citation
1995	2×1	integrated piezoelectric sensor and piezoresisitive sensor for both tips	parallel constant-force AFM imaging	139
1995	2×1 5×1	single tip feedback (piezoresistive levers)	bias-induced oxidation of silicon (100-200 nm line patterns)	119
1996	2×1	integrated piezoelectric actuators for each tip	bias-induced oxidation of silicon (micron patterns)	121
1998	10×1 32×1 50×1	thermal actuation of individual probes, piezoresisitive sensors and integrated ZnO actuators.	bias-induced oxidation of silicon (1.1 micron line patterns), and parallel AFM imaging	120
1999	5×5	integrated piezoresistive sensing using 5 actuators	multiplexed AFM imaging	134
2000	2×1	thermal bimorph actuator, metal-oxide-semiconductor electronics	AFM imaging with constant height mode, tapping mode, constant force mode	126
2000	2×4	piezoresistive deflection sensors	parallel AFM imaging	123
2000	32×32	thermal actuation, corner sensors for z-feedback control of entire chip	data storage read/write operations	135, 136
2001	5×1	optical interferometric detection	parallel AFM imaging, constant height mode	124
2002	2×2 2×7	piezo-resisitive sensing with integrated electrical interconnects	parallel contact-mode imaging of large sample areas	122
2002	8×1 32×1	single tip actuation & optical deflection feedback	DPN with octadecanethiol/gold	131
2003	8×1	single tip actuation & optical deflection feedback	DPN with sol inks for chemical sensing	133
2003	10×1	Conductivity-based sensing of tip-surface contact	simultaneous DPN writing with eight probes	130
2004	10×1	integrated thermal actuation of probes with piezoresistive stress sensors	parallel constant-force AFM imaging	127
2004	12×1	thermal actuation of bimetallic probes, piezoresisitive Wheatstone bridge detection	AFM imaging and force-distance measurements	125
2004	10×1	individual tip control by thermal actuation of bimorph probes	simultaneous DPN writing with ten probes	128, 129

Dip-Pen Nanolithography (DPN) has been advanced to parallel processes through the use of one-dimensional cantilever arrays.[132, 133] Control of the horizontal and vertical movements of AFM probes can be achieved using the laser signal feedback of a closed-loop AFM scanner. Using an eight-cantilever array, a miniaturized combinatorial chemical sensor was produced with DPN by writing multiple inks as sensor elements.[134] Also, examples have been reported using tip arrays for simultaneously writing multiple patterns of octadecanethiol using DPN.[129-131]

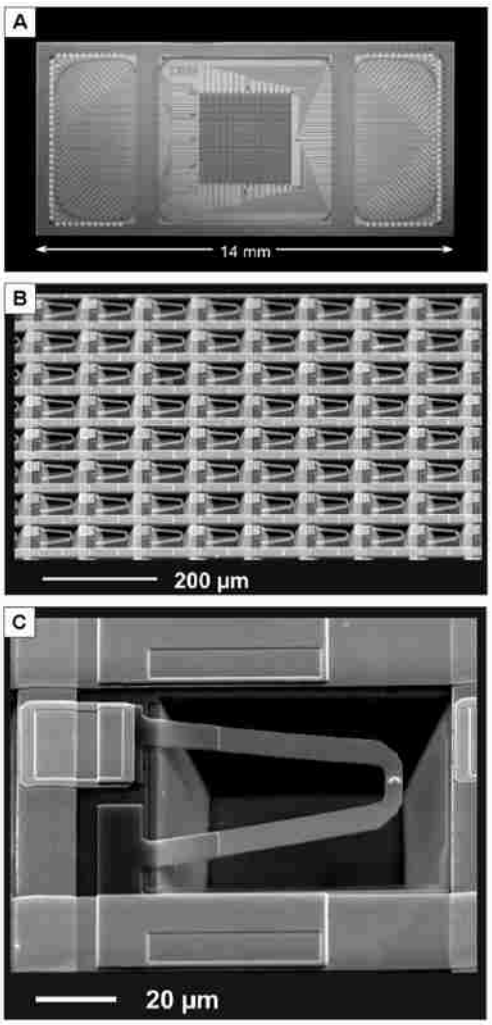

Figure 2.15 The "millipede" array of 1024 cantilevers. [A] Photo of the entire chip; [B] SEM images of cantilevers of the 32 x 32 array; [C] A single cantilever with integrated silicon tip. Reproduced with permission from *J. MEMS.*[135]

Two-dimensional cantilever arrays have been developed and tested, including designs which combine passive (feedback from deflection of a single tip) and active control through actuation of multiple tips.[136] A group at IBM has implemented an addressable 32 x 32 probe array designed for high density data storage.[135, 137] The "millipede" array format with 1024 cantilevers measures 3 x 3 mm and each cantilever is assigned to read and write 100 x 100 μm^2 areas. The millipede approach is not based on individual z-feedback for each cantilever; feedback control is applied for the whole chip. This design requires stringent control of tip fabrication parameters via micromachining to generate uniform probe dimensions (Figure 2.15). Although the Millipede design is intended for read/write data storage, other applications can be envisioned using scanning probe lithography.

2.10 Concluding Remarks

Fundamental understanding of the interactions of protein binding to substrates or antibodies is essential for developing workable technologies for life sciences. The new capabilities to study and control processes on the nanometer scale are emerging as valuable assets in both fundamental and applied research. At present, SPM and SPL are primarily used as research tools in laboratories rather than as tools for manufacturing. However in the future, nanoscale technology in manufacturing is predicted to bring an even greater impact and benefit to society than present-day microfabrication technologies. Potential applications include the development of a new generation of chemical and biosensors, biochips, and molecular electronic devices. We anticipate that nanoscale research will define new directions in areas such as biosensing, biomimetic surfaces for drug delivery and biomolecule-based electronics. This chapter has provided insight on the tremendous versatility of several new SPL methods applied for protein nanopatterning. In addition, there are many new nanofabrication methods

being developed which may be suitable in the future for engineering surfaces for nanoscale protein assays.

Applying the *in situ* tools of lithography with proteins will enable systematic evaluation of the differences in bioaffinity for various chemical immobilization strategies, with direct views of how the morphology and geometry of nanoengineered surfaces direct and influence the binding of antibodies and proteins. Conceptually, by arranging and orienting proteins on well-defined surfaces, the selectivity and sensitivity of surface-based protein assays can be substantially improved. These studies will facilitate the development of new and better approaches for immobilization and bioconjugation chemistries, which are key technologies used in manufacturing biochip and biosensing surfaces.

CHAPTER 3. ACHIEVING PRECISION AND REPRODUCIBILITY FOR WRITING PATTERNS OF *n*-ALKANETHIOL SAMS WITH AUTOMATED NANOGRAFTING

3.1 Introduction

Automated scanning probe lithography (SPL) combined with high-resolution AFM imaging furnish valuable new tools for nanoscale research, enabling control of parameters such as the size, arrangement, geometry, spacing, the packing density, and the composition of nanopatterned test elements. Automated SPL offers tremendous advantages for the speed and reproducibility of nanopatterning and can produce highly sophisticated pattern arrangements and geometries with superb precision for writing nanopatterns.[74] Nanopatterned arrays of self-assembled monolayers written by nanografting[69, 138] furnish 2-D planar test platforms for further measurements of surface properties,[139] and can also serve as a foundation for bottom-up assembly of complex nanostructures of polymers,[140] metals,[141] and proteins.[76, 142, 143] At present, scanning probe microscopes (SPM) and scanning probe-based lithography are primarily used for laboratory research investigations rather than as tools for manufacturing. However in the future, nanoscale technology in manufacturing is predicted to bring an even greater impact and benefit to society than present-day microfabrication technologies.[144, 145] Potential applications include the development of a new generation of chemical and biosensors, biochips, and molecular electronic devices.[146, 147]

Nanografting was first introduced in 1997 by Xu et al. for writing nanopatterns of self-assembled monolayers (SAMs).[138] Since then, a broad range of thiolated molecules have been

---

Reproduced with permission from John Wiley & Sons Inc.: Ngunjiri, J. N.; Kelley, A. T.; Lejeune, Z. M.; Li, J.-R.; Lewandowski, B. R.; Serem, W. K.; Daniels, S. L.; Lusker, K., Achieving Precision and Reproducibility for Writing Patterns of n-alkanethiol Self-assembled Monolayers with Automated Nanografting. *Scanning* **2008,** 30, (1).

nanografted which provide flexibility in choosing the desired molecular lengths and terminal groups for experimental designs.[69-73] Nanografting is an AFM-based lithography method which applies mechanical force to an AFM tip to inscribe patterns of thiolated molecules (ink) within a matrix SAM. To accomplish nanografting, the AFM tip is completely submerged in a liquid containing the *ink* molecules for writing and AFM characterizations are accomplished *in situ* without exchanging tips. Instruments for AFM have remarkable capabilities for controlling the force applied to the tip, ranging from pico to nanonewtons. When low forces are used for AFM imaging (<1 nN) the SAM surfaces are not disturbed and can be characterized with high resolution using contact mode imaging. However, when higher forces are applied to the tip, areas of the matrix SAM are shaved from the surface, which enables fresh molecules from solution to immediately self-assemble onto the uncovered areas following the track of the scanning tip. By returning to low force the same tip can be used to characterize the nanostructures.

Due to their stability, ease of preparation and well-ordered surface structures, SAMs of *n*-alkanethiols furnish excellent models for studying molecular binding, since layers of defined thickness and designed properties can be generated.[26, 27] The endgroups of *n*-alkanethiols bond via thiol chemisorption to metal surfaces. The properties of SAM surfaces can be flexibly controlled by changing the functional (head) groups of the alkyl chain; also these functional groups can be used for further chemical reactions. The acidity, adhesion, wetting and structural properties of surfaces can be modified by choosing specific chemical headgroups (such as NH_2, OH, COOH, CH_3, glycol, etc.).[28, 29] The preparation, characterization, and properties of SAMs have been described and reviewed previously.[29-33]

Several other approaches for writing nanopatterns of *n*-alkanethiol SAMs have been developed with SPM, such as Dip-Pen Nanolithography (DPN),[85, 148-150] bias-induced replacement lithography,[151, 152] bias-induced oxidation,[66, 67, 153] and catalytic probe lithography.[154] The nature of the desired surface chemistry dictates which scanning probe lithography (SPL) approach is most suitable and convenient for investigations. All SPL methods use an SPM tip as a tool for nanofabrication; a suitable analogy is to describe the tip as a "pen" for writing nanopatterns. The "inks" for writing are self-assembled monolayers or other molecules, and various substrates provide the "paper" for nanolithography. The dimensions of the AFM tip determine the resolution of writing, patterns as small as 3×5 nm^2 have been reported.[138] Commercial AFM instruments furnish software with capabilities to control the length, direction, speed, bias pulse duration, residence time, and the applied force for the motion of the AFM tip. Thus, SPL can be completed with little instrument modification. For example, DPN and catalytic probe lithography are achieved by using a coated AFM tip. To accomplish oxidation or replacement lithographies, a conductive probe is used to apply elevated bias voltages. Nanografting is accomplished in dilute solutions of thiol inks by applying greater force to the AFM tip for writing nanopatterns. Details about the writing strategies and mechanisms for various SPL methods have been previously reviewed.[151, 155-157]

Nanografting provides significant advantages for *in situ* investigations, since the steps of characterization and writing are accomplished in liquids without exchanging AFM tips. The successive changes in surface topography can be viewed after each step: nanopatterning SAMs, rinsing, and introducing new adsorbates. With *in situ* nanografting, the SAM patterns remain in a carefully controlled environment and solutions within the liquid cell can be exchanged by rinsing to introduce new reagents for chemical reactions. Another important advantage of

conducting experiments in liquid media is the dramatic increase in the resolution of AFM imaging. By imaging in liquid media the strong capillary interactions between the tip and sample which are present in ambient air can be reduced or eliminated.[158-160] Binding between molecules is a nanometer-sized phenomena, thus intuitively, a close-up view of molecules on surfaces furnishes a fresh perspective on how reactions occur. Nanografted patterns can be incubated with desired nanomaterials or molecules, and the progressive changes in height and surface morphology of the nanostructures provides insight about surface reactions and mechanisms. *In situ* investigations with nanografting have been reported for adsorption of proteins,[76, 142, 143, 161-165] electroless deposition of copper on nanografted gradients of carboxylate-terminated SAMs,[141] and for pattern transfer reactions with polymers.[140]

Despite the intrinsic *in situ* advantages and capabilities for high spatial resolution, nanografting has not yet become widely applied for surface investigations as compared to other ambient *ex situ* writing methods. The complexity of imaging in liquids requires advanced skills and training for experimentalists. This report will provide strategies and technical details for automated writing of SAM nanopatterns by nanografting. A few key experimental parameters can be systematically optimized for nanografting to enable exquisite control of pattern geometry, pitch and reproducibility at the nanoscale.

3.2 Materials and Methods

3.2.1 Materials.

Alkanethiol compounds such as hexanethiol, decanethiol, dodecanethiol, hexadecanethiol, octadecanethiol (ODT), 11-mercaptoundecanol (11-MUD), 11-mercaptoundecanoic acid (11-MUA) and 16-mercaptohexadecanoic acid (16-MHA) were obtained from Sigma Aldrich (St. Louis, MO, USA) and used without further purification.

Ethanol (200 proof) was purchased from AAper Alcohol and Chemical Co. (Shelbyville, KY, USA). Self-assembled monolayers were prepared by immersing gold substrates in ethanolic solutions (0.01 mM) of *n*-alkanethiols for at least 12 h. For AFM imaging, the sample surfaces were rinsed with fresh ethanol and placed into an AFM cell holder assembly. The sample surfaces were not exposed to air for more than a few minutes, to minimize surface oxidation. Two types of atomically flat gold substrates were used for experiments. Flame-annealed gold-coated mica substrates with 150 nm gold films were obtained from Agilent Technologies, Inc. (Chandler, AZ). However, Figures 3.4, 3.5, and 3.6M were produced using template-stripped gold films.[166, 167] The AFM tips for several experiments (Figures 3.4A, 3.4B, 3.4C, 3.6E, 3.6F) were coated with octadecyltrichlorosilane (OTS) purchased from Gelest, Inc, (Morrisville, PA).[160] A hydrophobic coating of OTS is often helpful for preventing contamination of the tip by removed matrix molecules. The tips were exposed for 45 min to UV light (254 nm) to remove impurities. The cantilevers were then immersed in a solution of OTS (1 mM) in a 7:3 mixture of hexadecane:chloroform for 1 h followed by chloroform rinsing. The tips were then dried in air and stored until needed.

3.2.2 Atomic Force Microscopy

Atomic force microscope (AFM) images were acquired using either a hybrid SPM system from RHK Technologies, Inc. (Troy, MI) with a PicoSPM scanner (XPMPro v.1.2.1.0) or with an Agilent 5500 AFM/SPM system with Picoscan v5.3.3 software. All of the images presented in this article were acquired using contact mode in ethanol solutions. Images were acquired with 256 lines/frame, with the exception of Figures 3.2A, 3.4, 3.6E and 3.6F which were acquired with 512 lines/frame. The scan rate for acquiring images ranged from 1.2 to 2.5 μm/s. Oxide-sharpened Si_3N_4 probes (MSCT-AUHW) from Veeco Probes (Santa Barbara, CA)

were used to pattern the alkanethiol monolayers on gold. The probes have V-shaped cantilevers and relatively low force constants (k_{avg} = 0.5 N/m), and the same probes were used for both fabrication and imaging procedures. The imaging and writing forces were calculated from corresponding force-distance curves using the manufacturer's reported values for the spring constant. The values include both the capillary/meniscus contribution and the force of cantilever bending. Images were processed using Gwyddion, which is available on the internet, free of charge (http://gwyddion.net).

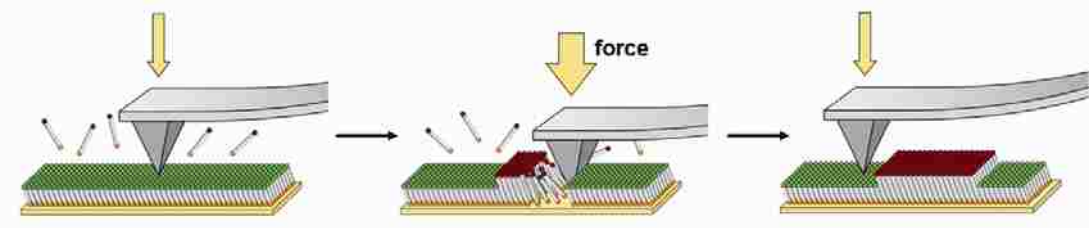

Figure 3.1 Steps for nanografting. [A] A flat area is selected by imaging under low force, the tip and surface are immersed in a solution of thiol (*ink*) molecules; [B] Nanopatterns are written by applying greater force; [C] The nanografted patterns can be characterized *in situ* by returning to a low force setpoint.

3.2.3 Nanografting

Nanografting with SAMs is achieved by applying mechanical force to an AFM tip while scanning (Figure 3.1). Writing is accomplished in dilute SAM solutions (0.003 – 0.01 mM) containing the selected *ink* molecule to be patterned by exerting a high local force on an AFM tip, pushing through the surface monolayer to contact the underlying gold surface. When the tip is rastered across the surface under high force, the molecules underneath the tip are shaved away and replaced by molecules from solution. When the matrix SAM molecules are removed, new thiol molecules from solution immediately adsorb onto the uncovered areas of the substrate to

produce designed nanopatterns, following the scanning track of the tip. The inscribed patterns can then be characterized *in situ* without exchanging tips by returning to low force (< 1 nN).

3.3 Results

3.3.1 Automated Writing via Nanografting

Controllers for AFM can be programmed for automated nanografting, to rapidly and consistently generate desired surface arrangements of SAM nanopatterns.[74] Commercial instruments typically provide software with capabilities to control the length, direction, speed, bias pulse duration, residence time and the applied force of the scanning motion of the SPM tip, analogous to a pen-plotter. Example arrays of square nanopatterns written by nanografting are presented in Figure 3.2. The topographs display 1.4×1.4 μm^2 and 1×1 μm^2 views of nanopattern arrays in Figures 3.2A and 3.2D, respectively.

By changing the length of the alkane chains of the ink molecules, the height of the nanopatterns can be tailored to be shorter (Figure 3.2A) or taller (Figure 3.2D) than the surrounding areas of the matrix SAM. The patterns of 11-mercaptoundecanol (11-MUD) are 0.5 ± 0.3 nm shorter than the surrounding octadecanethiol (ODT) matrix (Figure 3.2B), in agreement with the theoretically predicted differences in monolayer thickness as depicted in the model (Figure 3.2C). The height of the terrace steps of the underlying gold substrate are clearly visible in the AFM images, and furnish an internal reference for height calibration. The holes and valleys between terrace domains are common defects of naturally formed gold surfaces. There are three patches of matrix areas which exhibit a brighter contrast at the center and bottom right of the image in Figure 3.2A. The bright bands were introduced artificially by the image processing algorithm for slope subtraction.

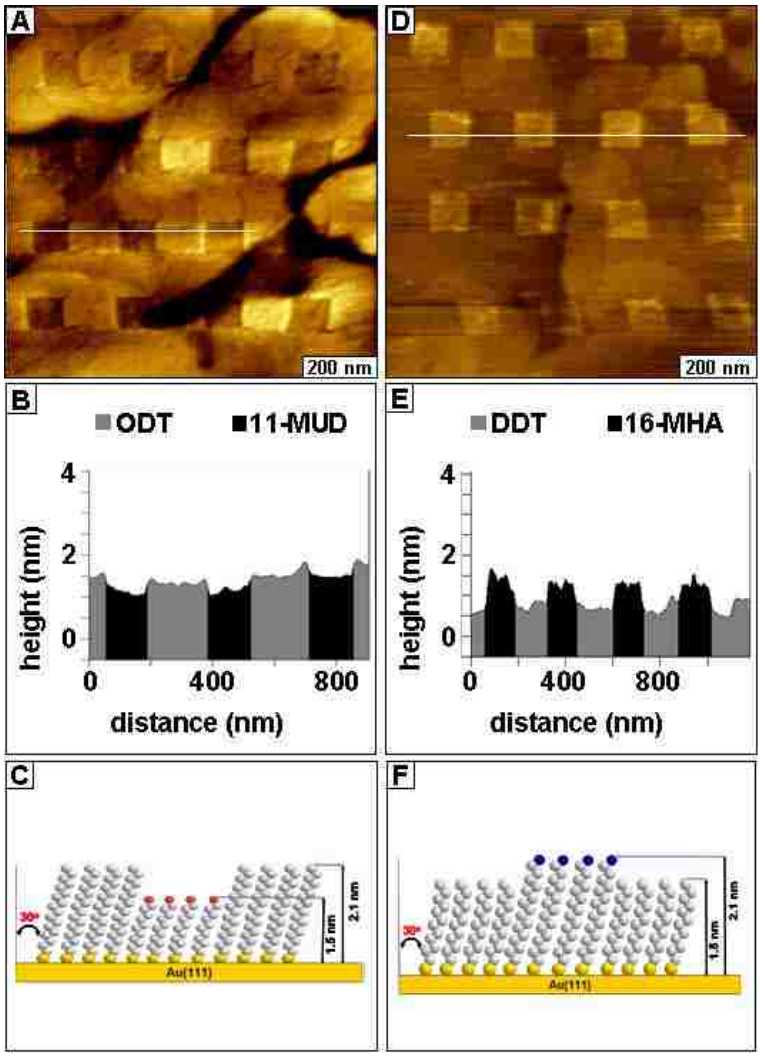

Figure 3.2 Example arrays of nanografted patterns that are either shorter or taller than the matrix SAM. [A] AFM topograph of 150 nm square patterns; [B] Cursor profile for the line across three squares in **A**; [C] Structural model for nanografted patterns. [D] Array of 100 nm square patterns; [E] Cursor profile for the white line in **D**; [F] Model of molecular heights.

The 150 nm square patterns are spaced at 200 nm intervals horizontally and 200 nm pitch vertically between rows. Note that the color of the nanografted squares is homogeneous, which is evidence that the ODT matrix layer has been entirely replaced by the shorter ink molecules of 11-MUD. Each square was written using a simple raster pattern, with a single

sweep over the surface from bottom to top at 5 nN of applied force. Writing the 16 patterns of the entire array was completed within 10 min.

An example array of nanopatterns with a positive height with respect to the matrix is presented in Figure 3.2D, for a 1×1 μm^2 view. Each square measures 100 ± 5 nm and patterns are spaced at 100 ± 5 nm pitch in the horizontal direction and 200 ± 5 nm distance in the vertical direction between rows. The array of square nanopatterns was written using an applied force of 6 nN. A similar writing strategy (a single raster scan from bottom to top) was applied to produce the positive-height array, requiring 25 seconds to write each pattern. The patterned molecules of 16-mercaptohexadecanoic acid (16-MHA) are 0.4 ± 0.2 nm taller than the dodecanethiol (DDT) matrix SAM (Figures 3.2E and 3.2F). The shapes of the nanopatterns are square and regular, as evident in the representative cursor profile across one row of patterns.

Even smaller nanopatterns of filled circles (diameter 45 ± 5 nm) of 11-mercapto-undecanoic acid (11-MUA) were inscribed within a matrix monolayer of ODT (Figure 3.3). The patterns are spaced at 30 ± 5 nm horizontally and vertically. The AFM topography and frictional force images (350×350 nm^2) reveal differences in height and surface chemistry for the 4×4 array of patterns, sited on a fairly flat terrace area. Six concentric circular step edges are visible at the right and bottom edges of the topograph (Figure 3.3A). Etch pits and the fine details of the lacey contours of the step edges can be resolved, disclosing typical landmarks of a natural SAM surface on Au(111). The height difference between the matrix and patterns measures 0.7 ± 0.3 nm as indicated in the representative line profile across the third row of patterns (Figure 3.3C). The expected difference in thickness between ODT and 11-MUA is 0.7 nm. A few bright spots are visible on the surface of half of the nanopatterns in the topography image. The heights of the spots are identical to the thickness of the surrounding matrix and are

likely attributable to incomplete removal of the matrix SAM within the nanopatterns. The frictional force image also discloses tiny dark or bright spots within the otherwise bright contrast of the circular nanopatterns, suggesting that the surface chemistry of the patterned areas is not completely homogeneous. An outline of the path of the AFM tip is shown in Figure 3.3D, with the position of the pickup and landing point of the writing area at the right of each pattern. A corresponding small protrusion at the edges of the patterns that were written is also evident in the topography and friction images (Figures 3.3A-3.3B). The writing path was outlined manually by directing the motion of an optical mouse to generate a computer drawing.

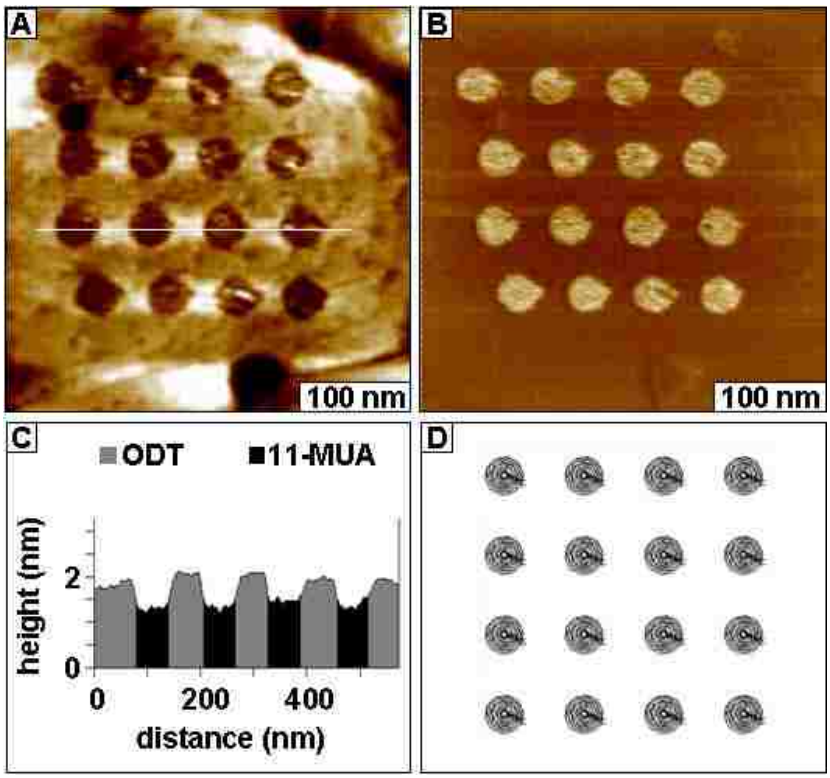

Figure 3.3. Nanografted array of filled circle patterns. [A] Topography image of 16 filled circle patterns; [B] corresponding friction image; [C] cursor profile along the third row of patterns; [D] graphic design for writing the array.

Once a single pattern was traced, the same outline was copied and pasted fifteen times within the 2-D grid of a computer drawing board. (PicoLith beta version 0.4.5, Agilent

Technologies, Inc.) Such a method of filling the pattern by drawing circles using hand was not 100 % effective for removing all of the matrix molecules within the pattern during nanografting.

3.3.2 Line Resolution of Nanografting

To investigate the resolution of nanografting line patterns, an array of nine Mickey mouse patterns was produced (Figure 3.4). The design enables multiple measurements of the linewidths of nanografted rings for evaluating the resolution of writing, as well as for assessing the capabilities for reproducibly inscribing adjacent rings in close proximity. A SAM of dodecanethiol formed on template-stripped gold was used as the matrix monolayer (*paper*) and the patterns were written with hexanethiol (*ink*). The topograph (1.5×1.5 μm^2) exhibits fairly large flat terraces, ranging from 200-700 nm in lateral dimensions (Figure 3.4A). Natural landmarks of SAMs/Au(111) such as etch pits are clearly visible within the *in situ* topograph, verifying that a sharp AFM tip persists after writing the patterns using 4.8 nN applied force. The circles range from 40 to 210 nm in diameter, and are spaced 220 ± 5 nm horizontally and 200 ± 5 nm vertically. A zoom-in view of the center pattern is presented in Figure 3.4B and the corresponding frictional force image is shown in Figure 3.4C.

The matrix and patterns are terminated with methyl groups, so the friction image displays only a small difference in contrast due to edge effects. The depth of the line patterns measures 0.7 ± 0.2 nm (Figure 3.4D) in close agreement with the expected 0.6 nm height difference between dodecanethiol and hexanethiol SAMs. The AFM tip (*pen*) is not lifted from the surface when outlining the circles; instead the traces are connected together as mapped in Figure 3.4E. All nine patterns were written in less than 2 min. The "ears" of the mouse patterns were formed by writing four concentric circles in a bullseye target arrangement, with an interpattern spacing of 11 ± 2 nm.

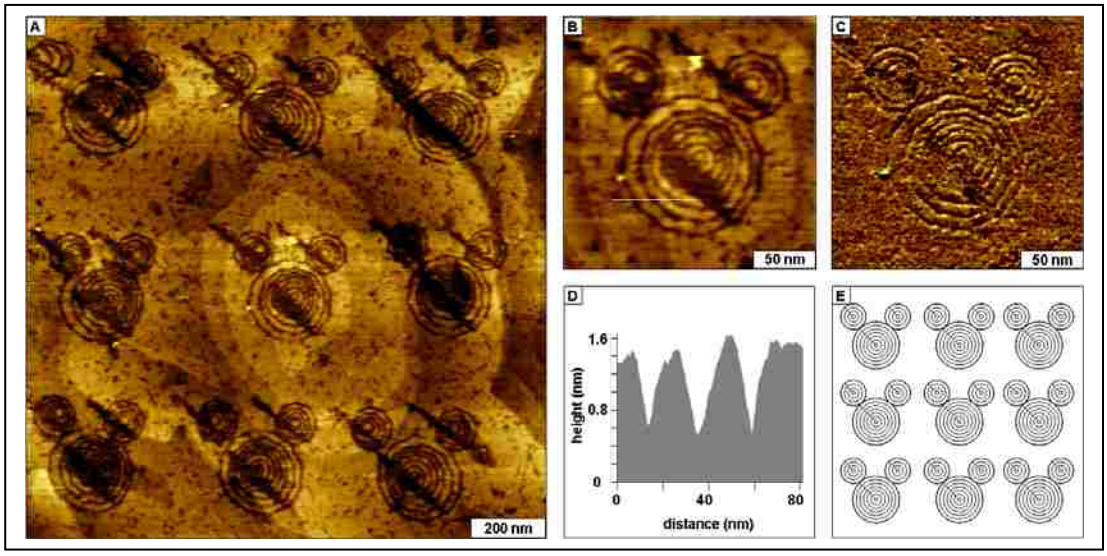

Figure 3.4 Mouse ear designs produced by nanografting. (A) AFM topograph of concentric rings written with hexanethiol ink within a dodecanethiol SAM; (B) Zoom-in view of a single set of patterns; (C) corresponding frictional image for **B**; (D) cursor plot for the line in **B**; (E) writing path of the designed nanopatterns.

The "face" of the pattern was produced by writing seven concentric circles at 12 ± 2 nm intervals. The diameter of the smallest circle at the center of the designs measured 23 ± 2 nm. Each circle was outlined twice by the AFM tip to produce a linewidth of 8 ±1 nm.

Nanografted letter patterns written with a positive height with respect to the matrix were generated in Figure 3.5. In this example, the *ink* molecules were 16-MHA written within a dodecanethiol SAM with an applied force of 7 nN. The wide view topograph (Figure 3.5A) displays four writing areas within the 11×11 μm^2 frame. The underlying substrate (template-stripped gold) exhibits flat triangular facets, often viewed for Au(111) surfaces. Dark defect holes with a depth of ~ 1.4 nm are present, and contaminants are visible at the bottom left of the image. This example illustrates the practical aspects of nanografting, it is helpful to navigate around defect areas to locate atomically flat and defect-free areas for nanoscale writing. Although nanografted patterns can be successfully inscribed on rougher substrates, flat surfaces without defects provide improvement for the resolution of topographic images.

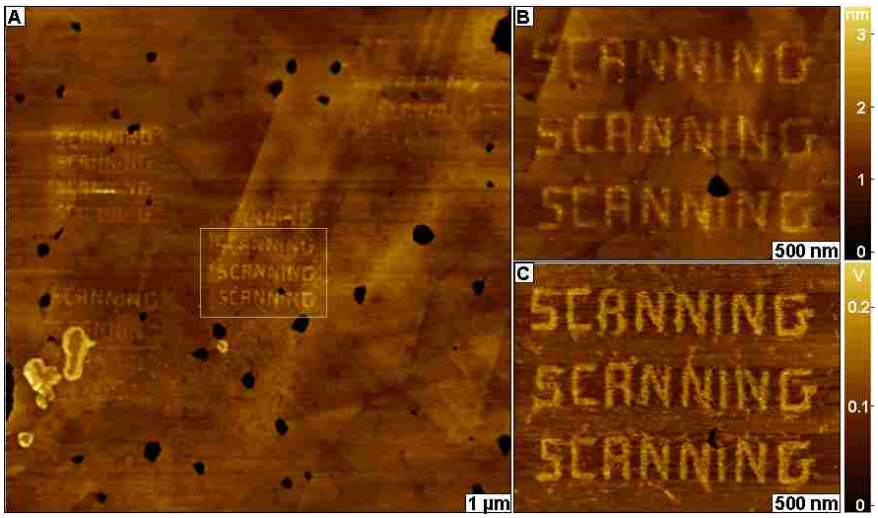

Figure 3.5 Nanoscale graffiti written by nanografting. [A] Topographic (11 × 11 μm^2) view of multiple written areas; [B] Zoom-in view of the central area; [C] corresponding frictional force image for **B**.

To resolve height differences of a few angstroms for nanografted patterns, it is helpful to have a narrower color scale for image contrast. Zooming in to view the central set of patterns, (Figures 3.5B and 3.5C) the writing fidelity and reproducibility achievable with nanografting is showcased in the 2.4 × 1.8 μm^2 view. The height of the patterns is 0.4 ± 0.1 nm, and each 100 nm letter is spaced at 50 nm intervals. The entire set of patterns was written within 3 min. Each letter was outlined three times by the AFM tip to produce a 50 nm linewidth. The friction image displays uniform contrast for the patterns, which is evidence that the matrix molecules were fully replaced by *ink* molecules.

3.3.3 Range of Pattern Geometries

A variety of geometries can be designed and written by nanografting, several examples are displayed in Figure 3.6. Cross-shaped patterns of 11-mercaptoundecanol (11-MUD) inscribed within a taller octadecanethiol SAM are presented in Figures 3.6A and 3.6B. Both the topography and frictional force image clearly reveal the location of the 300 nm crosses displayed with dark contrast in comparison to the surrounding matrix. The 11-MUD pattern is

0.4 ± 0.2 nm shallower than the matrix as measured with a representative cursor line across the top arm of the cross on the right (Figure 3.6C). The arms of the crosses measure 100 nm laterally, and were traced by a left-right raster pattern advancing 2 nm increments between linesweeps. The pattern for writing is traced in Figure 3.6D. The patterns were written in less than two min using a writing speed of 0.5 μm/s and an applied force of 5 nN.

Filled circles of hexanethiol were written within a dodecanethiol SAM (Figure 3.6E). The four patterns (130 nm diameter) are spaced 50 ± 5 nm apart vertically and horizontally, and are located on triangular shaped terraces of ultraflat Au(111). The AFM topograph reveals that the patterns are darker than the surrounding dodecanethiol SAM; the circles were filled by outlining six concentric rings. A zoom-in topographic view of the bottom left pattern (Figure 3.6F) reveals faint tracks of matrix which were not completely replaced. The cursor profile in Figure 3.6G shows a height of 0.3 ± 0.1 nm above the matrix, which is in agreement with the theoretical difference between hexanethiol and dodecanethiol (0.4 nm). The Picolith design for the patterns (Figure 3.6H) was executed twice to produce the four patterns, using an applied force of 4.8 nN and writing speed of 0.1 μm/s.

Ring patterns of 16-mercaptohexadecanoic acid (16-MHA) with successively decreasing sizes were nanografted (Figure 3.6I) within a dodecanethiol matrix SAM. The diameters of the rings within the three rows of patterns from left to right are 125 nm, 90 nm, 70 nm, and 50 nm with an approximate error term of ± 5 nm. The array was written in 75 seconds on a naturally formed gold film on mica, and despite the defects one can clearly distinguish the locations of the ring patterns in the both topography and frictional force (Figure 3.6J) images. The patterns are spaced at 80 nm intervals horizontally, and the vertical distance between rows ranges from 40 to 90 nm. The line width for the rings ranges from 20 to 30 nm. The brightest contrast in the

friction image represents carboxylate-terminated areas written with 16-MHA ink. The friction image also reveals small bright spots scattered throughout all areas of the sample. The tiny spots indicate the position of etch pits in the methyl-terminated SAM matrix. The etch pits are not observed in the topography image because of the color saturation, but were evident with zoom views of individual patterns (data not shown). The friction contrast of the etch pits is lighter than the nanopatterned areas, which is evidence that the spots are not caused by surface-solution exchange reactions.

When exchange occurs after extended immersion in the imaging media (> 4 h) the height changes from exchanged molecules will become clearly apparent in the topography images. The force applied to the AFM tip for writing was 4.2 nN, and each ring was outlined multiple times. The rings are 0.5 ± 0.1 nm taller than the matrix, as viewed with a representative cursor line profile in Figure 3.6K. This measurement matches the expected thickness difference between 16-MHA (1.9 nm) and dodecanethiol (1.5 nm). As the tip is placed on or lifted from the surface, the up/down movement of the AFM tip is often non-linear, and systematically produces a writing track at the edge of each pattern as observed for the nanografted rings. A sketch of the writing map is presented in Figure 3.6L, with arrows to pinpoint the start and stop positions at the right of each ring. Five rectangular patterns of 16-MHA were nanografted within a dodecanethiol SAM on template-stripped gold (Figure 3.6M). Fine details of the surface morphology are visible within the larger 2 × 2 μm^2 frame (acquired *in situ* in ethanol), because of the sharp color saturation obtained when using an ultraflat surface.

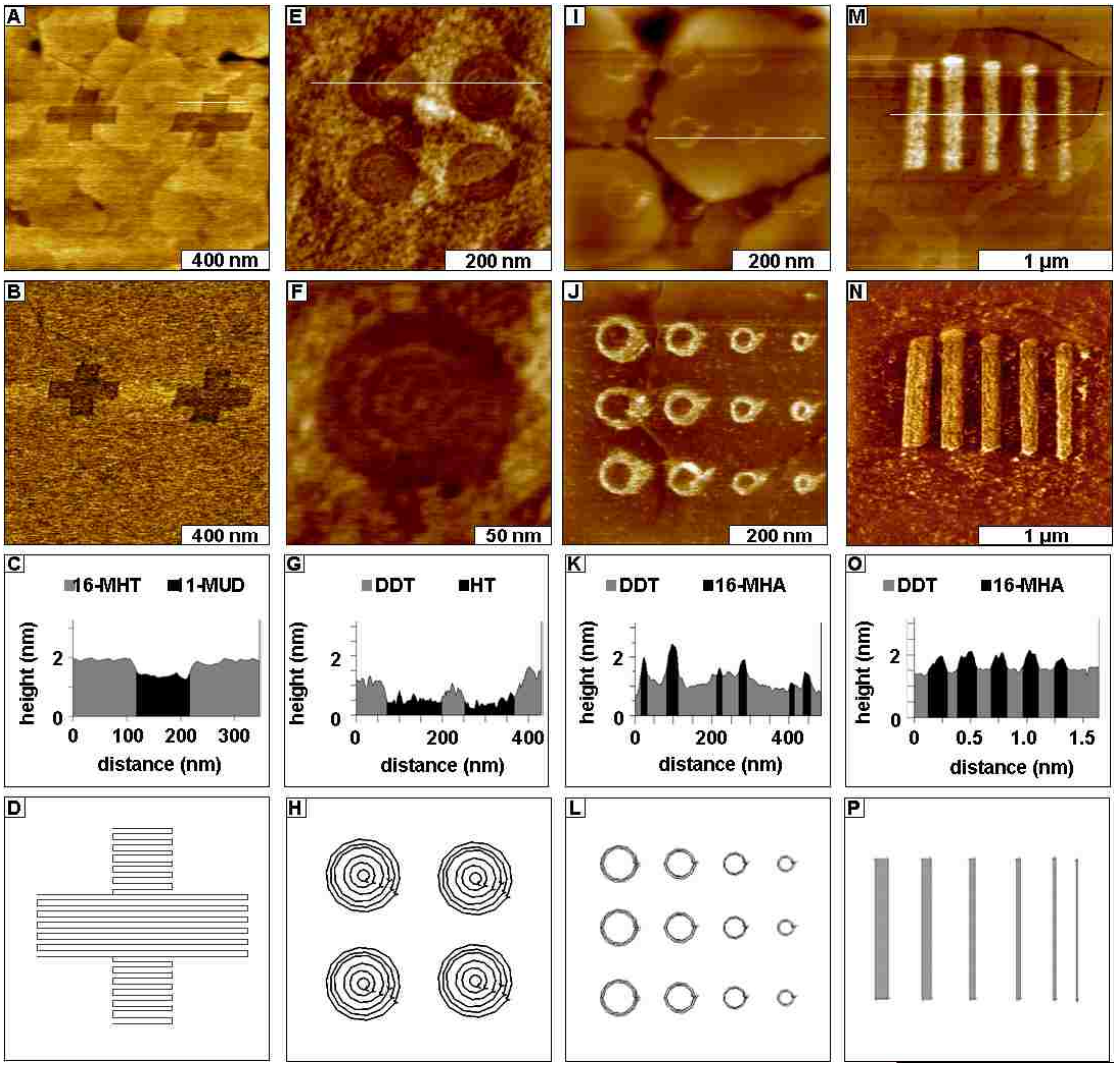

Figure 3.6 Patterns with varied geometries and molecular inks written by nanografting. [A] Cross patterns of 11-mercaptoundecanol nanografted within octadecanethiol; [B] corresponding frictional image; [C] cursor profile for **A**; [D] design for writing the cross patterns. [E] Filled circles of hexanethiol fabricated in dodecanethiol; [F] close-up view (topography) of a single pattern; [G] cursor profile for E; [H] PicoLith sketch for writing the circle patterns. [I] Array of ring patterns using 16-mercaptohexadecanoic acid as ink within a dodecanethiol SAM; [J] corresponding friction image; [K] height profile across three rings in I; [L] map of the tip trajectory for writing the rings. [M] Rectangular stripes of 16-mercaptohexadecanoic acid nanografted into a dodecanethiol SAM; [N] friction image for **M**; [O] line profile across the patterns in **M**; [P] Picolith outline for writing the patterns.

The vertical length of the rectangles measures 850 ± 40 nm; and the horizontal widths of each pattern from left to right are 170 ± 7 nm, 150 ± 4 nm, 125 ± 15 nm, 110 ± 15 nm, and 90 ±15 nm respectively. The lines were written by a single pass of the AFM tip using a horizontal raster pattern (150 linesweeps) from top to bottom with interpattern spacing (left to right) of 120 nm, 160 nm, 160 nm, and 150 nm. The probe was picked up and placed on the surface once for each rectangle, thus the AFM tip was not lifted during the writing process when inscribing the rectangular patterns. When acquiring the AFM topography image, a few linespikes were produced in the image where the tip intersects the top of the patterns. The linespikes are caused by stick-slip adhesion of the tip to the surface. The friction image (Figure 3.6N) provides a distinct view of the pattern geometries, the areas of bright contrast indicate the carboxylate-terminated regions of nanografted 16-MHA. Notice the bright spots throughout areas of the surrounding matrix monolayer, which identify the locations of etch pits for the dodecanethiol SAM. Linespikes are not detected in the simultaneously acquired frictional force image. The height of the 16-MHA patterns above the matrix measures 0.4 ± 0.2 nm (Figure 3.6O) which is in agreement with the expected theoretical height difference. The graphic design used to generate the set of patterns is shown in Figure 3.6P.

3.4 Discussion

Automated nanografting offers advantages for the speed and reproducibility of nanopatterning, and can produce sophisticated pattern arrangements and geometries. The precision and reproducibility of nanografting for the alignment, spacing and shapes of nanopatterns is superb, due to the exquisite control of small forces with piezoscanners. The geometry and fidelity for reproducibly writing patterns depends on the fabrication and

experimental parameters. To achieve high resolution at the nanoscale, the force, speed and the scan direction for writing need to be optimized for each experiment.

3.4.1 *In situ* Determination of the Threshold Force for Writing

Automated SPL rapidly achieves sophisticated pattern shapes, high precision and reproducibility for the alignment, spacing and geometry of nanopatterns. Instrument controllers for AFM can be interfaced with a programmable scanning module for automated lithography.[74] Commercially available soft Si_3N_4 cantilevers have mostly been applied for nanografting *n*-alkanethiol SAMs, with force constants ranging from 0.03 to 2.0 N/m. Although substantial improvements have been made in recent years for the manufacturing processes for AFM tips, the spring constants of individual AFM probes can vary widely for microfabricated levers.[168-170] The variations in tip geometry/sharpness as well as differences in surface adhesion for different monolayers makes it necessary to derive the optimized fabrication force for each experiment. A rapid and systematic approach for finding the threshold force is to write a number of small patterns with successively increasing applied force. The optimized force is chosen by imaging the patterns and selecting the minimum force which produces a distinct nanopattern. The chosen threshold force can then be used to write hundreds of nanopatterns during an experiment without evidence of tip damage. Certainly if too much force is applied for writing then the tip or substrate can be damaged. The fabrication forces used for nanografting typically are greater than 1 nN, dependent upon the system under investigation and the geometries and spring constants of the cantilevers. For the examples presented in Figures 3.2-3.6, the fabrication forces ranged from 2 to 10 nN. In contrast, for characterizing surfaces with nondestructive forces in liquid, the total force applied for imaging is typically less than 1 nN to prevent damage to the sample.

3.4.2 Optimization of the Writing Speed for Nanografting

Among the parameters for successful nanografting, the speed of tip translation does not strongly influence nanopattern quality when writing with *n*-alkanethiol inks.[69] Dense patterns can be nanografted over a relatively wide range of writing speeds. For the most part, slower tip movement has not produced observable changes for patterns of n-alkanethiol SAMs. A general rule of thumb is that whatever writing speeds are suitable for imaging (0.1-0.5 um/s) will also work well for nanografting.

3.4.3 Design Parameters for Tip Translation

Writing at the nanoscale with an AFM tip is analogous to digging a trench of molecules; the removed material can pile up on the sides of the nanopatterns. Therefore, when designing the parameters for tip translation a practical strategy is to translate the tip to push material to both sides of the pattern for clean removal of the matrix SAM. Depending on the solvent chosen for imaging, the shaved molecules eventually dissolve in the liquid imaging media after sweeping the surface a few times with the AFM tip at reduced force. The images presented in Figure 3.2-3.6 evidence clean removal of the matrix and replacement with ink molecules from solution. Nanografting is not the best approach for writing micron-sized patterns of SAMs, because for larger patterns the shaved molecules can persist and re-adsorb at the edges to form thick borders. (data not shown) However, nanografting is an excellent choice for writing SAM patterns that are smaller than one micron, as viewed in the examples. Dozens of small patterns can be rapidly inscribed with various shapes and arrangements.

Mechanical parameters to consider are the nonlinearity of piezoceramic scanners, hysteresis and electronic drift. When voltage is applied to a single segment of a piezotube scanner, the movement of the tip follows a linear trajectory. However, when voltages are

applied to two segments simultaneously the tip is often moved unpredictably to different positions, such as for triangulating vector movements. The problems in nanoscale translations result from mechanical imperfections in the manufactured sizes of scanner segments. If voltages are applied to the scanner simultaneously for the x and y directions, this will often produce distortions and misalignment of nanopatterns. Thus, to optimize pattern geometries and arrangements, it is a good strategy to program separate movements to define displacements in either the x or y direction individually. Another strategy to incorporate when defining the writing parameters is to program brief pauses after translating the tip between rows and columns of patterns. There are nanoscopic displacements of the cantilever as the piezoscanner is momentarily relaxed. The array in Figure 3.2D displays an example where the bottom row of nanopatterns is slightly out of alignment with the upper three rows. The rows of patterns were written from left to right, beginning with the bottom row and proceeding to the top. The registry of the bottom row is offset approximately 50 nm compared to the upper three rows of squares caused by relaxation of the lever position. The example in Figure 3.2A, on the other hand, is nearly perfectly aligned for all four rows and columns because the programmed parameters issued a brief pause (5 s) before beginning the writing operations.

Another imperfection introduced with nanografting is apparent when the tip is picked up or placed on the surface. In the process of writing stray lines may be produced at the corners of patterns, which are caused by the tilt of the cantilever under pressure. As the tip is picked up or placed on the sample there is often a nonvertical sliding motion produced as an artifact of open loop scanners. This becomes apparent by viewing the writing tracks at the locations where the tip was picked up or removed from the surface (Figure 3.6J). These artifacts can be prevented by changing the lithography parameters to use a slower speed for approaching or lifting the tip

from the surface, and by choosing a minimal threshold force for writing. When the force is optimized nearly perfect shapes can be nanografted, even when using an open-loop scanner for feedback control.

3.4.4 Nanografting Gradient Patterns

It was previously established that nanografted patterns of *n*-alkanethiols form dense close-packed structures with crystalline order.[138] Periodic lattices were revealed by zooming-in for molecular views of the surfaces of nanografted patterns. The AFM images revealed a two-dimensional periodic structure with a lattice constant of 0.5 nm, which is consistent with the well-known $(\sqrt{3}\times\sqrt{3})R30°$ structure of alkanethiol SAMs where hydrocarbon chains are close-packed and tilted ~27° with respect to the surface normal. Depending on the sharpness of the AFM probe, gradient patterns of a mixture of matrix and ink molecules can be nanografted by changing the spacing between linesweeps.[141] The array of nanopatterns in Figure 3.2D was written with successive changes in line spacing between rows. The distance between horizontal linesweeps was programmed to be different for each row, from top to bottom with 5, 3, 2 and 1 nm increments between linesweeps in the y direction. No differences in the heights of the patterns were observable from row to row, because there is sufficient writing density to produce dense patterns. However, when such patterns are further reacted with biomolecules or metals the nanoscale gradients become apparent by differences in adsorption.[141]

3.5 Advantages of the *In Situ* Approach of Nanografting

A significant advantage of using nanografting for AFM investigations is the ability to conduct experiments *in situ*, successively viewing changes for nanofabricated structures with high resolution in liquid media. Analogous to time-lapse photography, after writing nanopatterns further reactions can be conducted selectively on spatially defined regions of the

surface with nanoscale control of the reactivity of SAM headgroups. The surrounding areas of a matrix SAM can be chosen to provide non-reactive or insulating headgroups to spatially direct reactions to occur only for the nanografted areas.[140] Within the liquid cell, solutions can be introduced with fresh reagents and molecules for surface confined reactions. Sequential real-time AFM images display reaction steps at a molecular level, providing details of the adsorption and conformational changes that take place over time.[76] An important criteria for *in situ* investigations with AFM is to use highly dilute solutions for reactions. Since there is no need to generate milligram quantities of products on surfaces when studying nanoscale phenomena, the reactions for AFM experiments require picomolar to nanomolar concentration levels. As an example, for reactions with *n*-alkanethiol SAMs, introducing solutions at millimolar concentrations will potentially cause problems with surface exchange reactions, in which molecules from solution change place with matrix molecules to form a mixed monolayer on the surface. For nanoscale investigations the reagents need to be scaled to dilute regimes to provide optimized conditions to control surface reactions. Consequently, as a benefit, very small amounts of reagents are needed to conduct reactions in an AFM liquid cell.

3.6 Applications of Nanografting

Nanografting has mainly been applied for fundamental studies of surface chemistry, assembly mechanisms, kinetics and properties of thin films.[171] Nanografted patterns of SAMS can be applied as reference structures for measuring the dimensions of the tip apex *in situ*.[172] Also, SAM patterns produced by nanografting can serve as a molecular ruler for local measurements of the thickness of films.[173-175] The desorption and stability of nanografted patterns over time has been investigated for different spacer lengths of *n*-alkanethiol SAMs.[69] Bottom-up assembly has been accomplished to produce 3-D nanostructures by reactions with

octadecyltricholorosilane,[140] and electroless deposition of copper has been achieved selectively on SAM nanopatterns.[141] An emerging area of research is enabled for molecular-level investigations of biochemical reactions with nanografted protein structures, in which nanopatterns are monitored during *in situ* protocols in aqueous buffers. [76, 142, 143, 161-165, 176] Nanografted arrays offer potential as a convenient test platform to define the chemistry and placement of nanomaterials on surfaces. Designed 2-D arrays of patterns of SAMs with tunable dimensions can be applied with AFM measurements of surface properties such as friction and elasticity.[139] Well-defined nanostructures provide precise reproducible dimensions for multiple measurements, and enable tunable material compositions for studies of size-dependent properties.[174] Advancement of viable nanotechnologies will require a thorough understanding of properties at the molecular scale, and AFM-based lithographies such as nanografting furnish a practical toolkit for nanoscale research.

3.7 Future Prospectus

Methods of SPL are becoming indispensable for fundamental investigations of the interrelations between chemical structure and properties of thin film materials. Nanografted patterns of SAMs provide 2-D planar test platforms for studies of size-dependent physical properties. In nanometer-scale structures, size effects give rise to novel electronic, magnetic, and optical properties which occur at length scales between 1 and 150 nm. When nanografting *n*-alkanethiol SAMs, surfaces can be designed to anchor materials such as DNA, proteins, polymers, metals, organic molecules and polymers for the bottom-up assembly of nanomaterials. Writing individual patterns may not be a practical strategy for manufacturing devices, in which millions of structures may be needed for a single memory chip or circuit design. The serial nature of SPL is problematic for future applications, which will require high

throughput and speed. This problem has been addressed by the on-going development of arrays of multiple probes for parallel writing, as well as by increasing the speed of writing processes. Prototype arrays of 1024[177] and 55,000[178] AFM probes have been developed for high throughput nanopatterning. Scanning probe lithography approaches such as nanografting with self-assembled monolayers extends beyond simple fabrication of nanostructures to enable control of the surface composition and reactivity at the nanoscale.

CHAPTER 4. SELF-ASSEMBLY OF α,ω-ALKANEDITHIOLS ON Au(111)

4.1 Self-Assembly of *n*-alkanethiols Versus α,ω-alkanedithiols on Au(111)

Methyl-terminated *n*-alkanethiols have been widely studied and are known to form ordered commensurate monolayers for a range of experimental conditions (e.g. concentration, immersion intervals). Self-assembled monolayers (SAMs) with sulfur headgroups have not been as extensively characterized. Monolayers of *n*-alkanethiols on coinage metal surfaces such as gold have promising applications as lithographic resists,[179-183] and chemical/biological sensors.[184-190] Dithiol SAMs are promising materials for wires in molecular electronic devices[191-194] or can provide linker groups for attaching nanoparticles to surfaces.[195-202] Upon immersion of a gold substrate into a thiol solution, the -SH endgroups of *n*-alkanethiol molecules bind spontaneously to metal surfaces by chemisorption to form densely-packed monolayers.[203-205] Molecules within *n*-alkanethiol SAMs typically adopt a standing-up configuration to form a close-packed monolayer, presenting various headgroups at the surface. The basic structure of an *n*-alkanethiol SAM consists of three parts: the sulfur endgroup, the carbon backbone, and the headgroup. The endgroup is composed of thiol molecules for chemisorptive attachment to metal surfaces.[206] A thiol group is located at the terminus of an alkane chain (backbone) of the molecules. The carbon chain is capped with a headgroup (esters, alkyls, hydroxyls, carboxylates, amides, etc.). The length of the alkane chain and the nature of the SAM headgroup largely determines surface properties such as wettability.[207-209] Readers are directed to previous reports for details regarding synthesis, preparation, and characterization of *n*-alkanethiol SAMs.[210]

From the perspective of the molecular formula, α,ω-alkanedithiol molecules should form SAMs presenting a free SH group at the surface. However, this assumes that the

molecules attach to gold through only one sulfur in an upright configuration. Ultrahigh vacuum scanning tunneling microscopy (UHV-STM) studies[211-213] reveal that *n*-alkanedithiol SAMs prepared either from a vapor phase deposition or from immersion in ethanolic solutions predominantly assemble with a lying-down configuration on gold. Because of the affinity for chemisorption to gold, most α,ω-alkanedithiol molecules assemble with a side-on orientation without free thiol groups presented at the surface. Monolayers of α,ω-alkanedithiols are not densely-packed and are less ordered than methyl-terminated *n*-alkanethiol SAMs, because the molecules bind to the surface through both endgroups in a lying-down orientation. Interactions between the thiol groups and gold have an important role in the self-assembly of α,ω-alkanedithiol molecules. In contrast, methyl-terminated *n*-alkanethiols form SAMs with the single thiol endgroup chemisorbed to Au(111) with the carbon chains oriented in an upright configuration. According to previous studies, the alkyl chains of *n*-alkanethiol SAMs tilt approximately 30° with respect to the surface normal.[214-220] Thiol endgroups of SAMs are thought to bind to the triple hollow sites of Au(111) lattice by chemisorption.[203, 221, 222] The self-assembly of *n*-alkanethiol SAMs on bare gold is reported to occur in two phases. A mobile physisorbed phase forms when thiol molecules initially make contact with the surface, in which the backbone of the molecules are oriented parallel to the plane of the substrate in a lying-down configuration. However, over time *n*-alkanethiol molecules rearrange into a standing upright orientation with the molecular backbone tilted 30^{o} from surface normal. The mature crystalline phase forms an enthalpy favorable, close-packed commensurate $(\sqrt{3} \times \sqrt{3})R30^{o}$ configuration with respect to the Au(111) lattice.

For certain applications of α,ω-alkanedithiols, a standing-up configuration of the molecules within the SAMs to present a thiol headgroup at the surface is compulsory. In an

upright orientation, the free thiol is available for further chemical reactions. For example, catalysis or oxidation reactions with the thiol group will produce a sulfonate-terminated surface that can react to form hybrid multilayer assemblies.[173, 223, 224] The upright orientation offers a route to form stable multilayer structures with S-S bonds for interlayer covalent linkages. Considerable research effort has been invested to gain better control for constructing thiol-terminated surfaces with the favored standing-up conformation. One reported approach used alkanedithiols with a rigid molecular backbone containing either aromatic rings or double/triple bonds in the molecular linker.[225-227] The inflexible nature of conjugated structures prohibits the twisting of the backbone and thus makes it difficult for both ends of dithiol molecules to have good contact or to simultaneously interact with the gold surface.

A second approach for preparing thiol-terminated surfaces was to induce exchange reactions by soaking a previously formed SAM into an alkanedithiol solution. In this method, a standing-up configuration for α,ω-alkanedithiols is obtained through a replacement reaction that occurs with a previously formed *n*-alkanethiol SAM after immersion in a dithiol solution.[228, 229] Exchange reactions can produce domains of upright dithiols on gold because the matrix *n*-alkanethiol SAMs can sterically prevent the incoming dithiol molecules from lying-down to form a side-on configuration. Exchange reactions prefer to initiate at surface defects sites, such as step edges and domain boundaries. Therefore, the "exchange" approach does not provide precise control of the location and geometry of dithiols in the resulting dithiol SAM.

A third approach follows a stepwise protection/deprotection strategy to prepare SAMs presenting thiols at the interface.[230-233] One of the thiol groups is first protected by thioacetyl or thioester groups. After the organothiolate adlayer is formed, the protected thiolate group can be restored to –SH under controlled conditions, such as by immersion in a sodium hydroxide

solution. This strategy involves extra steps for sample preparation and requires delicate control of acid/base deprotection chemistry.

Writing nanopatterns of dithiol SAMs via nanografting provides an approach for presenting free thiols at surfaces, since thiol adsorption on gold during nanografting follows a different reaction pathway due to the effects of spatial confinement.[171] For self-assembly during nanografting, very small areas of freshly exposed gold are produced by scanning with a high force applied to the AFM tip. The transient reaction environment is sufficiently small to prevent the molecules from assembling in a lying-down position. The surrounding matrix areas are surrounded and spatially confined by thiol SAMs. The confined area uncovered by the AFM tip has dimensions less than the molecular length of the thiols, therefore the ink molecules in solution do not have sufficient room to assemble in a lying-down configuration. Thus, the initial physisorbed phase is bypassed and molecules assemble directly onto gold with the favored standing-up configuration during nanografting.

4.2 Results and Discussion

Approaches which are most commonly applied to prepare α,ω-alkanedithiol SAMs are vapor phase deposition[211] and solution immersion,[230] which produce films with the molecular backbone oriented parallel to the substrate. Nanografting is a new strategy for surface self-assembly which bypasses the formation of an intermediate (lying-down) phase to directly produce an upright molecular configuration.[171] In these investigations, nanografting is applied as a means to produce densely-packed, well-ordered layers with a single thiol endgroup attached to the surface. Due to a different assembly mechanism, nanografting generates patterns of α,ω-alkanedithiols presenting free –SH groups at the interface. In addition, nanografted patterns can be used to determine the orientation of naturally-formed SAMs of 1,8-octanedithiol and 1,9-nonanedithiol. Local AFM views of nanografted patterns enable a side-by-side comparison of

the morphology of different SAM headgroups, and provide an internal height reference for measuring differences in molecular thickness.

4.2.1 Naturally Grown 1,8-octanedithiol SAMs Characterized by AFM.

The surface of a naturally grown dithiol SAM after one week of immersion in 1,8-octanedithiol (0.02 M) is viewed in Figure 4.1. The AFM topograph (Figure 4.1A) reveals predominantly flat matrix areas interspersed with nanoscopic protruding islands, and the underlying triangular shapes of terraces of Au(111) are apparent. The bright spots exhibit relatively uniform sizes, suggesting regular vertical and lateral dimensions for the protrusions. A cursor profile (Figure 4.1B) corresponding to the line drawn across two of the small islands indicates that the protrusions are about 0.8 nm taller than the surrounding matrix areas. The height for the islands corresponds closely to the expected theoretical difference in thickness between a standing-up (1.3 nm) versus a lying-down (0.4 nm) orientation for 1,8-octanedithiol. The protrusions cover approximately 7 % of the surface of Figure 4.1A. The theoretical dimensions for the molecular diameter assumes an all-trans alkyl chain (0.4 nm) and the thickness of an upright 1,8-octanedithiol layer (1.3 nm) relies on the assumption that molecules have the same orientation as 1-octanethiol in which the hydrocarbon backbone tilts ~30° from the surface normal. The dimensions are calculated by considering that 1,8-octanedithiol has an all-trans configuration for the alkyl chain and that the terminal thiol group of dithiol molecules is not bulkier than methyl functionalities as for *n*-alkanethiols.

Nanografting was accomplished *in situ* to measure the thickness of the naturally formed 1,8-octanedithiol SAM. The surface of the 1,8-octanedithiol SAM was immersed in a dilute decanethiol solution (ink molecules for writing) within the AFM liquid cell assembly. A

rectangular pattern (200 × 300 nm^2) of decanethiol was nanografted within the 1,8-octanedithiol SAM for a one week sample (Figure 4.1C).

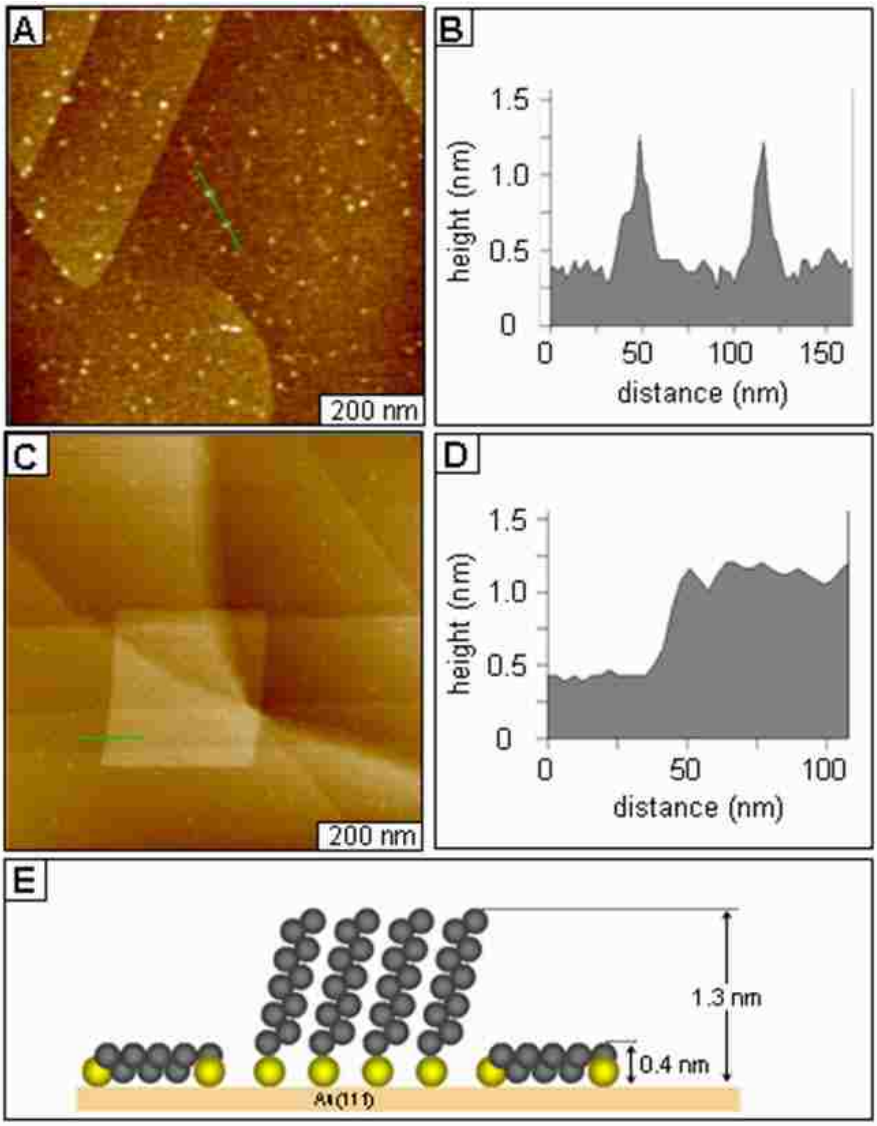

Figure 4.1 Surface morphology of naturally formed 1,8-octanedithiol. [A] Topograph; [B] Cursor profile for the line in A; [C] Square pattern (200 x 300 nm^2) of decanethiol nanografted within a SAM of 1,8-octanedithiol; [D] Corresponding cursor profile; [E] Proposed model for the SAM thickness.

The surface of the pattern exhibits a smooth morphology typical of *n*-alkanethiol SAMs. The established dimensions of decanethiol provide a height reference or *molecular ruler* for nanoscale measurements. The height of the decanethiol nanopattern is 0.9 ± 0.2 nm taller than

the surrounding areas of 1,8-octanedithiol as shown by the representative cursor line profile in Figure 4.1D.

The thickness typical of a decanethiol SAM is 1.3 nm and the expected height for a lying-down orientation of 1,8-octanedithiol is 0.4 nm. The difference measured by nanografting decanethiol as a reference height matches well with the expected thickness for a side-on orientation of the 1,8-octanedithiol molecule for the matrix areas, as represented in the molecular model of Figure 4.1E. The nanografting measurements confirm that most of the areas of the naturally grown 1,8-octanedithiol SAM are composed of lying-down molecules, with the protrusions corresponding to isolated areas of standing molecules. Two distinct conformations are visible in Figure 4.1A, a lying-down orientation in which both sulfur atoms attach through chemisorption onto Au(111), interspersed with islands of upright molecules that attached through a single sulfur endgroup.

Combining the results from AFM using both high-resolution imaging and nanolithography establishes that 1,8-octanedithiol molecules assemble predominantly with a lying-down orientation for a naturally grown SAM. Images acquired for a sample prepared with 12 h immersion in 1,8-octanedithiol exhibited a similar morphology of mixed phases (data not shown). The results are in good agreement with previous studies of the same system with other techniques.[234] For example, structures of a 1,8-octanedithiol SAM prepared from one-day immersion in a 1 mM ethanolic solution were investigated using an ultrahigh vacuum scanning tunneling microscope (UHV-STM). It was observed that dithiol molecules within the 1,8-octanedithiol SAM were arranged with the molecular axis parallel to the gold surface. However, in our investigations, both lying-down and standing-up orientations of 1,8-octanedithiol molecules in the monolayer are clearly revealed in high-resolution AFM images of

Figure 4.1. The coexistence of the lying-down orientation with the nearly upright conformation is evident after intervals of either 12 h or extended immersion (7 days) and the surface morphology was not observed to rearrange into a densely-packed layer over time.

4.2.2 Nanografting of 1,8-octanedithiol.

A square nanopattern of 1,8-octanedithiol was written within a matrix of hexanethiol (Figure 4.2). A flat terrace area of the hexanethiol SAM is displayed in the topography images before (Figure 4.2A) and after (Figure 4.2B) nanografting a pattern of 1,8-octanedithiol. The characteristics typical of the surface of an *n*-alkanethiol SAM such as etch pits are observed throughout areas of the surface for Figure 4.2A, where relatively broad flat terrace domains were chosen for writing. As an internal reference for z calibration, the heights at the edge of the Au(111) steps measure 0.23 nm, also the distinct outline of the square-shaped terraces provide landmarks for *in situ* imaging. The surrounding areas of the hexanethiol SAM exhibit a smooth surface and thus the features of the underlying substrate such as the Au(111) steps are clearly visible.

The same area is shown in Figure 4.2B after a square pattern was nanografted. The topography of the patterned area has a rougher morphology, and there are several bright spots of adsorbate molecules attached to the nanopattern. The brighter contrast of the square indicates that the pattern is taller than the hexanethiol monolayer. The trace and retrace friction images acquired simultaneously with the topographic image of Figure 4.2B are presented in Figures 4.2C and 4.2D, respectively. The friction images furnish evidence that the functionality exposed on the surface of the pattern is different than the surrounding SAM. In comparison to the surrounding methyl-terminated matrix, the patterned area of dithiol SAM exhibits a difference in contrast for the two images, indicating greater frictional force between the

headgroups of the dithiols and the AFM tip while the tip is scanning in contact mode. Compared to the methyl headgroup of a hexanethiol SAM, the -SH group is more hydrophilic due to higher polarity. The silicon nitride AFM tip is also relatively hydrophilic, therefore a higher frictional force between the -SH head group of dithiols and the AFM tip results from the stronger hydrophilic-hydrophilic adhesive interactions.

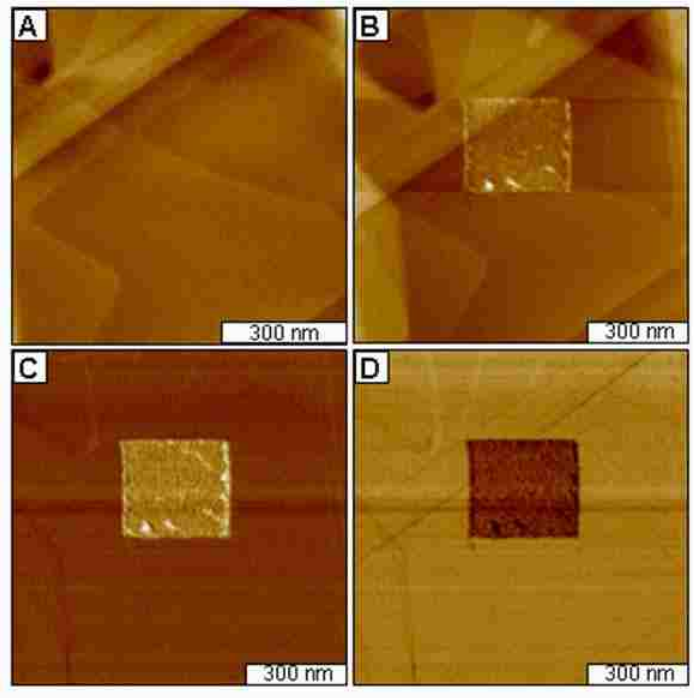

Figure 4.2 Selected area of a SAM of hexanethiol before and after nanografting. [A] AFM topograph of hexanethiol/Au(111); [B] Same area after writing a square pattern of 1,8-octanedithiol by nanografting; [C] Corresponding frictional force trace and [D] Retrace images.

Patterns written by nanografting provide a molecular ruler for locally comparing the thickness differences of SAMs. A close-up view (500 × 500 nm^2) of the same square pattern of Figure 4.2 is displayed in Figure 4.3. The fine details of the edges of the square pattern are visible for the zoom-in image.

The clustered morphology of the surface of the thiol-terminated pattern is visible and distinctive differences are revealed when compared side-by-side with the surrounding methyl-

terminated areas of hexanethiol matrix (Figure 4.3A). A representative cursor line was drawn at a flat edge of the square pattern to measure the height difference between the nanografted 1,8-octanedithiol pattern and hexanethiol SAM (Figure 4.3B). The pattern measures 0.4 ± 0.2 nm taller than the hexanethiol monolayer, which matches a standing orientation for 1,8-octanedithiol. The theoretical height difference between hexanethiol and 1,8-octanedithiol is 0.3 nm, assuming an orientation with an all-trans alkyl chain tilted ~30 degrees from surface normal (Figure 4.3C).

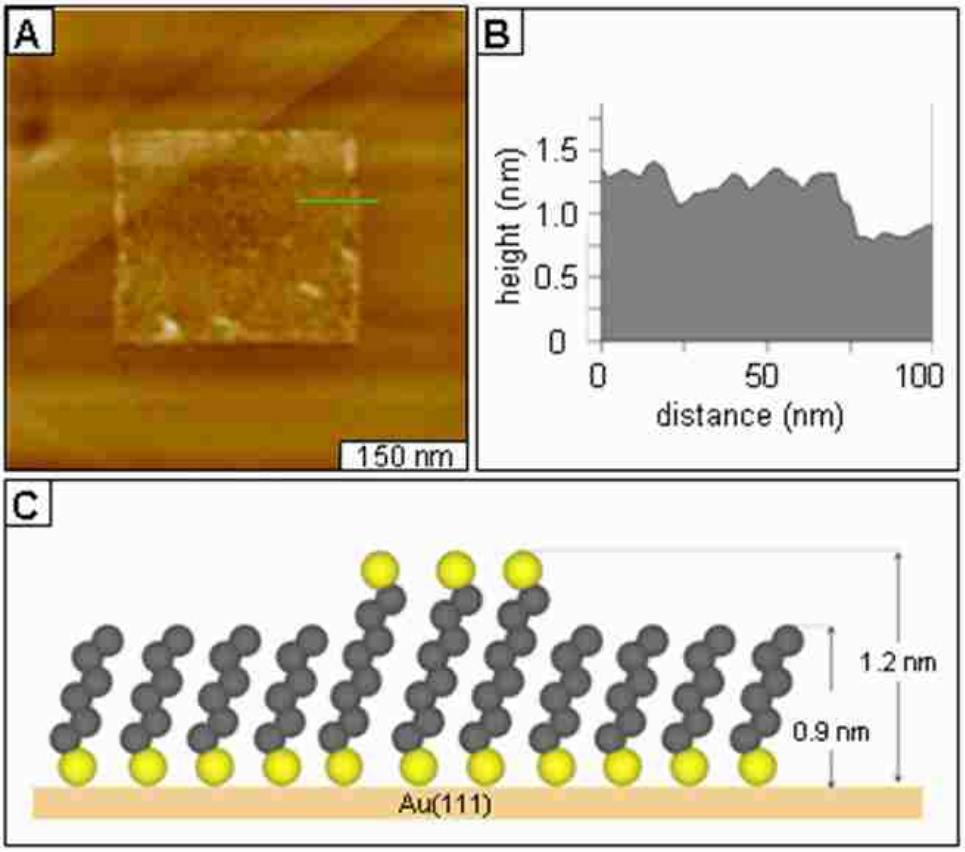

Figure 4.3 Close-up view of the 1,8-octanedithiol pattern. [A] Zoom-in view of the pattern surface; [B] Selected cursor for the line in **A**; [C] proposed model.

These results demonstrate that with nanografting, dithiol molecules are directed to assume an upright configuration. Due to an effect of spatial confinement, when nanografting the molecules adsorb to the surface immediately following the track of the AFM tip in a standing orientation.[171] During writing, there is not sufficient substrate area exposed for dithiol molecules to assemble in a lying-down orientation, therefore the assembly mechanism when nanografting occurs in a single step. Without a lying-down step during molecular assembly, there is no opportunity for both sulfur groups to bind to gold. If the 1,8-octanedithiol molecules had assembled in a lying-down orientation, the nanopattern would be shorter than the hexanethiol matrix with a depth of 0.5 nm. Thus the spatial confinement effect of nanografting can be used to engineer an upright orientation of 1,8-octanedithiol molecules.

4.2.3 Nanoshaving of 1,9-nonanedithiol.

To corroborate the observations for 1,8-octanedithiol SAMs, AFM characterizations were accomplished for a naturally-formed monolayer of 1,9-nonanedithiol prepared by 3 days of immersion in a 0.02 mM ethanol solution (Figure 4.4). A surface composed of mixed phases is viewed in the AFM topographs of Figures 4.4A and 4.4B, with random bright islands scattered throughout the surface. The height of the protrusions measures 0.9 ± 0.1 nm above the matrix areas of the SAM, and the taller features cover approximately 6 % of the surface (Figure 4.4B). Nanoshaving was used to measure the thickness of the 1,9-nonanedithiol SAM.[156] A selected area of the SAM can be shaved away by applying a higher force (0.5 nN) and sweeping the tip across the region several times. A rectangular area of the substrate (300 x 340 nm^2) is exposed in Figure 4.4C which is easily distinguished from the surrounding areas of 1,9-nonanedithiol. The clean removal of 1,9-nonanedithiol adsorbates from the nanoshaved area is confirmed in the corresponding frictional force image (Figure 4.4D) which evidences a brighter contrast for the

nanoshaven pattern. The thickness of the SAM can be measured directly by acquiring a cursor profile across the edges of the nanoshaved region, referencing the uncovered area of the substrate as a baseline.

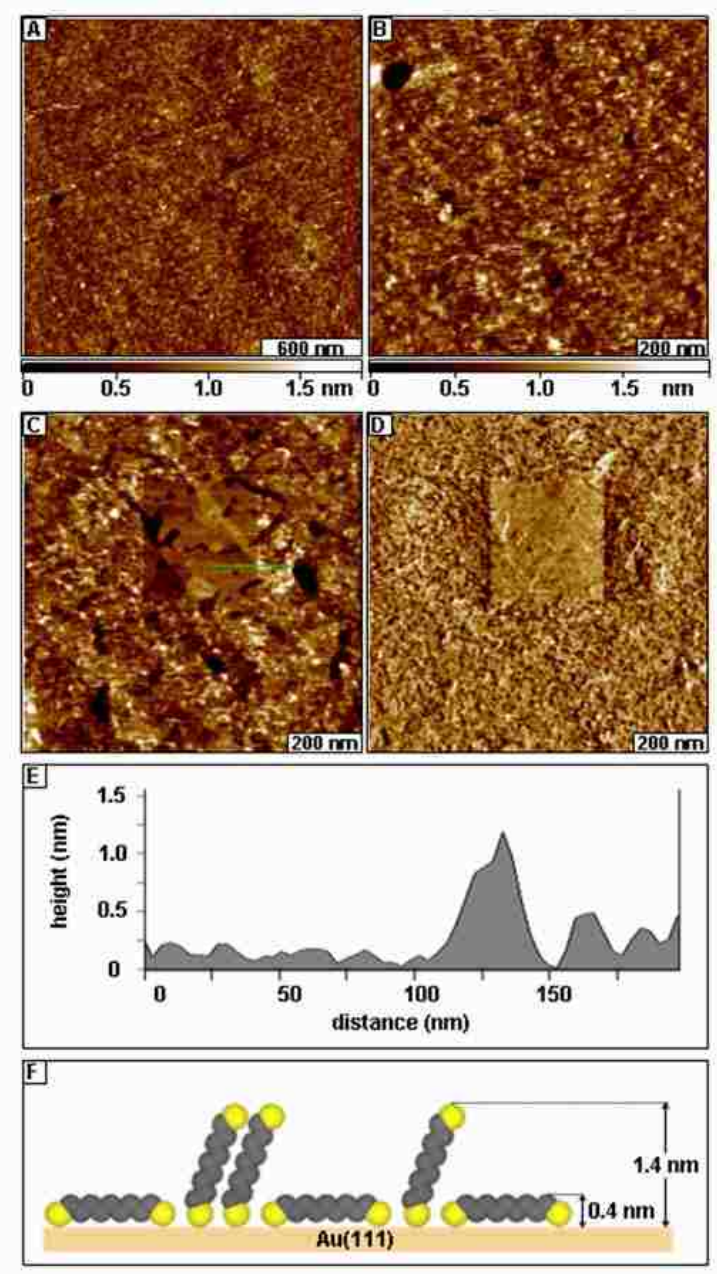

Figure 4.4 Nanoshaving of 1,9-nonanedithiol. [A] Topographic view before fabrication (2 x 2 μm^2); [B] Zoom in view of **A** (0.9 x 0.9 μm^2); [C] After shaving a 300 x 340 nm^2 pattern; [D] Friction image for **B**; [E] Corresponding profile for the line in **B**; [F] Proposed model for mixture of surface orientations of 1,9-nonanedithiol.

The morphology of the underlying template-stripped gold surface has small irregular terraces, therefore the placement of the representative cursor line was chosen to provide a relatively even background. Two different heights are displayed in the corresponding cursor plot (Figure 4.4E) measuring 1.3 ± 0.1 nm and 0.4 ± 0.1 nm, which correspond well with the predicted dimensions for upright and lying-down orientations of 1,9-nonanedithiol, respectively.

As with the previous example of 1,8-octanedithiol SAM formed spontaneously by natural self-assembly, SAMs of 1,9-nonanedithiol adopt both lying-down and standing-up orientations on gold, with a predominance of lying-down molecules. Thus, as for 1,8-octanedithiol SAMs, for naturally-formed SAMs of 1,9-nonanedithiol, both of the thiol endgroups chemisorb to the surface and lock the molecules in a side-on orientation. A model is proposed showing the dimensions and different orientations (Figure 4.4F) observed for 1,9-nonanedithiol molecules. The height of the protrusions measures 1.0 ± 0.2 nm, which matches with the expected thickness difference between the upright and lying-down phases (1.0 nm).

4.2.4 Nanografting Dodecanethiol into a SAM of 1,9-nonanedithiol.

Nanografting was accomplished within a SAM of the mixed phases of 1,9-nonanedithiol using dodecanethiol as ink molecules for writing (Figure 4.5A). The morphology of the 300 x 300 nm^2 pattern appears smooth and even for the area written with methyl-terminated dodecanethiol, providing a side-by-side view to compare the surfaces of a methyl-terminated SAM versus the surrounding 1,9-nonanedithiol matrix. The thickness of a densely-packed dodecanethiol SAM is 1.5 nm, which would be expected to be 1.1 nm taller than the lying-down phase of 1,9-nonanedithiol which covers most of the areas of the surface surrounding the pattern. The cursor profile (Figure 4.5B) displays a thickness difference of 1.0 ± 0.2 nm, which

matches the expected theoretical height difference between a lying-down alkane chain and upright orientation of dodecanethiol of the pattern.

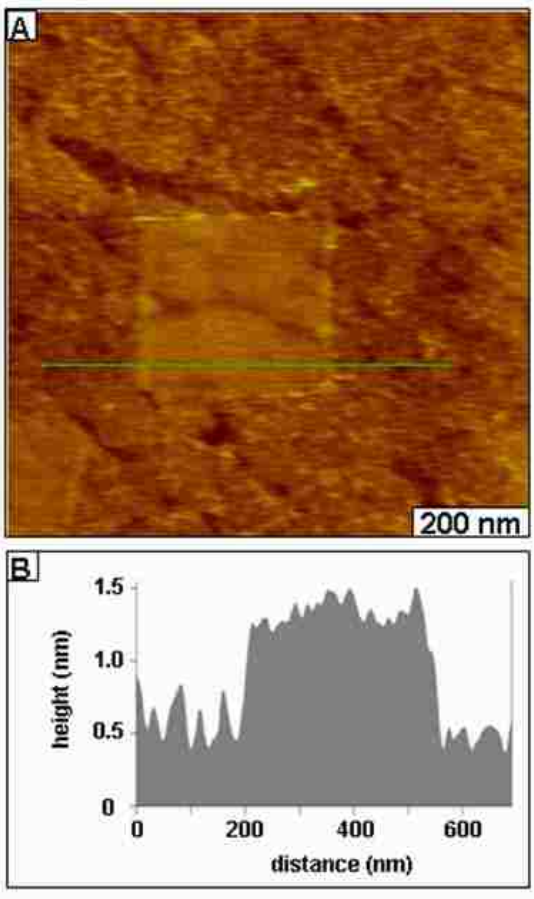

Figure 4.5 Nanografted pattern of dodecanethiol within a 1,9-nonanedithiol matrix. [A] Topograph of a 300 x 300 nm^2 pattern; [B] simultaneously acquired friction image.

4.2.5 Natural Versus Spatially Constrained Self-assembly of α,ω-alkanedithiols.

The natural and spontaneous self-assembly process for α,ω-alkanedithiols begins in a similar manner as for *n*-alkanethiols, with molecules attaching to the surface in a lying-down mobile phase. However, for α,ω-alkanedithiols at this initial stage both ends of the molecule chemisorb to the Au(111) substrate and thus trap the molecules in a lying-down orientation. Over time, more molecules attach to the surface via chemisorption until there is no longer

sufficient room for molecules to assemble in a fully-stretched, lying-down configuration with the backbone of the molecule oriented parallel with the surface. However, due to the randomness of spontaneous adsorption there are still pinhole areas of the surface which are uncovered. At a later stage of self-assembly the dithiol molecules attach between the adsorbed side-on molecules at the pinhole sites of uncovered gold, adopting a standing orientation. This description of natural self-assembly for α,ω-alkanedithiols fits well with the observations of Figure 4.1 and Figure 4.4 which reveal the coexistence of both lying-down and standing-up phases. The initial adsorption step with a lying-down orientation for α,ω-alkanedithiols favors both ends of the molecules binding to gold forming alkanedithiolates. The additional binding of a thiolate (20 k cal/mol) dramatically stabilizes the lying-down phase and thus increases the activation energy barrier for transformation to a standing-up conformation. As a result, a further transition beyond the intermediate phase is inhibited and dithiol molecules remain in a lying-down configuration for the resulting alkanedithiol monolayer.

When *n*-alkanethiols assemble naturally, there is a phase transition from a physisorbed side-on orientation with the backbone of the molecule oriented along the surface, to a chemisorbed standing orientation in which the molecules adopt an upright and tilted configuration. In the case of self-assembly during natural growth of *n*-alkanethiols, monothiol molecules go though multiple steps to form a densely-packed commensurate SAM.[235, 236] Molecules initially adsorb to the surface with the molecular axis of the hydrocarbon chains oriented parallel to the substrate. The physisorbed or lying-down phase is observed to be mobile because it rearranges over time as surface coverage increases. When the surface density of the lying-down phase reaches near saturation coverage, continuous collisions of thiols from solution induce a lateral pressure, which leads to a two-dimensional phase transition. The thiol

molecules rearrange into a standing-up configuration with the hydrocarbon axis tilted approximately 30° with respect to the surface normal. The energy barrier of the phase transition for organothiols with only one thiol endgroup is moderate, thus even at room temperature thiol molecules can readily convert from a lying-down to an upright monolayer. On the other hand, for α,ω-alkanedithiol molecules the formation of alkanedithiolates with both –SH groups chemisorbed to gold stabilizes and anchors the lying-down phase to the surface, which increases the activation barrier between the two intermediate states (lying-down and standing-up). Therefore, a kinetic trap inhibits the phase transition and results in a percentage of dithiol molecules persisting in a lying-down configuration.

The spatially constrained self-assembly of α,ω-alkanedithiols is the same as for *n*-alkanethiols during nanografting. The mechanical process of writing with nanografting enables the molecules to bypass the lying-down phase and assemble immediately into a standing configuration because there is insufficient space on the surface for the molecules to assemble on the surface in lying-down orientation.[171] A key element of nanografting is that *n*-alkanethiols chemisorb spontaneously to surfaces in an upright arrangement to form a crystalline phase, due to a mechanism of spatial confinement. A kinetic Monte Carlo model of natural and nanografted deposition of *n*-alkanethiols on gold surfaces was developed by Ryu and Schatz, which reproduces experimental observations for the variation of SAM heterogeneity with AFM tip writing speed.[210] The speed of the AFM tip influences the composition of the monolayers formed along the writing track. Nanografting can be performed routinely in thiol solutions with concentrations as dilute as 1 μM. Therefore, using nanografting in liquid media, single layer nanopatterns of α,ω-alkanedithiols molecules can be written directly on gold with a standing-up configuration using a lower concentration than that required in a natural growth process.

4.3 Summary

For naturally grown α,ω-alkanedithiols from ethanol solutions, the resulting SAM is composed of lying-down dithiol molecules with isolated islands of upright molecules. The chemisorption of both -SH groups locks the lying-down phase on the surface and prevents the transition from a lying-down to standing upright configuration. Thus, the "mobile" phase of physisorption typically observed with *n*-alkanethiols was not observed for the natural self-assembly of α,ω-alkanedithiols. After 7 days immersion, the lying-down orientation of 1,8-octanedithiol was observed to persist and did not rearrange into a standing-up configuration. High-quality thiol-terminated SAMs can be written directly on gold by nanografting, even from simple α,ω-alkanedithiols without rigid backbones. Using 1,8-octanedithiol and 1,9-nonanedithiol as examples, SAMs were prepared by both natural growth and a new approach of nanografting with spatially confined self-assembly. High-resolution AFM characterizations demonstrate that molecules of nanografted SAM patterns of α,ω-alkanedithiols are densely packed with a preferred standing-up conformation, which generates a surface presenting free –SH groups.

4.4 Methods

4.4.1 Materials

Reagents such as decanethiol, hexanethiol, 1,8-octanedithiol, 1,9-nonanedithiol were purchased from Sigma Aldrich (St. Louis, MO, USA) and used as received. Ethanol (200 proof) was purchased from Aaper Alcohol and Chemical Co. (Shelbyville, KY, USA). Two types of atomically flat gold substrates were used for experiments. Flame-annealed gold-coated mica substrates with 150 nm gold films were obtained from Agilent Technologies, Inc. (Chandler, AZ). However, Figure 4.4 was produced using template-stripped gold films.[166, 167]

4.4.2 Preparation of Self-Assembled Monolayers

Monolayers were prepared by immersion of Au(111)/mica substrates in ethanolic solutions of desired thiols for at least 12 h. Glassware used for preparing SAMs was cleaned in piranha solution and rinsed with deionized water followed by ethanol. To minimize photooxidation of SAMS, the containers were wrapped with aluminum foil and stored in the dark at room temperature. The surfaces were rinsed with ethanol and then immersed in clean ethanol solutions within a liquid cell for AFM imaging.

4.4.3 Atomic Force Microscopy

Topography and friction images were obtained using a model 5500 AFM/SPM operated with Picoscan v5.3.3 software, from Agilent Technologies, Inc. (Chandler, AZ). Picolith beta version 0.4.5 software was used to apply force and to position the AFM tip for nanografting. Gwyddion software was used for image procession, which is freely available on the internet (http://gwyddion.net/). The instrument has an optical-deflection configuration in which the tip is mounted on the piezotube scanner for imaging. Images were acquired using contact-mode AFM in ethanol. Oxide-sharpened silicon nitride probes (MSCT-AUHW) with an average force constant of 0.5 N/m were used for imaging writing nanopatterns (Veeco Probe Store, Santa Barbara, CA).

4.4.4 Nanografting

Nanografting was applied to write nanopatterns of *n*-alkanethiol and α,ω-alkanedithiol SAMs (Figure 4.5).[69, 138] The imaging media contains fresh "ink" molecules for writing *in situ*. Both the AFM tip and sample are submerged in dilute ethanolic solutions containing the ink molecules selected for writing. First, the surface is characterized under low force (less than 1 nN) to identify a flat area for nanofabrication (Figure 4.6A). A flat area is helpful for clearly

distinguishing the thickness differences for molecular height measurements. With low force the sample can be characterized without modifying the surface. To accomplish writing, the force applied to AFM-probe is increased (2-20 nN). Under higher force, the tip is pushed through the matrix monolayer to shave away selected areas, and ink molecules from solution immediately assemble onto the surface following the scanning track of the AFM tip. The same probe can then be used for imaging the SAM nanopatterns by returning to a low force setpoint. Depending on the choice of molecules, nanografting can generate patterns of various thickness. Nanografting provides capabilities to fabricate thiol-terminated SAMs combined with other advantages such as high spatial resolution, flexibility to introduce multiple components of thiols on the same surface, enabling one to modify the fabricated nanostructures *in situ* and providing well-defined placement and geometries for constructing SAM patterns.[69]

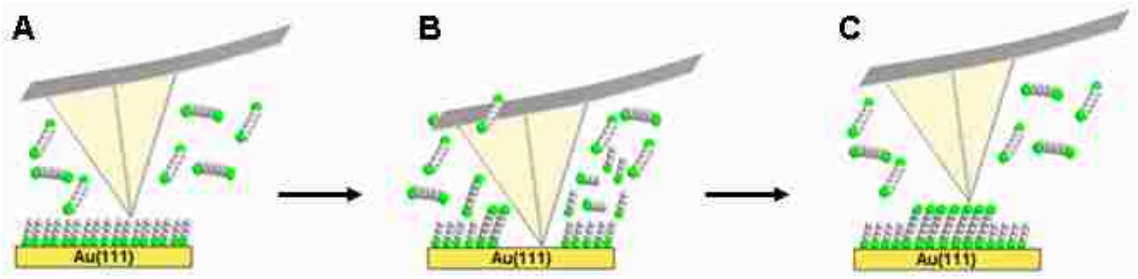

Figure 4.6 Steps for nanografting. [A] Characterization of the SAM using low force; [B] Writing step with high force applied to the AFM tip while scanning; [C] Returning to low force, the nanopattern can be characterized *in situ*.

CHAPTER 5. APPLYING AFM-BASED LITHOGRAPHY FOR NANOSCALE PROTEIN ASSAYS

5.1 Introduction

Imagine the tremendous revolution in medical diagnostics if we had the capabilities to screen thousands of proteins in an immunosensing array, using a single drop of serum and a biochip the size of the head of a pin! Scientists have begun to explore the frontier of nanoscale chemistry to attain the ultimate miniaturization for protein assays using atomic force microscopy (AFM). Of course, we have a long way to go before we achieve such futuristic technology. At this point, researchers have begun to develop analytical methods for detecting proteins using nanoscale surface assays. This article describes recent efforts at developing nanoscale protein assays with AFM-based lithography.

There are many practical reasons for developing protein assays at the nanoscale. New information can be gained from nanoscale studies to address fundamental questions about protein binding and biological function. Adhesion (e.g. protein–protein, protein–nucleic acid, and between small molecule), elasticity and morphology (visualization of the arrangement and the orientation of biomolecules with molecular resolution) data can be obtained over time. Moreover, these data sets can provide crucial information regarding multiprotein assemblies that have not yet been obtained using microarrays. Miniaturization provides rewards such as reduced quantities of analytes and reagents, increased density of sensor and chip elements and faster reaction response. Array-based technologies in proteomics, including protein-based

---

Reproduced with permission from the American Chemical Society: Ngunjiri, J. N.; Garno, J. C., AFM-Based Lithography for Nanoscale Protein assays. *Analytical Chemistry* **2008,** 80, (1).

biochip and biosensing devices, will significantly advance biotechnology, clinical diagnostics, tissue engineering and targeted drug delivery.

The reliability, selectivity and sensitivity of protein biosensors and biochips greatly depend on the affinity and viability of surface-bound biological components. One of the analytical challenges with current technology for biochips and biosensors is that surface-bound bioassays usually are just not as sensitive as solution chemistry methods. One problem is that some of the proteins become denatured when bound to a surface, which makes it difficult to predict how much of the surface is still viable for binding. Another problem is that confining molecules to a surface may reduce the accessibility of binding sites.[237]

Nanoscale assays provide tremendous new possibilities for directly detecting and visualizing the binding of antibodies to immobilized protein layers *in situ*, analogous to time-lapse photography. In nanoscale protein assays, AFM can be applied as a tool for both fabrication and characterization. Nanostructures written by an AFM tip provide highly controllable test environments for exquisite images of protein binding. AFM can be used for not only close-up views of structural changes when proteins bind to surfaces but also for exploring the surface chemistry of selected nanoscale areas by using advanced imaging modes to acquire information with simultaneously acquired channels of phase or frictional force images.

5.2 Chemistry of SAMs

Self-assembled monolayers (SAMs) such as alkanethiols on atomically flat gold surfaces or alkylsilanes on glass, mica, or silica surfaces have been applied successfully for linking proteins to surfaces.[238] The first step in designing a surface-bound bioassay is to choose the appropriate chemistries for attaching proteins to surfaces. Unfortunately, when proteins bind randomly and non-specifically to surfaces during drying denaturation can occur.[237, 239, 240] For

many proteins, the structure and activity can be destroyed by the drying step during microspotting. To maximize the binding activity of proteins for surface assays, gentle chemistries are required that preserve tertiary structure of fragile biomolecules A spacer or linker molecule that attaches proteins to a surface can enable proteins to retain their functionality.[241, 242] Close-packed monolayers of SAMs can be easily prepared and offer a wide variety of functional groups to bind proteins (Figure 5.1A). The chemical and physical properties of various of ω-functionalized monolayers such as alkyls, amides, esters, alcohols and nitriles have been studied on flat gold surfaces.[31, 243] Thus, a broad range of SAM molecular head groups are available for designing linker chemistries. When proteins are immobilized on SAMs, the linker groups can mimic the role of a biological membrane for preserving protein structure.[244, 245]

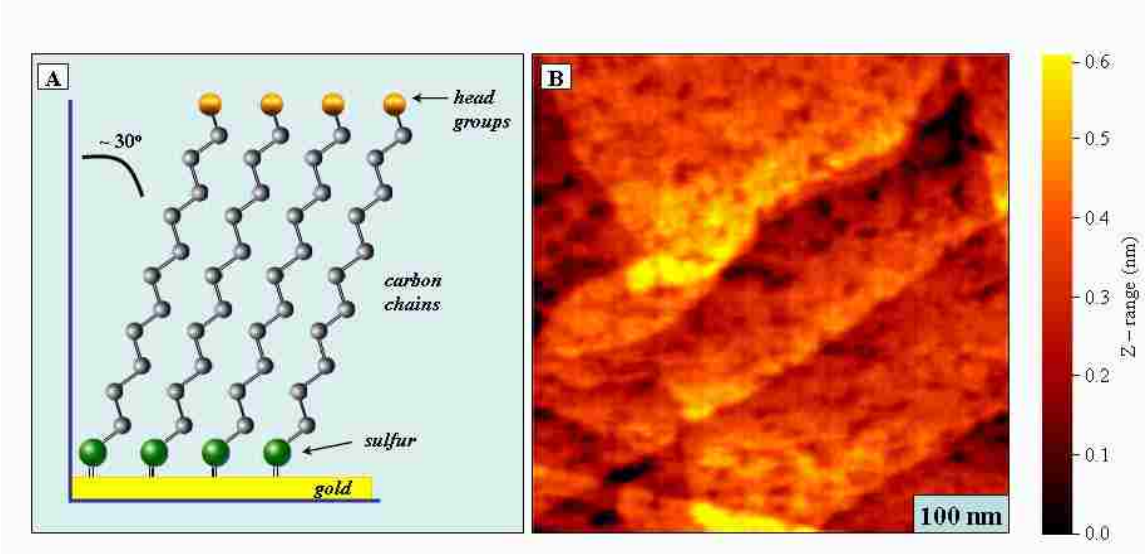

Figure 5.1 Structures of *n*-alkanethiol self-assembled monolayers. [A] Side view; [B] Surface of an octadecanethiol SAM imaged in ethanol by AFM.

An AFM topography image is essentially a map of surface heights. The color scales for AFM topographs in this article show bright areas for tall features and dark areas for short features. Few surfaces are truly flat from an atomic perspective. To assess whether or not an

AFM image has high resolution, look for defects and sharp details at the edges of surface features. A high resolution AFM image should disclose naturally produced defects of a real-world surface such as pinholes, scars or missing atoms. An example image of an octadecanethiol SAM is shown in Figure 5.1B which exhibits surface features characteristic of *n*-alkanethiol SAMs. Although the surface appears to be bumpy and rough, in actuality the step-like terraces are only 0.25 nm high. Notice the irregular contours of the edges of the terraces, details that can only be observed with a sharp AFM tip. The small holes scattered over the surface are etch pits, which are produced by surface reconstruction and are a characteristic landmark of a high resolution image of a SAM.[222] Such high-resolution topography image of a SAM can be routinely acquired using AFM in liquid environments.

The properties of SAMs enable control of the functional groups present on the surface; therefore, these molecules are good model systems for nanofabrication and for studies of protein adsorption. Nanofabricated SAM surfaces can be designed to avoid random protein adsorption, yet enable highly specific interactions with the proteins to be assayed. This design can be accomplished by surrounding nanopatterns of adhesive SAMs with a matrix which resists protein adsorption, such as ethylene-glycol or hydroxyl-terminated alkanethiols.[246-248] Few surfaces resist the adsorption of proteins, and it remains a major research focus to understand the mechanisms that contribute to protein resistance or adhesion.[249, 250]

5.3 AFM-Based Lithography with SAMs

For AFM imaging, a microfabricated sharp probe is rastered across the sample to profile the surface topography.[251-253] A laser is focused on the back of the cantilever and deflected to a four-segment photosensitive detector. As the surface is scanned in contact mode, the tip moves up or down according to surface roughness. The changes in position of the reflected laser spot

incident on the four segments provide a way to continuously monitor the deflection of the tip. As the position of the focused laser spot shifts up or down, images of topography are generated; the left and right movements of the laser spot correspond to frictional forces which cause torsional twisting of the cantilever. An electronic feedback loop maintains constant deflection of the tip, to control of the force applied during scans. Height and friction data are collected line-by-line to generate maps or images of the surface.

Concurrent with the invention of AFM and scanning tunneling microscopy (STM), researchers noticed that the surfaces under investigation were accidentally altered under certain conditions. Essentially, scanning probe lithography (SPL) was brought about by the development of well-controlled "damage" to surfaces. SPL methods selectively and intentionally change the surface chemistry of small areas under the tip of an AFM or STM instrument. Bias-induced nanolithography,[254, 255] dip-pen nanolithography (DPN),[256] catalytic probe lithography[154] and nanografting[56, 257] are types of SPL with different writing mechanisms. The height and surface chemistry of nanopatterns can be tailored by the selection of molecules to be patterned, with designated chain lengths and surface groups. The mechanism for writing with bias-induced nanolithography is thought to involve surface electrochemistry. A conductive AFM or STM tip is required and writing is accomplished by applying pulses of elevated bias voltage (between 2 – 20 V) between the tip and surface (Figure 5.2A, left). The substrates must be conductive or semiconductive, and are coated with an insulating SAM layer (Figure 5.2A, middle). The surface in contact with the tip becomes oxidized under elevated bias, which then provides a reactive site for attaching new molecules to nanopatterns. An example of bias-induced lithography is shown in a frictional force image (Figure 5.2A, right) that reveals rows of 90 nm dot patterns, which were written within a silane SAM on a silicon surface.[254]

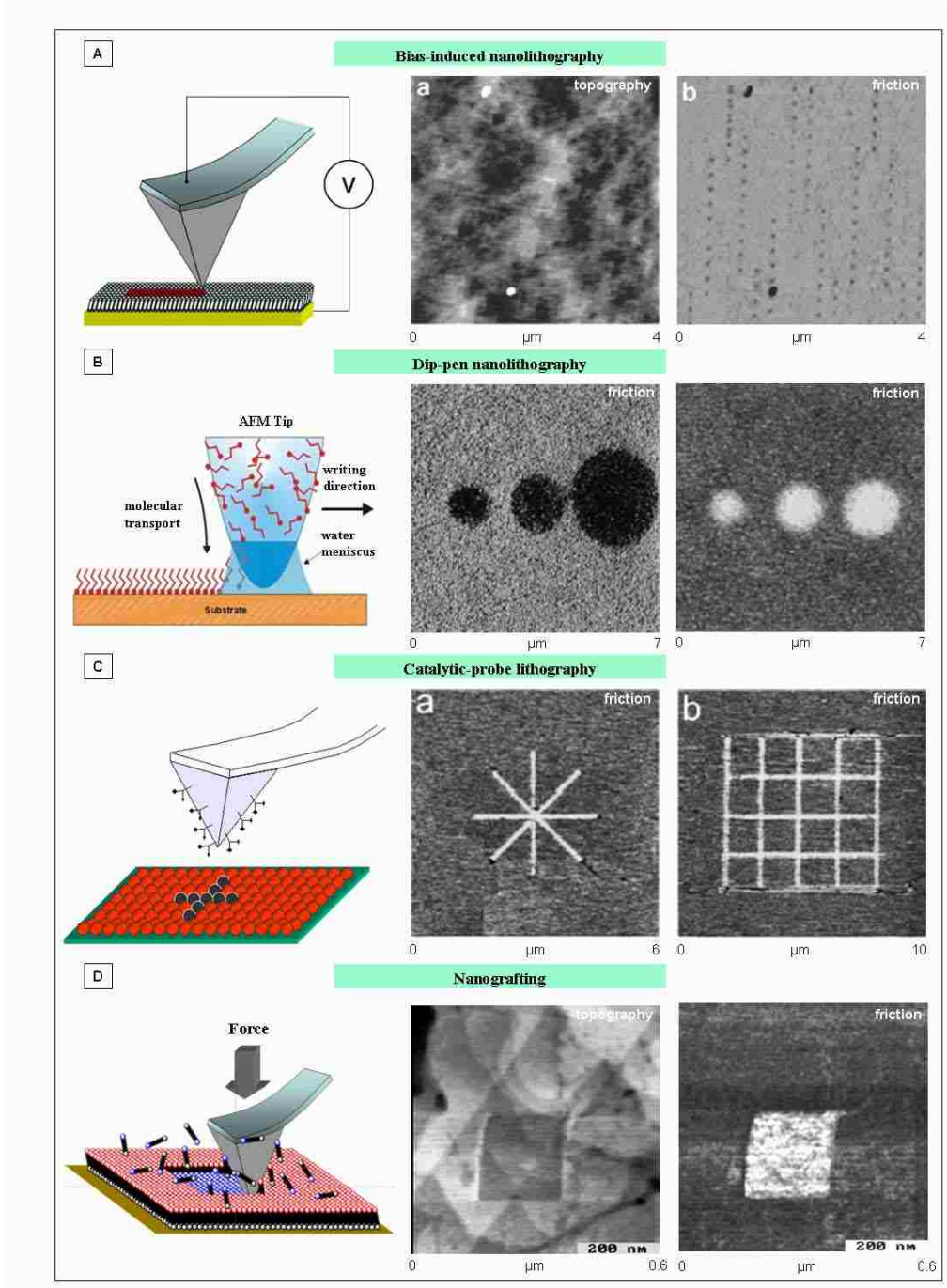

Figure 5.2 Mechanisms for scanning probe lithography methods with SAMs. [A] Bias-induced nanolithography;[254] [B] Catalytic probe lithography;[154] [C] Dip-Pen Nanolithography (DPN);[256] [D] Force-induced nanolithography (nanografting). Images were reproduced with permission from references cited.

The nanopatterns were generated by applying 17 V pulses of 2 μs duration at 270 nm intervals. The dots are composed of carboxylic acid groups produced by oxidizing the methyl head groups of the silane SAM. Often, nanopatterns written with bias-induced lithography do not produce height changes so that surface modifications cannot be detected with topographic imaging. However, the differences are easily distinguishable in frictional force images which sensitively detect nanoscale changes in surface chemistry.

A tip is used as a "pen" and is coated with a molecular "ink" for writing on clean substrates in air (Figure 5.2B, left;).[256, 258] The writing mechanism of DPN involves transfer of molecules to the surface through a nanoscopic meniscus that forms between the tip of the atomic force microscope and the substrate. A water meniscus forms when an AFM tip is placed on the surface for a certain amount of time under humid conditions. The resolution of written patterns depends on the amount of time the tip is held in contact with the surface and the size of the AFM tip.[256] After writing nanopatterns using DPN, an uncoated AFM tip can be used to characterize the structures that were written.

The time-dependency for writing with DPN is demonstrated by frictional force images of patterns written with an atomic force microscope tip coated with *n*-alkanethiol molecules (Figure 5.2B). As the duration of contact between the tip and surface is increased, the circular patterns become larger. The DPN patterns also demonstrate that there are differences in diffusion properties for different SAM molecules. Three dark spots of ODT in the center image were written with tip-contact durations of 2, 4, and 16 minutes (min) from left to right, respectively (Figure 5.2B middle). The white spots in the image were written with 16-mercaptohexadecanoic acid with tip-surface contact of 10, 20 and 40 s, respectively (Figure

5.2B, right).[259] Protein patterns have been written using DPN by directly writing proteins as a molecular ink[260-262] or by adsorbing proteins onto SAM patterns written by DPN.[263, 264]

A newly emerging technique known as catalytic-probe lithography offers exciting possibilities for SPL. Similar to DPN, a coated atomic force microscopy tip is coated to write patterns; however, the tip coating is a catalytic agent that reacts with the head groups on a SAM (Figure 5.2C, left). As the tip touches areas of the surface, the molecular coating of the tip induces a catalytic reaction to write nanopatterns by chemically changing the terminal groups of the SAM (Figure 5.2C, middle and right). [154] An atomic force microscope tip coated with an acidic SAM induced hydrolysis of silyl ether head group of the example nanopattern written with catalytic-probe lithography in the frictional force image in Figure 5.2C.

Nanografting uses force to inscribe patterns within a matrix SAM while the tip is immersed in a solution containing the molecules for writing (Figure 5.2D, left). Instruments for AFM have tremendous capabilities for controlling the force applied to the tip, ranging from piconewtons to nanonewtons. When low forces are used for AFM imaging (<1 nN) the SAM surfaces are not disturbed and can be characterized with high resolution. However, when high forces are applied to the tip, areas of the matrix SAM are shaved from the surface. Fresh molecules from solution immediately assemble onto the shaved areas, following the track of the scanning tip. By returning to low force, the same tip can be used to characterize the nanostructures.

A topographic AFM image of a single square nanopattern (100 x 100 nm^2) written by nanografting is displayed in (Figure 5.2D, middle). To fabricate the nanopattern, the tip was swept 50 times, across the pattern at a force of 3 nN, advancing 2 nm between each sweep. It took only 30 s to write the nanopattern. The brighter colors surrounding the nanostructure

correspond to tall regions of the sample that are covered with a 16-mercaptohexadecanoic acid (MHA) SAM whereas the dark color indicates shallow regions which are covered with dodecanethiol. A frictional force image acquired simultaneously with topography displays differences in surface chemistry for the nanopattern as shown in the bottom right panel of Figure 5.2D, right. The color scales for friction images depend on the surface frictional forces interacting with the AFM tip and are unrelated to molecular heights. In this example, the carboxylate groups of the nanopattern exhibits colors that are brighter than the surrounding methyl groups of the dodecanethiol matrix.

A useful analogy is that the tip is like a "*pen*" for writing on surfaces. Molecules of SAMs are the "*ink*" and various surfaces are "*paper*". A comparison for the different mechanism for writing nanopatterns of SAMs is presented in Figure 5. When choosing a suitable SPL method, researchers need to consider what types of surface functionalities are desired, the imaging medium, and the nature of the surfaces under investigation (Table 5.1).

The capabilities of SPL enable researcher to advance beyond imaging for nanoscale experiments; spatial parameters can be engineered with nanometer precision for placing molecules of well-defined composition. Modern scanning probe microscope instruments provide programs for directing the scanner movement to write complicated designs, with excellent control for variables such as the force, speed, bias voltage, residence time and direction of movement of an AFM tip. Automated SPL provides superb control for rapidly and reproducibly writing arrays of nanopatterns of SAMs. Parameters such as the size, arrangement, geometry, spacing, the packing density and composition of patterned test elements of SAMs can be systematically varied for nanoscale protein assays. Patterns of

various sizes, arrangements and geometries require only the creativity and ingenuity of the experimentalist.

Table 5.1 Comparison of SPL methods used for writing nanopatterns of SAMs.

	Bias-induced Nanolithography	**Dip-Pen Nanolithography**	**Catalytic Probe Nanolithography**	**Nanografting**
Pen	conductive AFM tip (metal-coated)	coated AFM tip	Catalyst coated AFM tip	plain, uncoated AFM tip
Ink	SAMs	SAMs and many other classes of molecules	molecules in solution	thiol molecules in solution
Paper	conductive or semiconductive substrate	clean, uncoated surfaces	SAM/Au(111)	SAM/Au(111)
Environment	air or liquids	air	air or liquids	liquids containing thiol molecules
Writing mechanism	elevated bias at a local area	liquid transfer through a capillary meniscus	catalysis at a local area under an AFM tip	force-induced displacement and replacement by surface self-assembly

Example arrays of nanopatterns written with automated nanografting are shown in Figure 5.3; 11-MUA was used as the *ink* molecules and ODT as the matrix SAM. The array was written within a 1 x 1 μm^2 area, and each design consists of four rings that are inscribed symmetrically around a common focal point. The *in situ* AFM topography images were acquired in ethanol immediately after writing the nanopatterns without changing tips. High-resolution AFM images display etch pits and features of the underlying gold terraces, even after writing nanopatterns; this shows that the tip was not been broken or damaged during nanografting. The individual rings are 100 nm in diameter and were produced by outlining a circle pattern three times with the tip. In Figure 5.3A, the dark contrast of the ring indicates that the molecules of the patterns are shallower than the surrounding ODT. The patterns were written

at 100 nm spacing in the x and y directions. The close-up image in Figure 5.3B, reveals the intricate details of the geometry and fidelity for reproducibly writing a complicated pattern of rings.

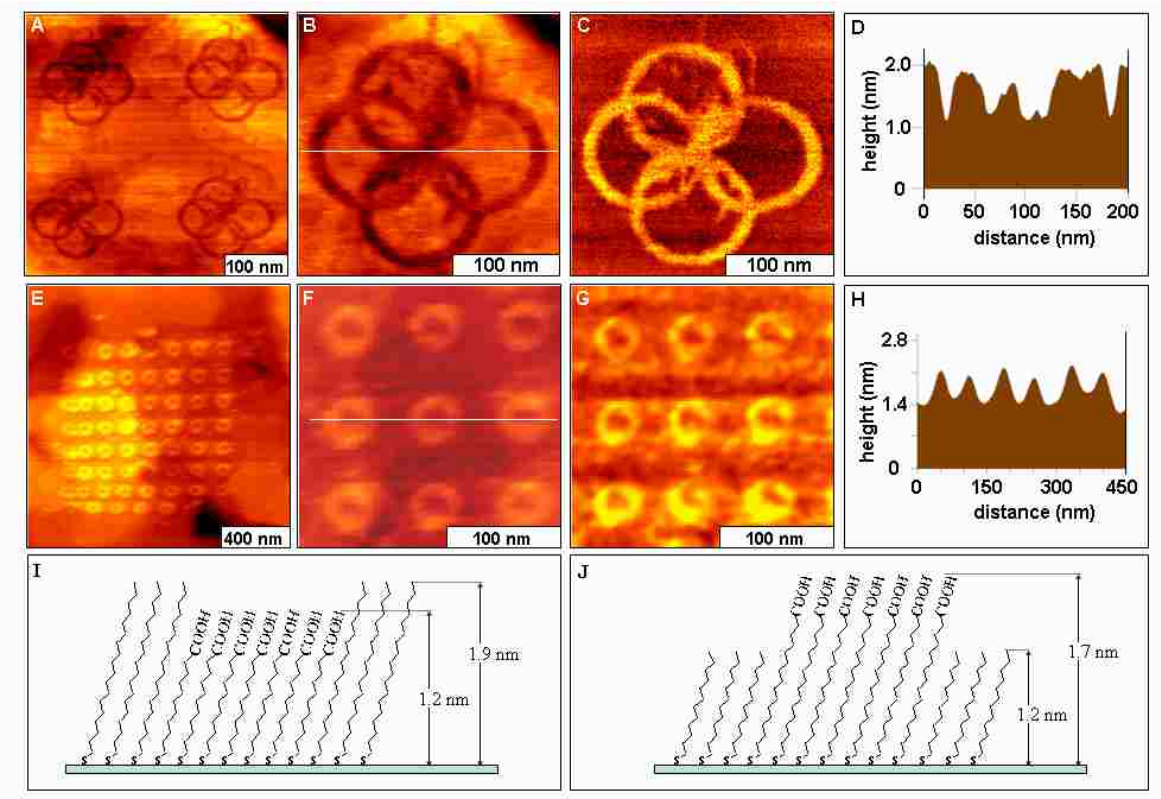

Figure 5.3 Nanopatterns of SAMs written with automated nanografting. [A] AFM topography image of four pretzel designs written with 11-MUA *ink* into a matrix octadecanethiol SAM; [B] Close-up view of a single pattern; [C] friction image for B; [D] cursor profile for the white line in B. [E] An array of sixty four rings of 16-MHA written within a matrix of 11-MUD; [F] zoom-in view of nine patterns; [G] corresponding friction image for F; [H] cursor plot for the line in F; [I] Proposed model for pattern heights in A and B. [J] Model for the patterns in E and F.

Bright colors in the frictional force image of Figure 5.3C, are the carboxylate-terminated; the dark matrix indicates the methyl-terminated ODT. The height difference between the ODT matrix and the 11-MUA rings is 0.7 ± 0.1 nm, as measured in the cursor profiles in Figure 5.3D. This agrees closely with the theoretical height difference of 0.7 nm

shown in the model (Figure 5.3I). The resolution of nanografting determined from the line width of the rings is ~10 nm, according to the cursor measurements.

Sixty-four ring patterns of MHA were written in only 3 min within a matrix SAM of 11-mercaptoundecanol (11-MUD) using automated nanografting (Figure 5.3E). The bright rings in the topography images indicate that molecules of the patterns are taller than the surrounding matrix areas. The nanostructures are nearly perfectly aligned at such small dimensions, even when using a scanner with open-loop feedback (Figure 5.3F); a close up image of 9 nanopatterns shows reproducibility and precise alignment of the 50 nm diameter rings. The cursor profiles display a height difference of 0.6 ± 0.1 nm between the 11-MUD matrix SAM and the 16-MHA rings; this corresponds well with the expected theoretical height difference of 0.6 nm (Figure 5.3H). In the friction image (Figure 5.3G), the contrast changes clearly distinguish the differences in terminal groups; the carboxylate-terminated rings are bright, whereas the matrix areas of the hydroxyl-terminated 11-MUD SAM are dark.

5.4 Attaching Proteins for Nanoscale Assays

Nanografted patterns of SAMs can be used to anchor proteins for *in situ* assays. Typically, the dimensions of an atomic force microscope tip are tens of nanometers. However, depending on the applied force and the geometry of asperities on the tip apex, the actual physical area of contact between the tip and surface may be much smaller; the smallest feature yet produced by nanografting is a 2 x 4 nm^2 dot of ~ 32 thiol molecules.[265] Because protein dimensions are on the order of tens to hundreds of nanometers, the nanopatterns produced by SPL are an ideal size for defining the placement of proteins on surfaces. The terminal moieties of nanopatterns mediate the type of binding for proteins, such as covalent,[266, 267] electrostatic,[268] specific interactions[254] or molecular recognition.[264] Lithography parameters can be used to

precisely control the arrangement and density of SAM binding sites at the nanometer level, in which areas of protein-adhesive terminal groups are written within a resistive matrix SAM.

Several of the initial nanoscale studies using nanografted SAM patterns for protein immobilization were conducted in 1999 by Liu and co-workers.[269] Since then, a growing number of investigators have taken advantage of the flexibility of SPL with SAMs and developed new techniques to probe the chemistry of biomolecular interactions.[162, 270] In the initial investigations of protein immobilization on nanografted SAMs, Wadu-Mesthrige and Liu used different functional groups of nanopatterned alkanethiol SAMs to mediate the electrostatic or covalent binding of immunoglobulin G (IgG) and lysozyme.[265]

The reactivity and stability of protein nanopatterns was also investigated, demonstrating the retention of specific binding activity of the immobilized proteins for antibodies.[265, 268] Protein patterns remained attached to nanopatterns, even after rinsing with buffer and surfactant solutions, and were stable for at least 40 hours (h) of AFM imaging. The smallest pattern of proteins produced by nanografting is a 10 x 150 nm^2 line containing three proteins.[268] A key advantage of the nanografting protocol is the ability to conduct experiments *in situ*, and visualize the successive changes in surface topography after the steps of nanopatterning SAMs, rinsing, and introducing buffers or protein solutions. The protein patterns remain immersed in an aqueous buffer throughout the experiment.

Microscale assays with biochips required that either the protein or antibody be immobilized on a surface.[271, 272] One such strategy is the sandwich assay for protein detection. A target protein or antibody is attached to a surface, and then, a solution containing tagged molecules is introduced. Tags include nanoparticles, fluorescent markers, quantum dots, radiolabels, and other nanomaterials. After binding to the surface, antibodies are sandwiched

between the marker molecules and the surface-bound proteins. The proteins are visualized by optical or fluorescence microscopy using labeled detection antibodies, or by chemically labeling proteins before applying them to arrays.

A good starting point for developing nanoscale protein assays is to investigate well-known model protein systems and surface immobilization chemistries. This is considered a "top-down," approach for nanotechnology, because the same conditions used for macroscopic assays are diluted to the nanoscopic regime. A practical protein for nanoscale assays is staphylococcal protein A (SpA), which has a molecular weight of 42,000 and an estimated Stokes radius of 4.0 nm.[273] Many immunological methods have been developed and refined with the use of SpA as a reagent, including immunoprecipitation techniques and sandwich immunoassays. The amino acid sequence of SpA is composed of five homologous immunoglobulin binding domains. Purified SpA is known to bind at least two IgG molecules, and the affinity constant is ~108 L /mol for human or rabbit IgG.[274] Protein A has a highly stable 3D structure over a wide range of temperature and pH conditions. We have chosen to investigate surface reactions with SpA because it provides a generic foundation for binding a broad range of IgG interactions.

Proteins can be covalently linked to nanopatterns by using 1-ethyl-3-(3-dimethylaminopropyl) carbodiimide hydrochloride (EDC) and N-hydroxy-succinimide (NHS) activation of SAM carboxylic acid head groups.[275] The activation of 11-MUA surface carboxylic acid is achieved by immersing the substrate in an aqueous NHS/EDC mixture for 30 min. Initially, the EDC converts the carboxylic acid groups into a reactive O-acylisourea intermediate that is unstable in aqueous solution, and does not have a sufficient lifetime for a two-step conjugation procedure.

Usually, EDC and NHS are used together in a 1:1 ratio to generate an activated complex with a more stable reactive intermediate (N-succinimidyl ester) to give a greater reaction yield. Cross-linking occurs during the 30 min incubation at room temperature. The resulting NHS-ester can interact via a nucleophilic substitution reaction with accessible α-amine groups present on the N-termini of proteins or the ε-amines on lysine residues. The proteins are covalently attached to the nanopatterns by forming a Schiff's base linkage to make complexes with the 11-MUA carboxylic acid groups (Scheme 5.1).

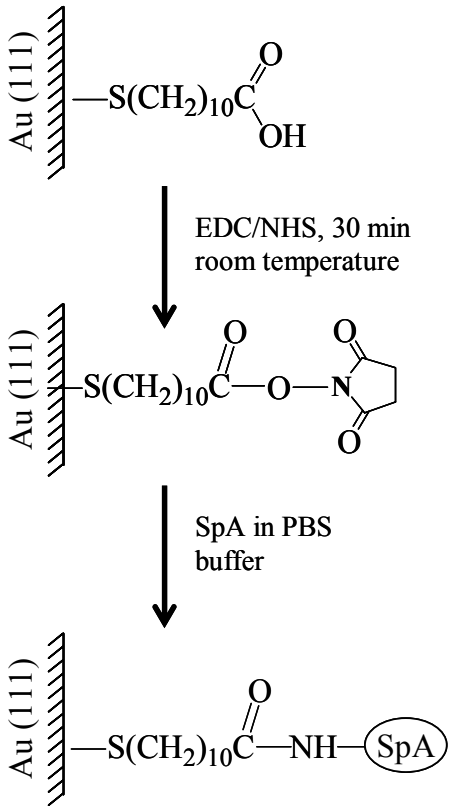

Scheme 5.1 Reaction sequence of the activation of 11-MUA carboxylate groups for immobilization of SpA.

For an *in situ* protein patterning experiment, 16 square nanopatterns (100 x 100 nm^2) of 11-MUA were written within ODT arranged in a 4 x 4 array (Figure 5.4A). The nanopatterns are spaced only 50 nm apart within each row, and the rows are spaced vertically at 100 nm

intervals. The geometry of each of the nanopattern is neatly square and regular at nanoscale dimensions, as evident in the friction image (Figure 5.4B). There are a few additional marks and line patterns caused by the tip. These small patterns are written by the slight twist of the tip as higher force is applied during writing. To achieve symmetrical square nanopatterns, the tip orientation must be well-aligned with the surface at the nanoscale, and the scanner must be precisely calibrated. If the tip is slightly tilted, then patterns will be written as parallelograms or rectangles rather than as squares.

Piezoceramic tube scanners are subject to the effects of drift, hysteresis and non-linearity.[276] These imperfections influence the alignment and spacing for arrays of nanopatterns written with SPL. Also, the tip shape can affect the outcome when writing nanopatterns.

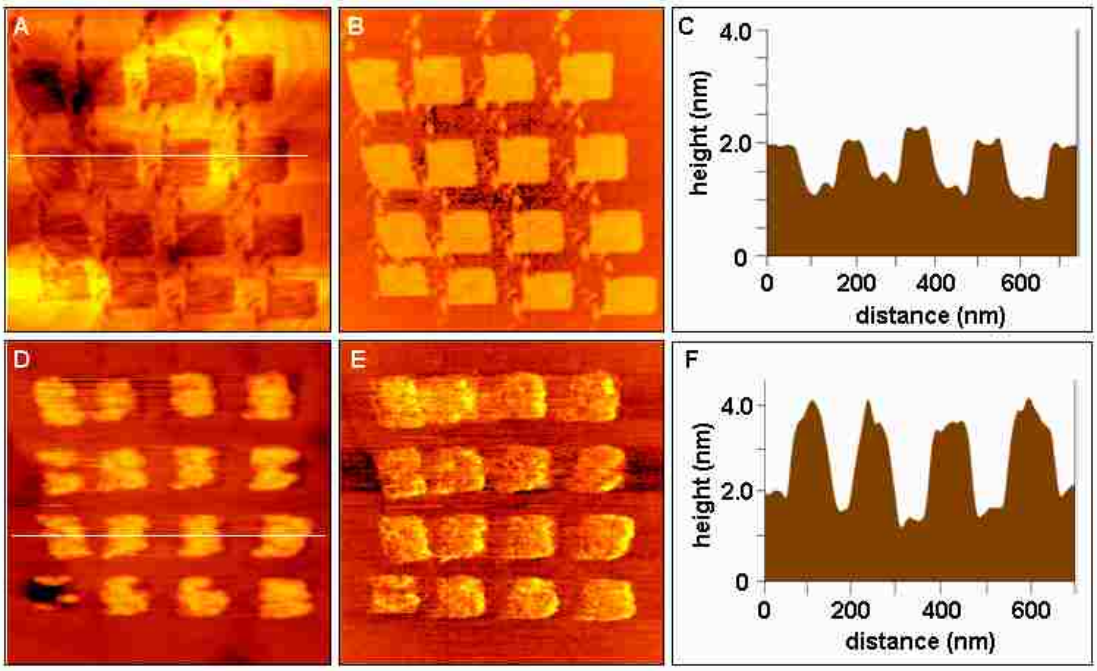

Figure 5.4 Nanoscale protein assay for the adsorption staphylococcal protein A on SAM nanopatterns. [A] An array of 11-MUA squares written in an ODT matrix; [B] corresponding friction image; [C] cursor plot along the line in A. [D] Same area after adsorption of SpA; [E] friction image for D; [F] Cursor measurement for height changes in D.

For the AFM images in Figure 5.4, the end of the tip has multiple asperities and a double tip artifact is observed. At the top left corner of each pattern, tiny dot patterns (15-20 nm) are produced by the second tip scratching the surface under high force. These smaller nanopatterns are clearly distinguishable in the frictional force image.

The difference in height between 11-MUA nanopatterns and ODT measures 0.7 ± 0.2 nm shown by the cursor profile for the white line (Figure 5.4C). After nanografting, a 1:1 aqueous solution of 0.2 M EDC and 0.05 M NHS was introduced into the atomic force microscope cell to react for 30 min. The cell was then rinsed twice with phosphate buffered saline, and a solution of 0.05 mg/mL SpA solution was introduced and incubated for 30 min. Finally, the cell was rinsed with water and ethanol to completely remove any unreacted protein. The tip used for this experiment was precoated with with octadecyltrichlorosilane to minimize tip-sample interactions and improve resolution.[160]

After the steps of chemical activation and protein immobilization, the same array of nanostructures were imaged in ethanol with AFM (Figure 5.4D). All of the steps of nanografting, EDC/NHS activation of carboxylate groups and protein adsorption were accomplished *in situ* with the same AFM tip, and the entire experiment was completed in ~3 h. The SpA molecules bind selectively onto the surfaces of 11-MUA nanopatterns, forming a single layer. After protein adsorption, the changes in surface morphology and chemistry are visible in the Figures 5.4D, and 5.4F, respectively. The contrast of the patterns in the frictional force image has changed, because soft and sticky proteins have friction and adhesive properties that are markedly different than the surfaces of 11-MUA patterns. The changes in height after protein adsorption can be measured with cursor profiles (Figure 5.4F). An average change in height of 4.0 ± 0.5 nm was measured, which corresponds to a "side-on" (3.5 nm thick)

orientation of SpA on the surface. Interestingly, the smaller nanopatterns at the left corners of the array elements do not exhibit SpA adsorption. Experiments in progress indicate that longer immersion intervals are needed for protein adsorption to take place on such small nanopatterns.

During successive *in situ* steps of an AFM-based nanoscale assay, changes in the height and morphology of protein nanopatterns can be monitored. As molecules bind to nanopatterned areas with well-defined chemistries, sequential real time AFM images reveal reaction details at a molecular level, providing a direct visualization of biochemical reactions. An additional advantage of an *in situ* AFM approach for protein assays is that environments can be well controlled by using aqueous buffers and temperature stages. Typically, only single layers of proteins attach to nanopatterns. High-resolution AFM images can even resolve the different orientations of proteins on nanopatterns by using height measurements. For example, height changes were used to determine whether the immobilization chemistry resulted in a side-on or end-on orientation for IgG molecules.[268] After sweeping the surface with the tip and imaging the protein patterns for 4 h, the proteins did not detach and were not swept away by the scanning motion of the tip. This robust attachment enables additional experimental steps, such as introducing peptides, antibodies, DNA or proteins.

Of course, there are a few experimental limitations. The immobilization chemistries that work best for nanoscale experiments should proceed under aqueous conditions to preserve protein activity. Also, investigations should be completed by using very dilute protein solutions to regulate the reaction rate so it transpires over time intervals of 20-30 min. One concern is that the motion and force of the scanning tip can sweep away adsorbates or perturb the reaction. To address this issue, the immobilization chemistry must be sufficiently robust to enable continuous imaging and scanning by the tip. Imaging in liquids facilitates the use of small

imaging forces, (0.05-0.2 N/m) because the adhesive interactions between the tip and sample are minimized.[277, 278] An intrinsic advantage of using AFM instruments is that forces can be controlled precisely on the order of piconewtons to nanonewtons.

In another example eight patterns of 11-MUA were written within an ODT-matrix SAM (Figure 5.5A). The topographic image does not exhibit sharp contrast, because the dark circular pits (defects in the underlying gold film) limit the range of contrast that can be digitally displayed. The simultaneously acquired frictional force image (Figure 5.5B) for the same area more clearly displays the geometries of the two rows of 100 × 90 nm^2 rectangular nanopatterns, which are horizontally spaced at 75-, 75- and 50- nm intervals from left to right. In the vertical direction, the rows are precisely spaced 65 nm apart. A few stray marks written on the left sides and above the top row are evident, caused by the tip during approach and retract cycles.

After the patterns were incubated in EDC/NHS solution for 30 min, SpA was introduced within the liquid cell, then the cell was rinsed several times with deionized water. After SpA adsorption, the heights of the patterns changed (Figure 5.5C).

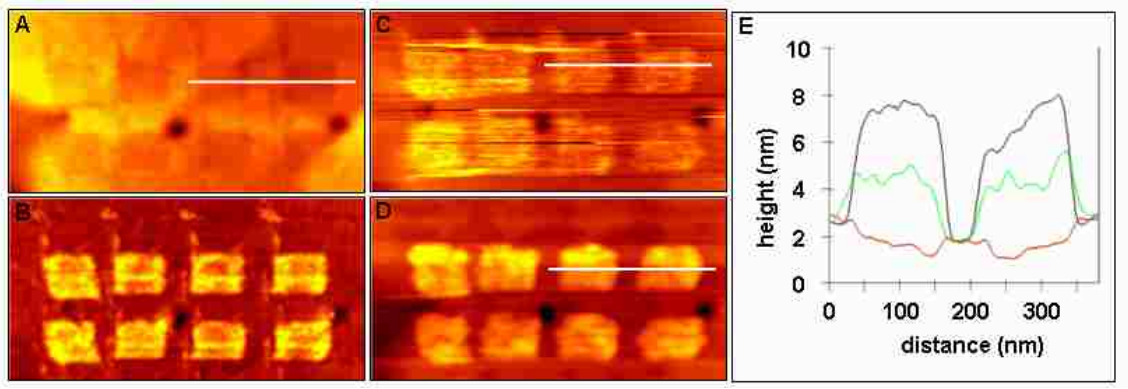

Figure 5.5 Successive AFM views of the steps of a nanoscale protein assay. [A] Topography image of 11-MUA nanopatterns nanografted within ODT; [B] friction image for A; [C] after SpA adsorption; [D] after binding IgG. [E] Combined cursor profiles for A, red line at the bottom; B, green line at the center; C, topmost black line.

The nanopatterns have brighter contrast than the matrix SAM, which indicates tall surface features. The proteins have a strong interaction with the tip operated in contact mode, and this interaction produces line spikes in the horizontal direction along the path of the scanning tip. Next, rabbit IgG was introduced to the liquid cell, which enables viewing the surface changes. After 30 min of incubation with IgG, the patterns became slightly taller and wider (Figure 5.5D). The tip-surface adhesion also changed, because the patterns no longer display line spikes which are cause by stick-slip interactions. A more quantitative nanoscale measurement is presented in the combined cursor profile for lines drawn across the two top-right nanopatterns in Figure 5.5A, 5.5C, and 5.5D. Successive changes in the nanopatterns heights after each step of the protein binding assay can be measured with angstrom precision during the *in situ* experiment. The height increased by 3.0 ± 0.4 nm after SpA adsorption and by 3.6 ± 0.4 nm after binding IgG; this is consistent with the expected protein dimensions for a single layer of proteins.

5.5 Future Directions

Nanoscale studies with proteins facilitated by SPL will assist in the development of approaches for immobilization and bioconjugation chemistries, which are key to manufacturing biochips and biosensing surfaces. Current technology can produce microscale topologies for surfaces, however, to realize further miniaturization at the nanoscale will require revolutionary new methods, such as SPL. The serial nature of SPL may be problematic for applications that require high throughput. Prototype arrays of 1024[177] and 55,000[178] AFM probes have been developed for high throughput nanopatterning. At this time, nanoscale studies with AFM enable new approaches to refine critical parameters used to link and organize proteins on surfaces of biochips and biosensors. With *in situ* AFM characterizations, the orientation, reactivity and

stability of protein molecules adsorbed on nanostructures of SAM can be monitored with successive time-lapse images using near-physiological conditions. These new investigations provide groundwork for advancing biotechnology towards the nanoscale, and furnish molecular-level information through the visualization of biomolecular reactions on surfaces.

CHAPTER 6. CONTROLLING THE SURFACE COVERAGE AND ARRANGEMENT OF PROTEINS USING PARTICLE LITHOGRAPHY

6.1 Introduction

Patterning proteins is important for emerging nanoscale biological and medical applications.[279, 280] There are few tools for writing or inscribing structures at the nanoscale, and this problem has been approached using electron or ion beam lithography techniques, reactive ion etching systems, high-powered lasers and clean rooms. Such methods are costly, require special skills, equipment or facilities and are not readily accessible to an average laboratory. There is a need for economical methods which can reproducibly create organized arrays of nanomaterials with high throughput and low-cost. Particle lithography provides an approach for rapidly preparing millions of exquisitely uniform nanometer-sized structures on flat surfaces using conventional benchtop chemistry - mixing, centrifuging, evaporation and drying. Particle lithography, which is often referred to as nanosphere lithography uses submicron-sized spherical particles as a mask or template to produce nanostructures on surfaces. This technique has been successfully applied to produce arrays of polymers,[281-284] proteins,[285-288] metals,[289-297] vertical nanorods/pillars,[298, 299] carbon nanotubes,[300] and self-assembled monolayers.[301-303] Robust, regular arrays of nanostructures can be reproducibly generated with well-defined dimensions, thickness and arrangement, even for fragile biological systems such as proteins.

Protein patterning is a critical technology for the integration of biomolecules into miniature biological-electronic devices. Direct applications of protein patterning are found in biosensing, medical implants, control of cell adhesion and growth, and for fundamental studies of cell biology.[304, 305] Surface-bound arrays of protein patterns have been applied for antibody

---

Ngunjiri, J. N.; Daniels, S. L.; Li, J.-R.; Serem, W. K.; Garno, J. C., Controlling the surface coverage and arrangement of proteins using particle lithography. *Nanomedicine* **2008**.

screening,[306, 307] testing protein activities,[308] and for analysis of antibody-antigen interactions.[309] Proteins such as bovine serum albumin (BSA), immunoglobulin G (IgG) and staphylococcus protein A have been patterned with particle lithography.[287, 288]

Understanding the interactions of protein binding to substrates or antibodies provides essential groundwork towards developing new technologies for biosensing. Immobilized biomolecules on surfaces serve as the receptor and in some cases as the signal transducer in biosensors and biochips. Surface-bound arrays of protein nanostructures provide a test platform that is readily probed using AFM. Using AFM for analysis enables label-free detection of pathogens and provides a means to monitor molecular interactions in real-time under physiological solutions.[310, 311] Detection for AFM is based on high-resolution imaging, as well as force and height measurements, and therefore does not require signal amplification which can introduce error. For protein studies, the drying step can cause denaturation of a portion of the surface-bound proteins. Also, proteins tend to aggregate and form multilayers when dried. The random, irregular distribution and surface coverage of proteins and problems with denaturation are detrimental for quantitation with surface-based assays. Therefore, the placement of biological ligands in precisely defined locations can increase the density of sensor elements and lead to improved detection limits and molecular-level control of the surface reactivity.[109, 312] Miniaturization of protein arrays provides high array densities, which dramatically reduce the quantities of analytes and sample volumes required for analysis.

6.2 Materials and Methods

6.2.1 Materials and Reagents

Ferritin and apoferritin were obtained from MP Biomedical Inc. (Solon, OH). Bovine serum albumin (BSA) and rabbit immunoglobulin G (IgG) were purchased from Sigma

Biochemicals (St. Louis, MO, USA) and used without further purification. Monodisperse latex and silica spheres were acquired from Duke Scientific (Palo Alto, CA). Hydrogen peroxide (30%), sulfuric acid (95.5%) were acquired from Sigma-Aldrich (Saint Louis, MO).

6.2.2 Preparation of Substrates

Three different substrates were used for AFM investigations. Ruby muscovite mica was acquired from S&J Trading Inc. (Glen Oaks, NY). Pieces of mica (1×1 cm^2) were cut and cleaved immediately before depositing sample solutions. Gold thin films (150 nm) evaporated on mica substrates were obtained from Agilent Technologies, Inc. (Chandler, AZ). A previously reported procedure for preparing ultraflat gold films on glass slides was applied to prepare template-stripped surfaces.[313] Round glass cover slides, diameter 12 mm were obtained from Ted Pella Inc. (Redding, CA). Glass slides were cleaned for 30 minutes by immersion in piranha solution, a 3:1 mixture of sulfuric acid and 30% hydrogen peroxide. (Caution: Piranha solution is highly exothermic and corrosive.) Next the slides were rinsed with deionized water and dried in air. For particle lithography, a volume of protein/mesosphere solution was deposited and dried on the cleaned slides.

6.2.3 Atomic Force Microscopy

Images were acquired using an Agilent 5500 AFM/SPM system equipped with Picoscan v5.3.3 software. An ambient environment was used for AC (tapping) mode imaging. Rectangular silicon nitride cantilevers (NSC 14/Al, resonance frequency 160 kHz, spring constant 5 N/m) from MikroMasch (Portland, OR) and silicon AFM probes (Tap 150AL, resonance frequency 150 kHz, spring constant 5 N/m) with an aluminum reflex coating from Budget Sensors (Redding, CA) were used for AFM imaging.

6.3 Particle Lithography with Proteins

Arrays of protein patterns were prepared by mixing aqueous solutions of proteins with monodisperse spheres of silica or latex at various ratios. A 10 μL drop of the mixture was deposited on a flat surface and dried at room temperature (Figure 6.1A). Surface coverage could be tuned to form at least one layer of spheres and varied between 1 and 4% wt/volume depending on the diameter of the particles.

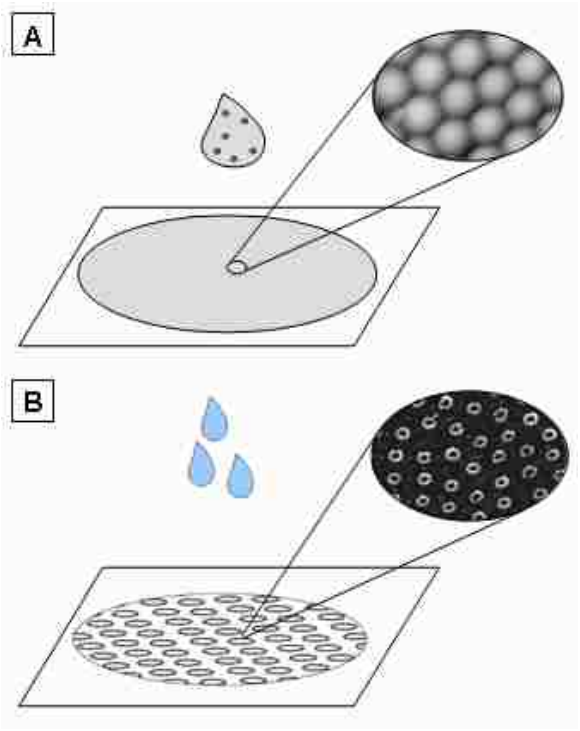

Figure 6.1 Steps of particle lithography with proteins.

The monodisperse spheres form a structural template which directs the placement of proteins on surfaces. During the drying step, mesospheres spontaneously assemble into a close-packed crystalline layer with the proteins surrounding the base of the spheres. The final step is to remove the particles by rinsing the sample surface with deionized water (Figure 6.1B). The larger spheres are easily displaced by rinsing the sample; however the proteins remain attached to the surface to form symmetric circular patterns surrounding the template spheres.

6.4 Results and Discussion

For particle lithography, the natural self-assembly of monodisperse mesospheres furnish a structural template to guide and direct the placement of proteins on surfaces. Because the spheres have the same diameter, a close-packed hexagonal arrangement of latex or silica particles is produced when aqueous solutions are dried on atomically flat surfaces (Figure 6.2). The tightly packed mesospheres do not fully cover the surface; areas between spheres provide a conduit for aqueous protein solutions to gravitate to the surface. The model proteins chosen for our investigations are highly soluble in water.

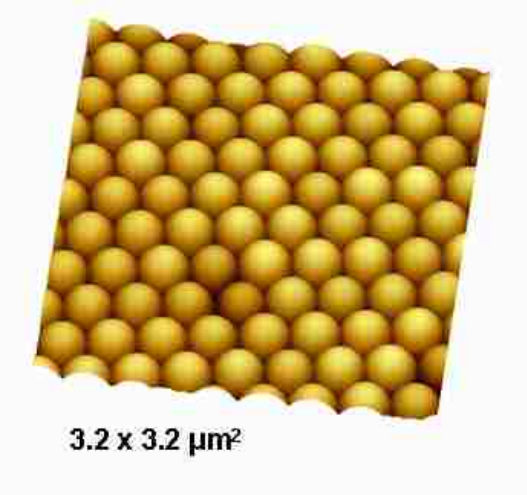

Figure 6.2 Example structural template formed by particle lithography with 300 nm latex mesospheres.

The proteins are carried with the water meniscus during ambient drying, to form regular, evenly distributed arrays of protein nanostructures at the base of the template particles. The mesospheres provide a structural template which masks spherical areas of the surface. After the templates are rinsed away, the protein nanostructures can be applied for surface investigations and assays. Ferritin and apoferritin,[314, 315] BSA,[316] and IgG[317] were chosen as model proteins for AFM investigations with particle lithography because of their well studied physical and

chemical properties. The direction for future investigations with the selected model proteins will be to image surface changes when binding secondary biomolecules to nanostructure arrays for fundamental analysis of protein interactions and events mediated by molecular recognition.

6.4.1 Films of Ferritin Formed by Direct Deposition at Different Concentrations

Ferritin forms the primary complex for the uptake and storage of iron in mammals. The shape of ferritin is nearly spherical with a diameter of 10-12 nm.[318, 319] The protein structure consists of 24 subunits forming a shell containing up to 4500 iron(III) ions.[314] Ferritin is a promising component for engineering diverse nanomaterials due to its catalytic,[315, 320-322] magnetic,[323-325] and electrical [326, 327] properties. The protein shell or cage of ferritin has been used in synthetic reactions with various metal ions, to form inorganic nanoparticles of materials such as Fe_3O_4, Co_3O_4, Mn_3O_4, CoPt, Pd, Ag, CdS and CdSe.[328] Monitoring levels of ferritin is required for diagnosis and treatment of anemia and complications which affect iron deficiency or iron metabolism. For AFM and surface investigations a problem is presented for controlling the distribution and surface coverage for studies of biomolecular reactions on various substrates. Methods of sample preparation which enable control of surface coverage are useful for a range of bioanalytical applications. The process of drying, surface forces, and intermolecular attractive interactions tend to pull proteins together into tightly packed aggregates.

An example is presented in Figure 6.3 for solutions of ferritin dried on mica under ambient conditions. Nearly monolayer coverage (84%) is achieved in Figure 6.3A, disclosing tightly-packed assemblies of ferritin spheres. The sample was prepared by drying a 10 μL drop of an aqueous solution of ferritin (0.5 mg/L) on a 1×1 cm^2 piece of freshly cleaved mica. The dark areas are uncovered areas of the substrate. For the examples in Figure 6.3, the AFM tip is unable to penetrate between proteins that are packed closely together. Thus, imaging and

measurements are limited to interrogating the exposed upper surface of the clusters. By diluting samples (0.2 mg/mL) lower surface coverage (36%) is achieved; however the proteins still tend

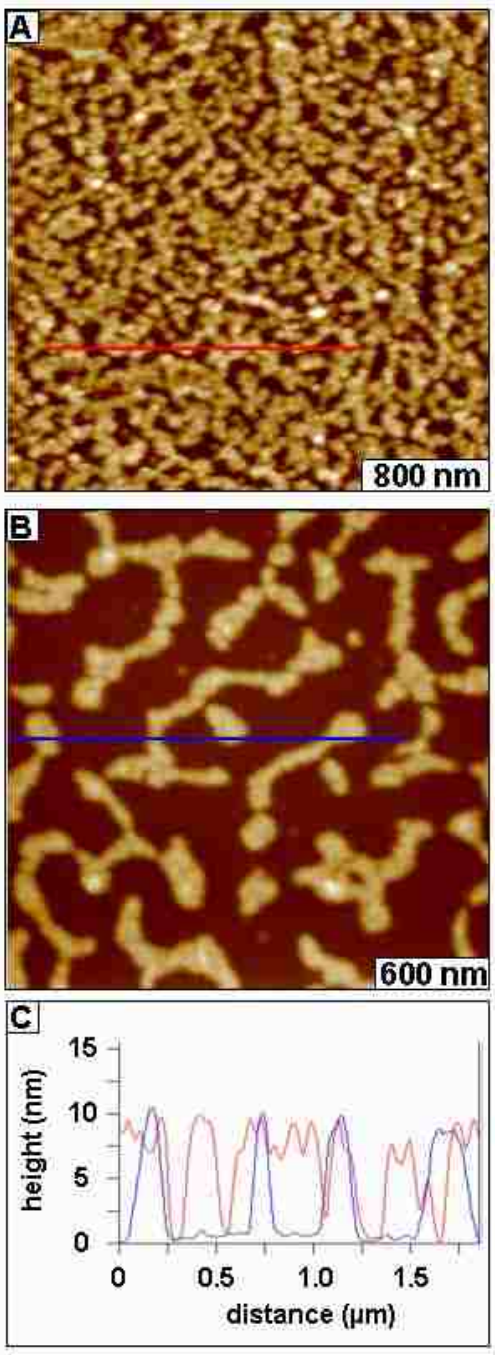

Figure 6.3 Aggregated domains of ferritin formed naturally on mica(0001). [A] High surface coverage produced with 0.5 mg/ml; [B] Lower coverage (0.2 mg/ml); [C] Combined line profiles for **A** and **B**.

to cluster together (Figure 6.3B). With an incomplete surface layer, there are only a few individual protein spheres visible between the larger domains of ferritin aggregates. A combined plot of the height of the protein layer is displayed for Figures 6.3A and 6.3B, with red and blue line profiles, respectively (Figure 6.3C). For both samples, the height measured 11 ± 2 nm, in close agreement with the known dimensions of ferritin (12 nm) obtained from x-ray crystallography.[329]

Aggregation is not simply a problem for AFM surface investigations. Scaling up from the nanoscale to microarrays, the self-aggregation of protein layers affects the sensitivity and reliability of bioassays and biosensor surfaces. The sensing elements of biochips and biosensors are composed of an adsorbed layer of biomolecules or proteins for selective reaction with targeted analytes. For surface assays, detection is mediated by molecular recognition. Thus, if the target sites of immobilized proteins are inaccessible or masked by neighboring proteins, then the necessary binding reactions cannot take place. Inherently, surface bound assays are often less sensitive than solution-based assays due to the effects of crowding and self aggregation.

6.4.2 Nanopatterns of Ferritin Produced on Mica, Gold and Glass Substrates

Patterns of ferritin molecules can be formed on various surfaces using particle lithography. The natural self-assembly of mesospheres provide a structural template to tune the surface coverage of proteins. Ferritin molecules can be organized into arrays of ring structures, as demonstrated for surfaces of mica, template-stripped gold and glass (Figure 6.4). Monodisperse spheres of colloidal silica (500 nm) were used as structural templates for the examples presented in Figure 6.4. For AFM topographs, the shapes of individual ferritin adsorbates can be resolved with better resolution than the previous example of Figure 6.3, because at lower surface coverage the tip can probe between molecules to more accurately

profile the shape of the proteins. Topographic images are a convolution of the tip geometry and the shape of the sample. Lateral dimensions often are broader than the expected geometry for AFM topographs; however height measurements furnish reliable information to measure the diameters of protein particles.

Successive zoom-in views of rings of ferritin on mica are viewed in Figures 6.4A-6.4C. Mica is commonly used for preparing biological samples with AFM, because of the hydrophilic nature of the surface.[330] After mica is cleaved, clean and atomically flat surfaces are produced, with roughness less than 0.1 nm. The flatness and hydrophilicity of the substrates provide an ideal platform for particle lithography. The shapes and interpattern spacing are uniform and symmetric. Since there are few defects on surfaces of mica, throughout broad areas of the surface the AFM images reveal long-range order and periodicity. A few individual proteins are scattered in areas between the ring patterns, however no proteins are detected inside the rings. The rings encircle bare areas of the substrate which were uncovered when the silica mesospheres were rinsed away. The displacement of template particles is complete, because the spheres are easily removed by the rinsing step. The surface coverage of ferritin is approximately 17 % for the sample prepared on mica. Each sample in Figure 6.4 was prepared at a ratio of 700 ferritin per silica sphere. Approximately 6400 ferritin proteins would fully encapsulate a silica sphere; therefore the ratio corresponds to a fraction of a monolayer shell for producing ring nanostructures. A close-up view (Figure 6.4B) reveals the hexagonal arrangement of the rings. A further zoom-in view of a single pattern reveals the morphology and arrangement of individual ferritin particles that form the ring (Figure 6.4C). The height of the rings measure 12 ± 1 nm, in close agreement with the expected diameter of ferritin. The outer diameters of the rings measure 350 ± 20 nm (Figure 6.4D). The center-to-center spacing

between rings measure 550 ± 30 nm, which corresponds well to the diameter for the template silica spheres.

Conductive films of gold provide an electrode for electrochemistry-based measurements for biosensors and voltammetry studies. Patterns of ferritin produced on surfaces of template-stripped gold are shown with successive zoom views in Figures 6.4E, 6.4F and 6.4G. Within the 4 x 4 μm^2 area of Figure 6.4E there are 21 rings, in comparison to a density of 40 rings formed within the same size area of mica in Figure 6.4. Approximately 12% of the surface is covered with ferritin for the gold substrate. At the nanoscale, the surface of gold is rougher than mica, the roughness of the template-stripped film is approximately 0.6 nm. Thus, a few defects such as cracks and domain boundaries are visible on bare areas of the surface. The long-range order and periodicity of the arrays are affected by the roughness of the surface, producing a few imperfections in the shapes of nanopatterns.

Gold surfaces are more hydrophobic than mica, which influences the ordering and packing density of silica spheres. Fine details of the shape of the proteins within rings are revealed in zoom-in views (Figures 6.4F and 6.4G). The diameter of the rings measures 200 ± 5 nm and the height measures 11 ± 2 nm (Figure 6.4H). There is a significant difference between the size of the ferritin rings formed on gold and mica, which is attributed to surface wettability. The hydrophilic surface of mica results in spreading of the protein rings to span a larger area.

Nanopatterns of ferritin can also be formed on glass surfaces using particle lithography (Figures 6.4I, 6.4J, 6.4K). Glass is an appropriate substrate for biosensing, due to the many possibilities for optical, microscopy and spectroscopy measurements. There are approximately 20 rings of ferritin within a 4 x 4 μm^2 area (Figure 6.4I), approximately 19% of the surface is coated with protein. Also, the shape of the rings is not as symmetric as for mica and gold

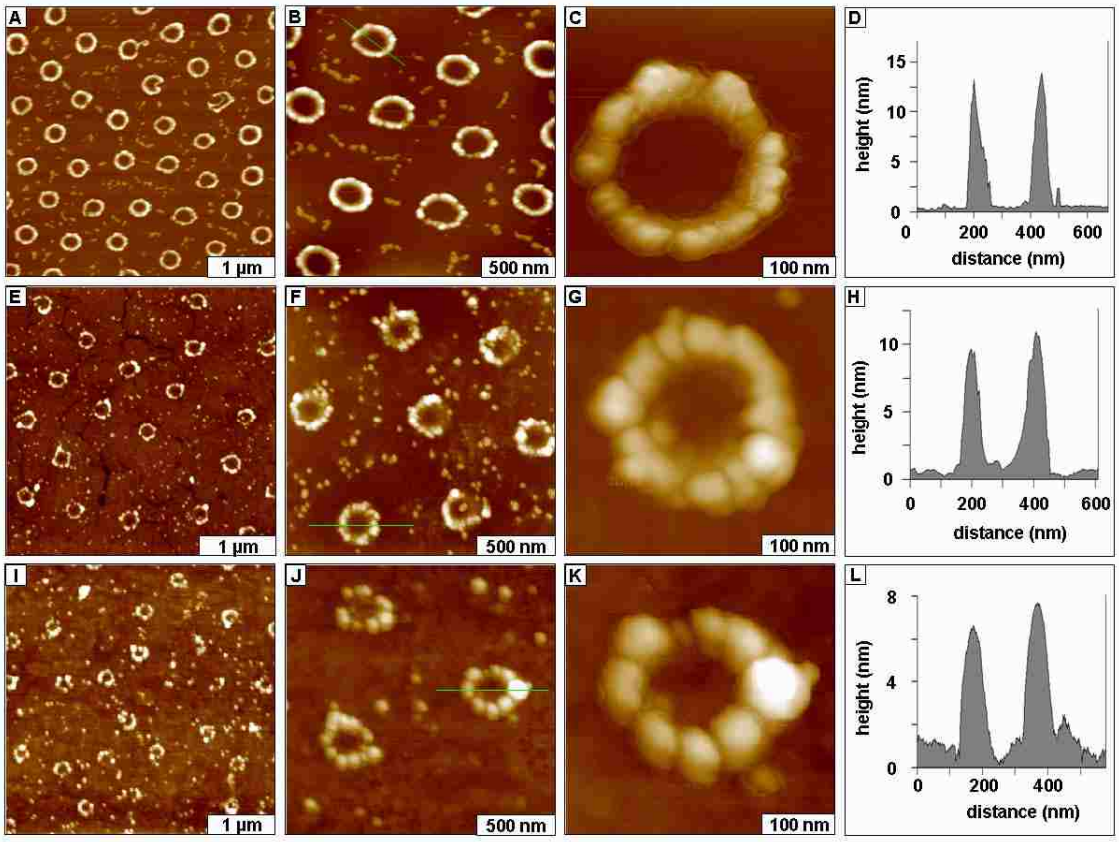

Figure 6.4 Arrays of ferritin rings produced on various surfaces using particle lithography; [A] Topograph (4 × 4 µm^2) for nanostructures on mica(0001); [B] Zoom-in view (2 × 2 µm^2); [C] Close-up of a single ferritin ring (0.45 × 0.45 µm^2); [D] Cursor profile for **B**. [E] Arrays of ferritin rings on template-stripped gold (3.5 × 3.5 µm^2); [F] Zoom-in view of **E** (1.7 × 1.7 µm^2); [G] A single ring pattern from **F** (0.6 × 0.6 µm^2); [H] Cursor profile for **F**. [I] Ferritin rings formed on glass (4 × 4 µm^2); [J] Zoom-in view of **I** (1.7 × 1.7 µm^2); [K] Close-up of a single ring from **J** (0.4 × 0.4 µm^2); [L] line profile for **J**.

surfaces; a number of rings formed on glass are incomplete with missing proteins. Zooming-in for a close-up view (Figure 6.4J) the spacing between rings measures 600 ± 30 nm, which is wider than the 500 nm diameter of the silica mesosphere template. The periodicity is influenced by a number of parameters such as surface treatment, roughness, hydrophobicity; however the surface coverage and periodicity can be optimized by changing the protein-to-particle ratios. The results of Figure 6.4 demonstrate that for different substrates the solution conditions need to be adjusted to optimize the density of nanostructures. By increasing the concentration of proteins a higher surface density can be produced. A single ring structure is viewed in Figure

6.4K, showing the circular arrangement of proteins. The size of ferritin adsorbates is actually quite uniform; the observed variances in height are caused by the pits and valleys of the rougher glass substrate, as well as the drying conditions of the sample. The cursor profile indicates that the rings are 7 ± 2 nm in height, which is smaller than the expected 12.5 nm dimension of ferritin (Figure 6.4L). The surface of glass is rougher than mica or gold, with an average roughness of 0.2 - 0.5 nm. The roughness profile of the glass surface is evidenced by the jagged baseline of the cursor outline (Figure 6.4L).

In comparing the ring structures of ferritin produced using particle lithography for various surfaces, as one can expect there are distinct differences in the periodicity, geometry and surface coverage (Table 6.1). Rings of proteins prepared on the hydrophilic surface of mica have larger diameters and more proteins surrounding each ring, whereas the nanopatterns formed on gold and glass have similar periodicity and ring diameters. The factors which influence the pattern morphologies are the surface roughness and wettability. During the drying step of particle lithography the amount of spreading at the macroscopic level affects the ordering and compactness at the nanoscale.

Table 6.1 Comparison of nanopattern morphologies on various surfaces.

substrate	**mica**	**gold**	**glass**
periodicity	600 ± 30 nm	650 ± 50 nm	650 ± 70 nm
ring diameter	360 ± 20 nm	270 ± 20 nm	290 ± 10 nm
number of proteins per ring	15-18	10-13	9-11
surface coverage	17 %	12 %	19 %

6.4.3 Rings of Apoferritin Produced on Surfaces of Glass

The protein shell of ferritin without an iron core is known as apoferritin. The shell or protein cage of apoferritin consists of the same 24 subunits as ferritin, with similar dimensions.

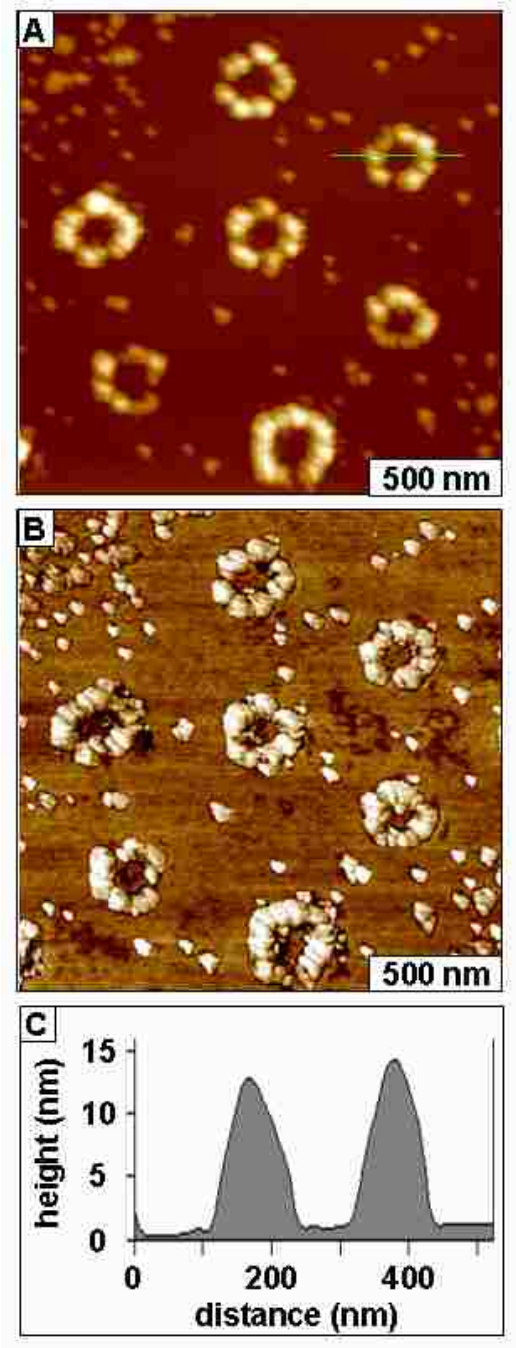

Figure 6.5 Nanopatterns of apoferritin molecules formed on glass. [A] Hexagonal arrangement of rings of apoferritin; [B] corresponding phase image; [C] cursor profile for the line in **A**.

Ring structures of apoferritin molecules were produced on glass substrates using 500 nm silica spheres as a template (Figure 6.5). An AFM topograph (Figure 6.5A) display well organized rings of apoferritin assembled in a hexagonal arrangement, with interpattern spacing matching the diameter of the templating silica spheres. A few individual molecules of apoferritin are scattered across the surface between ring patterns, the approximate surface coverage of ferritin is 15%. The ratio of apoferritin to silica spheres is 1000:1, approximately 15% of the number of proteins for a full layer surrounding a 500 nm sphere. In the corresponding phase image (Figure 6.5B) the soft and compressible areas of protein are distinct from the harder areas of the glass substrate. The morphologies of the individual proteins do not appear to be spherical; however, the shapes observed are an imaging artifact caused by the blunt, angular profile of the AFM tip. Images produced by AFM are a convolution of the shape of the imaging probe and the sample morphology. The height of the rings measure 12 ± 1 nm (Figure 6.5C), which is in close agreement with the known diameter of apoferritin (12 nm).

6.4.4 Patterns of IgG Formed by Particle Lithography

Antibodies such as IgG are used for a wide range of bioassays, such as for sandwich immunoassays.[312, 331, 332] Molecules of IgG have a Y-shaped geometry with two antibody binding domains at the ends of a Y-like fork, which are spaced 14.5 nm apart, according to X-ray diffraction studies.[333, 334] The tail of the Y-shaped molecule contains one or more carbohydrate chains. The distance between the two antibody-binding domains and the end of the carbohydrate domain is 8.5 nm. The thickness of the molecule is 4.0 nm. The hinge region at the center of the Y-shape link the amino acid chains together and is composed of disulfide bridges. High throughput patterning of IgG can be accomplished using particle lithography. An AFM topographic view displays 130 rings of IgG within the 10 × 10 μm^2 frame of Figure

6.6A, covering approximately 10% of the surface. At this density, roughly 130 million rings were produced for a 1 × 1 cm^2 sample.

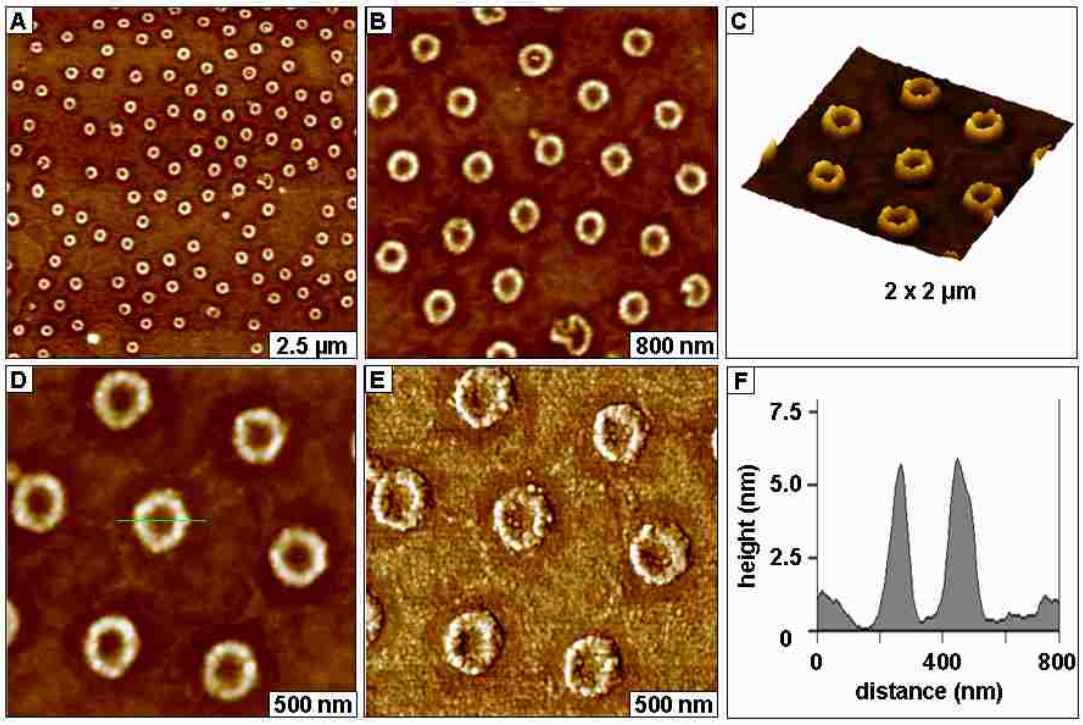

Figure 6.6 Ring patterns of IgG produced on mica. Successive zoom-in topographs: [A] 10 × 10 μm^2 ; [B] 3 × 3 μm^2 ; [C] 2 × 2 μm^2 ; [D] 2 × 2 μm^2 ; [E] phase image for D; [F] height profile for the line in **D**.

The ratio of IgG:spheres is 3300:1, however, since IgG has a smaller surface area than ferritin, 20,000 proteins would be needed for an encapsulating shell layer. In a close-up view (Figure 6.6B) the ring patterns exhibit a hexagonal packing arrangement, conforming to the periodicity and packing order of the structural template of 500 nm silica mesospheres. The pores of the IgG rings pinpoint the uncovered areas of the substrate where silica mesospheres were displaced by a rinsing step.

The proteins adsorb near the base of the spheres and are distributed evenly throughout the surface to form regular shapes and diameters. A 3-D view reveals the uniformity of the pattern heights (Figure 6.6C). The corresponding 2-D view (Figure 6.6D) and phase contrast

channel (Figure 6.6E) furnish details of the ring morphologies. Phase images often display surface details that cannot be clearly resolved in height images. Although the Y shape of IgG is not evident at this magnification, particles of individual proteins are apparent in the zoom views. The height of the rings of IgG measure 5 ± 1 nm (Figure 6.6F) which matches the dimensions for an IgG molecule which is lying flat on the surface.

6.4.5 Effect of Protein-to-Particle Ratios

Serum albumin is the most abundant protein found in plasma, and its affinity for binding materials has been well-studied.[335, 336] For surface bioassays, a blocking step is important to prevent nonspecific binding of proteins. Solutions of BSA are a common blocking reagent used to backfill uncovered areas of surfaces, applied for enzyme-linked immunosorbent assays (ELISA) and in agglutination assays. To develop a generic approach for surface-bound protein assays, the practical step is to nanopattern BSA to prevent nonspecific binding of proteins. Therefore, BSA is a sensible choice for AFM surface investigations with nanopatterning.

When changing the ratios of proteins to mesospheres, well-defined protein nanostructures are still produced, which generates differences in surface coverage and pattern morphologies. An example in which the ratio of proteins to mesospheres was systematically changed is presented for BSA patterns formed on mica in Figure 6.7. At a high BSA-to-latex ratio (13,600:1) AFM topographs reveal a continuous film of BSA with an organized arrangement of circular dark holes or pores (Figures 6.7A, 6.7B, 6.7C). The areas between particles fill completely with proteins to encircle the bare cavities where the mesoparticles were displaced. A honeycomb arrangement of pores within a film of BSA is displayed in Figure 6.7A, produced using 300 nm latex spheres as structural templates. The periodic arrangement of dark spots are uncovered areas of mica within a monolayer film of BSA. The uncovered areas

can be used to deposit a second molecule, or these vacant areas can furnish an *in situ* landmark for monitoring changes in height after biochemical assays. At a high ratio, the surface coverage of BSA is 83 % for Figure 6.7A. In comparison, approximately 22,600 BSA molecules would be required to completely surround and encapsulate a single 300 nm latex sphere. A close-up view of the surface (Figure 6.7B) displays the uniformity and periodicity of the patterned pores. There are 316 pores within the 6×6 μm^2 area, which extrapolates to a surface density of 877 million nanostructures produced with a single 10 μL drop of protein solution placed on a 1×1 cm^2 area of mica. The even surface profile, symmetric patterns and regular spacing of pores is clearly viewed with a 3D representation in Figure 6.7C.

The thickness of the protein film measures 3.8 ± 0.3 nm, matching the dimensions of a single layer of BSA (Figure 6.7D) in agreement with the 4.0 nm diameter of BSA obtained by x-ray crystallography.[337] The spacing between pores measures 270 ± 20 nm, which is 10% smaller than the expected 300 nm diameter of the latex spheres. The periodicity of the resulting nanopatterns depends on the separation of latex spheres, which is observed to be 5–15% smaller than the latex diameters. Since polystyrene latex are known to be deformable, the decrease in diameter is attributable to shrinking of latex particles when dried.[287]

By using a low BSA-to-latex ratio (6,800:1) ring-shaped nanopatterns of BSA were produced on mica(0001) with 300 nm latex (Figures 6.7E, 6.7F, 6.7G). The ratio of 6,800:1 corresponds to an incomplete shell of BSA encapsulating a 300 nm latex sphere, approximately half of a surrounding layer. The proteins closely surround the base of the latex to leave pore-shaped structures when the spheres are removed. The surface areas between the rings are not completely filled at this lower protein ratio (Figures 6.7E, 6.7F). A more ordered, tighter packing can be produced with changes in solution conditions.

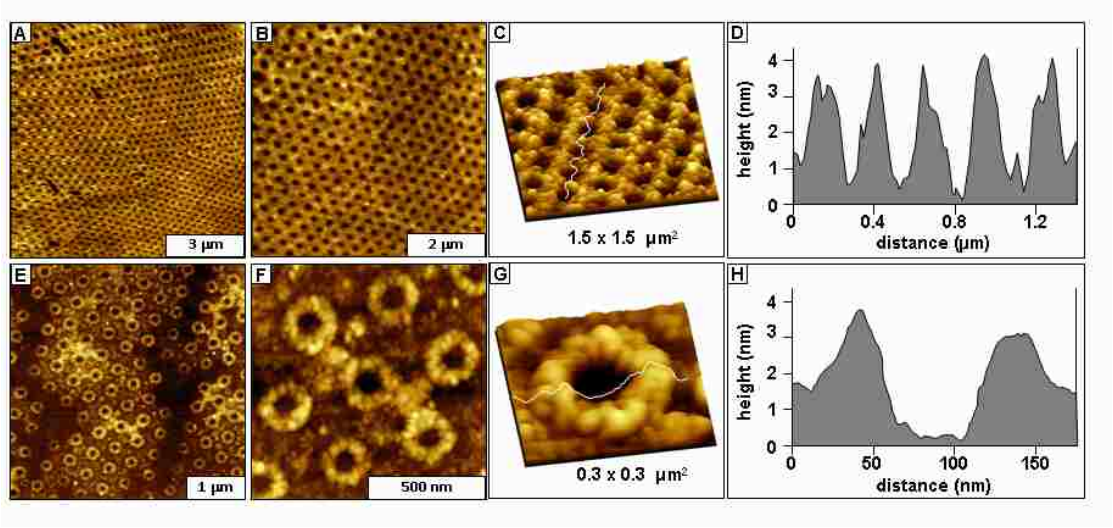

Figure 6.7 The ratios of protein:latex determine the morphology of patterns. [A] AFM topograph (10 × 10 µm^2) of pore-shaped structures produced at high ratio with 300 nm latex; [B] zoom-in view of pore structures (6 × 6 µm^2); [C] View of the 3-D surface morphology; [D] cursor profile for the line in **C**. At lower protein:latex ratio, ring-shaped structures were produced [E] using 300 nm spheres (4 × 4 µm^2); [F] zoom-in view of hexagonal arrangementof rings (1 × 1 µm^2); [G] view of a single ring of BSA; [H] line profile for **G**.

The compact hexagonal arrangement of patterns is clearly viewed in the 4 × 4 µm^2 frame, with a few BSA scattered between rings. The periodicity of the nanopatterns measures 283 ± 16 nm which matches well with the expected 300 nm diameter of the latex templating particles.

Approximately 26% of the surface is covered with rings of BSA, thus the surface coverage can be tuned by controlling the ratio of proteins and spheres. A zoom-in topograph (1 × 1 µm^2) in Figure 6.7F displays a hexagonal arrangement of BSA rings. A few BSA clusters are attached to the surface between the ring-shaped nanostructures. A 3D representation of a single ring clearly reveals the assemblies of BSA molecules (Figure 6.7G). The height of BSA nanostructures can be measured by referencing the uncovered areas of mica as a baseline. The height of the rings measure 3.7 ± 0.4 nm, matching the expected dimension of a single layer of BSA (Figure 6.7H).

Particle lithography provides a simple and effective approach for producing nanoscale protein structures. Once the experimental conditions have been chosen, dozens of samples prepared with those conditions reveal similar morphologies. The surface morphologies were highly consistent and reproducible for a given ratio and particle diameter. All of the examples of protein nanopatterns presented exhibit circular or ring shaped nanostructures, when using solution-based approach for particle lithography. These results are quite different from results cited from literature reports using methods of metal evaporation, which disclose triangular or pyramid nanostructures. Our approach for solution particle lithography does not use a mask and evaporation of metals at high temperatures; rather the mesospheres serve as a structural template during ambient drying. In solution, the proteins assemble surrounding the base of the latex or silica spheres when dried, conforming to the shape of the particle templates. Therefore, the circular ring or pore morphologies are determined by the spherical shape of the mesospheres.

6.5 Conclusion

Particle lithography is a highly reproducible approach applying straightforward bench chemistry steps to prepare millions of individual protein nanostructures on surfaces. Particle lithography provides a high throughput route to control the coverage and dimensions of surface structures of proteins at the scale of nanometers. The generality of this approach was demonstrated with various surfaces (mica, gold, glass) and different proteins (ferritin, apoferritin, IgG, BSA). By varying the ratio of proteins to mesoparticles, different pattern morphologies such as rings or pores are produced. The arrangement of proteins reflects the long range order, dimensions and periodicity according to the hexagonal packing of templating mesospheres.

6.6 Future Perspective

The examples presented with model proteins represent a solid beginning for development of more complex surface-bound bioassays. Periodic arrays of nanostructures offer a valuable test platform for studies of surface chemistry at the nanoscale. A number of possible experiments and potential applications are envisioned, since well-defined arrays of nanostructures enable precise reproducible dimensions for successive measurements. As an example, for fundamental AFM investigations of reactions mediated by molecular recognition, the changes in the morphology of protein nanostructures can be monitored after chemical agents, nanoparticles or other small molecules are introduced to protein nanopatterns. Well-defined protein arrays offer precise reproducible surface features for multiple measurements. By performing experiments in aqueous buffers, studies of protein-DNA interactions and antigen-antibody binding can be accomplished by imaging the evolution of surface changes during biochemical reactions. The particle templates used for preparing test platforms can be scaled to ever smaller dimensions, for studies of size-dependent properties at tens of nanometers, approaching single-molecule detection.

6.7 Executive Summary

There is a growing need for methods which can reproducibly create organized arrays of nanomaterials with high throughput and low-cost. Particle lithography provides such an approach for rapidly preparing millions of exquisitely uniform nanometer-sized structures on flat surfaces using basic steps of benchtop chemistry. Surface self-assembly is emerging as an indispensable approach for organizing materials at the molecular scale for practical reasons such as low cost, applicability to a wide range of nanomaterials, and capabilities for high throughput manufacture of regularly shaped surface structures. Unlike methods of particle lithography with

metal evaporation which produce periodic arrays of triangular structures, solution-based particle lithography creates rings and pore shaped geometries. Particle lithography provides a toolkit for fabricating protein nanopatterns on flat surfaces, providing superb control of the spacing and arrangement of nanostructures. With particle lithography, chemists can inexpensively produce robust, regular nanostructures using the conventional tools of mixing, centrifuging and drying. With particle lithography, millions of nanostructures can be prepared on a range of different surfaces with relatively few defects and high reproducibility. The nanopatterns may potentially be applied for engineering the surfaces of biochips and biosensors.

CHAPTER 7. CONCLUSIONS AND FUTURE PROSPECTS

7.1 Conclusions

New methods of nanolithography applying scanning probe microscopy and latex particle lithography were developed and applied to refine critical parameters used to link and to organize proteins on surfaces. The effectiveness of different bioconjugation chemistries were evaluated using protein binding experiments characterized by AFM. A key advantage of *in situ* AFM investigations is the capability to accomplish experiments under physiological conditions in aqueous buffers with molecular resolution. The versatility of nanografting with *n*-alkanethiol SAMs was demonstrated for protein nanopatterning, providing a systematic approach for directly viewing surface reactions with antibodies and proteins.

Methods for automated nanografting were developed for producing arrays of SAM nanopatterns as a platform to define the adsorption of proteins.[338] New protocols were developed for arranging and orienting proteins on arrays of SAM nanopatterns, towards improving the selectivity and sensitivity of surface-based protein assays. Nanografting is a valuable tool for controlling parameters such as the size, arrangement, geometry, spacing, packing density and the composition of nanopatterned test elements. Highly sophisticated arrangements and geometries were produced for *n*-alkanethiol nanopatterns using automated nanografting. Nanoscale precision and high reproducibility was achieved for arrays of nanografted patterns of SAMs.[339]

Nanografting provides a new self-assembly mechanism to direct the upright orientation of patterned α,ω-alkanedithiol molecules.[340] Designed surfaces that present thiol groups are ideal for adsorption of proteins,[339, 341] metal nanoparticles[342] and for selective metal deposition.[141] Chemical activation of SAM head groups was used to covalently attach proteins

to the nanostructure arrays for AFM investigations. Covalent attachment of proteins on nanostructures using EDC and NHS coupling reagents was accomplished for the first time at the nanometer scale to activate carboxylate groups of an array of SAM nanopatterns.[339]

Particle lithography was applied for high-throughput protein patterning to prepare millions of protein nanostructures on surfaces. The model proteins ferritin, apoferritin, IgG, and BSA were patterned on various surfaces such as mica, gold and glass, which illustrates the generality and reproducibility of the particle lithography.[343] For lithography with monodisperse mesoparticles of latex or silica, straightforward bench chemistry steps of mixing, drying and rinsing provided exquisite control for the surface coverage and periodicity of protein arrays for a range of surfaces. Periodic arrays of rings and pore shaped geometries were produced for protein-mesoparticle solutions, rather than the triangular structures more commonly reported to be formed with evaporative particle lithography of metals. Parameters such as the size of the template mesoparticles and the ratio of particle to proteins were varied to produce desired surface structures. Particle lithography with a low ratio of proteins to mesospheres produced ring patterns of a single layer of proteins. At higher ratios of proteins to mesospheres, a monolayer of proteins with uncovered pore structures was produced. Particle lithography is not only a high throughput method for nanostructuring surfaces, it is also time and cost efficient.

Insight can be gained towards improving the reliability and sensitivity of biosensor or biochip surfaces for optimizing experimental conditions such as concentration, buffer pH, reaction time and fabrication parameters. Few protein assays have been conducted using AFM, and this new direction holds promise for defining a new set of analytical methods for nanoscale investigations.

7.2 Future Prospectus

The results presented in this dissertation are groundwork for future nanoscale protein assays. Many new and exciting experiments are envisioned. For example, changes in morphology of proteins can be studied when chemicals, nanoparticles or other small molecules react with protein nanopatterns. As the capabilities of AFM and SPL improve with innovations and technical improvements by SPM manufacturers, one can anticipate that the technical difficulties and skill requirements for nanoscale surface investigations will not be as prohibitive for accomplishing biochemical assays with AFM.

Particle lithography is a rapid means to create protein nanostructures for *in situ* protocols, producing nanostructures which are amenable to even be used for micro scale fluorescence assays. Particle lithography with SAMs followed by selective protein adsorption would provide a further protocol to be developed for protein nanopatterning. Future directions will be to identify and develop assays of diagnostic importance, in which AFM provides the ultimate capabilities for small reagent volumes and molecular-level detection.

REFERENCES

1. Li, L.; Chen, S.; Jiang, S., Protein adsorption on alkanethiolate self-assembled monolayers: Nanoscale surface structural and chemical effects. *Langmuir* **2003,** 19, 2974-2982.

2. O'Brien, J. C.; Jones, V. W.; Porter, M. D., Immunosensing Platforms Using Spontaneously Adsorbed Antibody Fragments on Gold. *Anal. Chem.* **2000,** 72, 703-710.

3. Delamarche, E.; Sundarababu, G.; Biebuyck, H.; Michel, B.; Gerber, C.; Sigrist, H.; Wolf, H.; Ringsdorf, H.; Xanthopoulos, N.; Mathieu, H. J., Immobilization of antibodies on a photoactive self-assembled monolayer on gold. *Langmuir* **1996,** 12, (8), 1997-2006.

4. Rowe, C. A.; Tender, L. M.; Feldstein, M. J.; Golden, J. P.; Scruggs, S. B.; MacCraith, B. D.; Cras, J. J.; Ligler, F. S., Array biosensor for simultaneous identification of bacterial, viral, and protein analytes. *Anal. Chem.* **1999,** 71, (17), 3846-3852.

5. Lynch, M.; Mosher, C.; Huff, J.; Nettikadan, S.; Johnson, J.; Henderson, E., Functional protein nanoarrays for biomarker profiling. *Proteomics* **2004,** 4, 1695-1702.

6. Scouten, W. H.; Luong, J. H. T.; Brown, R. S., Enzyme or Protein Immobilization Techniques for Applications in Biosensor Design. *Trends Biotechnol.* **1995,** 13, (5), 178-185.

7. Zhang, S. G.; Yan, L.; Altman, M.; Lassle, M.; Nugent, H.; Frankel, F.; Lauffenburger, D. A.; Whitesides, G. M.; Rich, A., Biological surface engineering: a simple system for cell pattern formation. *Biomaterials* **1999,** 20, (13), 1213-1220.

8. Dillmore, W. S.; Yousaf, M. N.; Mrksich, M., A photochemical method for patterning the immobilization of ligands and cells to self-assembled monolayers. *Langmuir* **2004,** 20, 7223-7231.

9. Kane, R. S.; Takayama, S.; Ostuni, E.; Ingber, D. E.; Whitesides, G. M., Patterning proteins and cells using soft lithography. *Biomaterials* **1999,** 20, 2363-2376.

10. James, C. D.; Davis, R. C.; Kam, L.; Craighead, H. G.; Isaacson, M.; Turner, J. N.; Shain, W., Patterned protein layers on solid substrates by thin stamp microcontact printing. *Langmuir* **1998,** 14, (4), 741-744.

11. Lahiri, J.; Ostuni, E.; Whitesides, G. M., Patterning Ligands on Reactive SAMs by Microcontact Printing. *Langmuir* **1999,** 15, 2055-2060.

12. Bernard, A.; Renault, J. P.; Michel, B.; Bosshard, H. R.; Delamarche, E., Microcontact printing of proteins. *Adv. Mater.* **2000,** 12, (14), 1067-1070.

13. Bernard, A.; Delamarche, E.; Schmid, H.; Michel, B.; Bosshard, H. R.; Biebuyck, H., Printing Patterns of Proteins. *Langmuir* **1998,** 14, 2225-2229.

14. Whitesides, G. M.; Ostuni, E.; Takayama, S.; Jiang, X.; Ingber, D. E., Soft Lithography in Biology and Biochemistry. *Annu. Rev. Biomed. Eng.* **2001,** 3, 335-373.

15. Blawas, A. S.; Oliver, T. F.; Pirrung, M. C.; Reichert, W. M., *Langmuir* **1998,** 14, 4243.

16. Nicolau, D. V.; Taguchi, T.; Taniguchi, H.; Yoshikawa, S., Micron-sized protein patterning on diazonaphthoquinone/novolak thin polymeric films. *Langmuir* **1998,** 14, (7), 1927-1936.

17. Dontha, N.; Nowall, W. B.; Kuhr, W. G., Generation of biotin/avidin/enzyme nanostructures with maskless photolithography. *Anal. Chem.* **1997,** 69, (14), 2619-2625.

18. Delamarche, E.; Bernard, A.; Schmid, H.; Bietsch, A.; Michel, B.; Biebuyck, H., Microfluidic networks for chemical patterning of substrate: Design and application to bioassays. *J. Am. Chem. Soc.* **1998,** 120, (3), 500-508.

19. Patel, N.; Sanders, G. H. W.; Shakesheff, K. M.; Cannizzaro, S. M.; Davies, M. C.; Langer, R.; Roberts, C. J.; Tendler, S. J. B.; Williams, P. M., Atomic force microscopic analysis of highly defined protein patterns formed by microfluidic networks. *Langmuir* **1999,** 15, (21), 7252-7257.

20. Kinbara, K.; Aida, T., Toward Intelligent Molecular Machines: Directed Motions of Biological and Artificial Molecules and Assemblies. *Chem. Rev.* **2005,** 105, 1377-1400.

21. Fortina, P.; Kricka, L. J.; Surrey, S.; Grodzinski, P., Nanobiotechnology: the promise and reality of new approaches to molecular recognition. *Trends in Biotechnology* **2005,** 23, 168-173.

22. Kasemo, B., Biological surface science. *Surface Science* **2002,** 500, 656-677.

23. Wong, S. S., *Chemistry of protein conjugation and cross-linking*. CRC Press: Boca Raton, 1991; p 340.

24. Hermanson, G. T., *Bioconjugate techniques*. Academic Press: San Diego, 1996; p 785.

25. Nuzzo, R. G.; Allara, D. L., Adsorption of bifunctional organic disulfides on gold surfaces. *J. Am. Chem. Soc.* **1983,** 105, (13), 4481-4483.

26. Schreiber, S. L., Self-assembled monolayers: from 'simple' model systems to biofunctionalized interfaces. *J. Phys.: Condens. Matter* **2004,** 16, R881-R900.

27. Sagiv, J., Organized monolayers by adsorption - formation and structure of oleophobic mixed monolayers on solid surfaces. *J. Am. Chem. Soc.* **1980,** 102, (1), 92-98.

28. Ulman, A., *An Introduction to Ultrathin Organic Films: from Langmuir-Blodgett to Self-Assembly*. Academic: Boston, MA, 1991.

29. Witt, D.; Klajn, R.; Barski, P.; Grzybowski, B. A., Applications, Properties and Synthesis of w-functionalized n-Alkanethiols and Disulfides - the Building Blocks of Self-Assembled Monolayers. *Current Org. Chem.* **2004,** 8, 1-35.

30. Poirier, G. E., Characterization of Organosulfur Molecular Monolayers on Au(111) using Scanning Tunneling Microscopy. *Chem. Rev.* **1997,** 97, 1117-1127.

31. Schreiber, F., Structure and growth of self-assembling monolayers. *Prog. Surf. Sci.* **2000,** 65, (5-8), 151-256.

32. Dubois, L. H.; Nuzzo, R. G., Synthesis, Structure and Properties of Model Organic Surfaces. *Ann. Rev. Phys. Chem.* **1992,** 43, 437-463.

33. Ulman, A., Formation and Structure of Self-Assembled Monolayers. *Chem. Rev.* **1996,** 96, 1533-1554.

34. Porter, M. D.; Bright, T. B.; Allara, D. L.; Chidsey, C. E. D., Spontaneously organized molecular assemblies. 4. Structural characterization of Normal-alkyl thiol monolayers on gold by optical ellipsometry, infrared-spectroscopy, and electrochemistry. *J. Am. Chem. Soc.* **1987,** 109, 3559-3568.

35. Fenter, P.; Eberhardt, A.; Eisenberger, P., Self-assembly of n-alkyl thiols as disulfides on Au(111). *Science* **1994,** 266, 1216-1218.

36. Schreiber, F., Self-assembled monolayers: from 'simple' model systems to biofunctionalized interfaces. *J. Phys.: Condens. Matter* **2004,** 16, R881-R900.

37. Fenter, P.; Eberhardt, A.; Liang, K. S.; Eisenberger, P., Epitaxy and chainlength dependent strain in self-assembled monolayers *J. Chem. Phys.* **1997,** 106, (4), 1600-1608.

38. Dannenberger, O.; Weiss, K.; Himmel, H. J.; Jager, B.; Buck, M.; Woll, C., An orientation analysis of differently endgroup-functionalised alkanethiols adsorbed on Au substrates. *Thin Solid Films* **1997,** 307, 183-191.

39. Nuzzo, R. G.; Dubois, L. H.; Allara, D. L., Fundamental studies of microscopic wetting on organic surfaces. 1. Formation and structural characterization of a self-consistent series of polyfunctional organic monolayers. *J. Am. Chem. Soc.* **1990,** 112, (2), 558-569.

40. Qian, Y.; Yang, G.; Yu, J.; Jung, T. A.; Liu, G.-Y., Structures of Annealed Decanethiol Self-Assembled Monolayers on Au(111): an Ultrahigh Vacuum Scanning Tunneling Microscopy Study. *Langmuir* **2003,** 19, 6056-6065.

41. Camillone III, N.; Eisenberger, P.; Leung, T. Y. B.; Schwartz, P.; Scoles, G.; Poirier, G. E.; Tarlov, M. J., New monolayer phases of n-alkane thiols self-assembled on Au(111): Preparation, surface characterization, and imaging. *J. Chem. Phys.* **1994,** 101, (12), 11031-11036.

42. Yang, G.; Liu, G.-Y., New Insights for Self-Assembled Monolayers of Organothiols on Au(111) Revealed by Scanning Tunneling Microscopy. *J. Phys. Chem. B* **2003,** 107, 8746-8759.

43. Xiao, X.-D.; Liu, G. Y.; Charych, D. H.; Salmeron, M., Preparation, Structure, and Mechanical Stability of Alkylsilane Monolayers on Mica. *Langmuir* **1995,** 11, 1600-1604.

44. Peanasky, J.; Schneider, H. M.; Granick, S., Self-Assembled Monolayers on Mica for Experiments Utilizing the Surface Forces Apparatus. *Langmuir* **1995,** 11, 953-962.

45. Schwartz, D. K.; Steinberg, S.; Israelachvili, J.; Zasadzinski, J. A. N., Growth of a Self-Assembled Monolayer by Fractal Aggregation. *Phys. Rev. Lett.* **1992,** 63, (23), 3354-3357.

46. Chapman, R. G.; Ostuni, E.; Takayama, S.; Holmlin, R. E.; Yan, L.; Whitesides, G. M., Surveying for Surfaces that Resist the Adsorption of Proteins. *J. Am. Chem. Soc.* **2000,** 122, 8303-8304.

47. Ostuni, E.; Chapman, R. G.; Liang, M. N.; Meluleni, G.; Pier, G.; Ingber, D. E.; Whitesides, G. M., Self-Assembled Monolayers That Resist the Adsorption of Proteins and the Adhesion of Bacterial and Mammalian Cells. *Langmuir* **2001,** 17, 6336-6343.

48. Holmlin, R. E.; Chen, X.; Chapman, R. G.; Takayama, S.; Whitesides, G. M., Zwitterionic SAMs that Resist Nonspecific Adsorption of Protein from Aqueous Buffer. *Langmuir* **2001,** 17, 2841-2850.

49. Ostuni, E.; Chapman, R. G.; Holmlin, R. E.; Takayama, S.; Whitesides, G. M., A Survey of Structure-Property Relationships of Surfaces that Resist the Adsorption of Protein. *Langmuir* **2001,** 17, 5605-5620.

50. Luk, Y.-Y.; Kato, M.; Mrksich, M., Self-Assembled Monolayers of Alkanethiolates Presenting Mannitol Groups are Inert to Protein Adsorption and Cell Attachment. *Langmuir* **2000,** 16, 9604-9608.

51. Herrwerth, S.; Eck, W.; Reinhardt, S.; Grunze, M., Factors that Determine the Protein Resistance of Oligoether Self-Assembled monolayers - Internal Hydrophilicity, Terminal Hydrophilicity, and Lateral packing Density. *J. Am. Chem. Soc.* **2003,** 125, 9359-9366.

52. Tengvall, P.; Jansson, E.; Askendal, A.; Thomsen, P.; Gretzer, C., Preparation of multilayer plasma protein films on silicon by EDC/NHS coupling chemistry. *Colloids and Surfaces B: Biointerfaces* **2003,** 28, 261-272.

53. Binnig, G.; Rohrer, H.; Gerber, C., Surface Studies by Scanning Tunneling Microscopy. *Phys. Rev. Lett.* **1982,** 49, 57.

54. Binnig, G.; Quate, C. F.; Gerber, C., Atomic Force Microscope. *Phys. Rev. Lett.* **1986,** 56, 930.

55. Piner, R. D.; Zhu, J.; Xu, F.; Hong, S.; Mirkin, C. A., "Dip-Pen" Nanolithography. *Science* **1999,** 283, 661-663.

56. Xu, S.; Liu, G. Y., Nanometer-Scale fabrication by Simultaneous Nanoshaving and Molecular Self-Assembly. *Langmuir* **1997,** 13, 127-129.

57. Gorman, C. B.; Fuierer, R. R.; Kramer, S., Scanning Probe Lithography Using Self-Assembled Monolayers. *Chem. Rev.* **2003,** 103, 4367-4418.

58. Garno, J. C.; Amro, N.; Wadu-Mesthrige, K.; Liu, G.-Y., Production of Periodic Arrays of Protein Nanostructures Using Particle Lithography. *Langmuir* **2002,** 18, 8186-8192.

59. Liu, S.; Maoz, R.; Sagiv, J., Planned Nanostructures of Colloidal Gold via Self-Assembly on Hierarchically Assembled Organic Bilayer Template Patterns with In-situ Generated Terminal Amino Functionality *Nano Lett.* **2004,** 4, (5), 845-851.

60. Liu, G.-Y.; Xu, S.; Qian, Y., Nanofabrication of Self-Assembled Monolayers Using Scanning Probe Lithography. *Acc. Chem. Res.* **2000,** 33, 457-466.

61. Lewis, M. S.; Gorman, C. B., Scanning Tunneling Microscope-Based Replacement Lithography on Self-Assembled Monolayers. Investigation of the Relationship between Monolayer Structure and Replacement Bias. *J. Phys. Chem. B* **2004,** 108, 8581-8583.

62. Naujoks, N.; Stemmer, A., Using local surface charges for the fabrication of protein patterns. *Colloids and Surfaces A: Physicochem. Eng. Aspects* **2004,** 249, 69-72.

63. Chen, J.; Reed, M. A.; Asplund, C. L.; Cassell, A. M.; Myrick, M. L.; Rawlett, A. M.; Tour, J. M.; VanPatten, P. G., Placement of conjugated oligomers in an alkanethiol matrix by scanned probe microscope lithography. *Appl. Phys. Lett.* **1999,** 75, (5), 624-626.

64. Gorman, C. B.; Carroll, R. L.; He, Y.; Tian, F.; Fuierer, R., Chemically Well-Defined Lithography Using Self-Assembled Monolayers and Scanning Tunneling Microscopy in Nonpolar Organothiol Solutions. *Langmuir* **2000,** 16, 6312-6316.

65. Zhao, J.; Uosaki, K., Formation of Nanopatterns of a Self-Assembled Monolayer (SAM) within a SAM of Different Molecules Using a Current Sensing Atomic Force Microscope. *Nano Lett.* **2002,** 2, (2), 137-140.

66. Maoz, R.; Cohen, S. R.; Sagiv, J., Nanoelectrochemical Patterning of Monolayer Surfaces: Toward Spatially Defined Self-Assembly of Nanostructures. *Adv. Mater.* **1999,** 11, (1), 55-61.

67. Gu, J.; Yam, C. M.; Li, S.; Cai, C., Nanometric protein arrays on protein-resistant monolayers on silicon surfaces. *J. Am. Chem. Soc.* **2004,** 126, 8098-8099.

68. Xu, S.; Laibinis, P. E.; Liu, G.-Y., Accelerating Self-Assembly on Gold - A Spatial Confinement Effect. *J. Am. Chem. Soc.* **1998,** 120, 9356 - 9361.

69. Xu, S.; Miller, S.; Laibinis, P. E.; Liu, G.-Y., Fabrication of Nanometer Scale Patterns Within Self-Assembled Monolayers by Nanografting. *Langmuir* **1999,** 15, 7244-7251.

70. Hacker, C. A.; Batteas, J. D. B.; Garno, J. C.; Marquez, M.; Richter, C. A.; Richter, L. J.; van Zee, R. D.; Zangmeister, C. D., Structural and Chemical Characterization of Monofluoro-Substituted Oligo(phenylene-ethynylene) Thiolate Self-Assembled Monolayers on Gold. *Langmuir* **2004,** 20, 6195-6205.

71. Liu, J.-F.; Cruchon-Dupeyrat, S.; Garno, J. C.; Frommer, J.; Liu, G.-Y., Three-Dimensional Nanostructure Construction via Nanografting: Positive and Negative Pattern Transfer. *Nano Lett.* **2002,** 2, 937-940.

72. Brower, T. L.; Garno, J. C.; Ulman, A.; Liu, G.-Y.; Yan, C.; Golzhauser, A.; Grunze, M., Self-Assembled Multilayers of 4,4 -Dimercaptobiphenyl Formed by Cu(II) Oxidation. *Langmuir* **2002,** 18, 6207-6216.

73. Liu, M.; Amro, N. A.; Chow, C. S.; Liu, G.-y., Production of Nanostructures of DNA on Surfaces *Nano Lett.* **2002,** 2, (8), 863-867.

74. Cruchon-Dupeyrat, S.; Porthun, S.; Liu, G.-Y., Nanofabrication using computer-assisted design and automated vector-scanning probe lithography. *Appl. Surf. Sci.* **2001,** 175-176, 636-642.

75. Wadu-Mesthrige, K.; Xu, S.; Amro, N. A.; Liu, G.-Y., Fabrication and Imaging of Nanometer-Sized Protein Patterns. *Langmuir* **1999,** 15, 8580-8583.

76. Wadu-Mesthrige, K.; Amro, N. A.; Garno, J. C.; Xu, S.; Liu, G.-Y., Fabrication of Nanometer-Sized Protein Patterns Using Atomic Force Microscopy and Selective Immobilization. *Biophys. J.* **2001,** 80, 1891-1899.

77. Liu, G.-Y.; Amro, N. A., Positioning Protein Molecules on Surfaces: A Nanoengineering Approach to Supramolecular Chemistry. *Proc. Natl. Acad. Sci.* **2002,** 99, 5165-5170.

78. Zhou, D.; Wang, X.; Birch, L.; Rayment, T.; Abell, C., AFM Study on Protein Immobilization on Charged Surfaces at the Nanoscale: Toward the Fabrication of Three-Dimensional Protein Nanostructures. *Langmuir* **2003,** 19, 10557-10562.

79. Kenseth, J. R.; Harnisch, J. A.; Jones, V. W.; Porter, M. D., Investigation of Approaches for the Fabrication of Protein Patterns by Scanning Probe Lithography. *Langmuir* **2001,** 17, 4105-4112.

80. Jang, C.-H.; Stevens, B. D.; Phillips, R.; Calter, M. A.; Ducker, W. A., A Strategy for the Sequential Patterning of Proteins: Catalytically Active Multiprotein Nanofabrication. *Nano Lett.* **2003,** 3, (6), 691-694.

81. Case, M. A.; McLendon, G. L.; Hu, Y.; Vanderlick, T. K.; Scoles, G., Using Nanografting to Achieve Directed Assembly of de novo Designed Metalloproteins on Gold. *Nano Lett.* **2003,** 3, (4), 425-429.

82. Ginger, D. S.; Zhang, H.; Mirkin, C. A., The Evolution of Dip-Pen Nanolithography. *Angewandte Chemie* **2004,** 43, 30-45.

83. Hong, S.; Zhu, J.; Mirkin, C. A., A New Tool for Studying the in situ Growth Processes for Self-Assembled Monolayers under Ambient Conditions. *Langmuir* **1999,** 15, 7897-7900.

84. Hong, S.; Mirkin, C. A., A Nanoplotter with Both Parallel and Serial Writing Capabilities. *Science* **2000,** 288, 1808-1811.

85. Mirkin, C. A.; Hong, S.; Demers, L., Dip-Pen Nanolithography: Controlling Surface Architecture on the Sub-100 Nanometer Length Scale. *Chemphyschem* **2001,** 2, 37-39.

86. Sheehan, P. E.; Whitman, L. J., Thiol diffusion and the Role of Humidity in "Dip Pen Nanolithography". *Phys. Rev. Lett.* **2002,** 88, (15), 1561041-1561044.

87. Lee, K.-B.; Park, S.-J.; Mirkin, C. A.; Smith, J. C.; Mrksich, M., Protein Nanoarrays Generated By Dip-Pen Nanolithography. *Science* **2002,** 295, 1702-1705.

88. Kwak, S. K.; Lee, G. S.; Ahn, D. J.; Choi, J. W., Pattern formation of cytochrome c by microcontact printing and dip-pen nanolithography. *Materials Science and Engineering C* **2004,** 24, 151-155.

89. Cho, Y.; Ivanisevic, A., SiO*x* Surfaces with Lithographic Features Composed of a TAT Peptide. *J. Phys. Chem. B* **2004,** 108, 15223-15228.

90. Hyun, J.; Ahn, S. J.; Lee, W. K.; Chilkoti, A.; Zauscher, S., Molecular recognition-mediated fabrication of protein nanostructures by dip-pen lithography. *Nano Letters* **2002,** 2, (11), 1203-1207.

91. Smith, J. C.; Lee, K.-B.; Wang, Q.; Finn, M. G.; Johnson, J. E.; Mrksich, M.; Mirkin, C. A., Nanopatterning the Chemospecific Immobilization of Cowpea Mosaic Virus Capsid. *Nano Lett.* **2003,** 3, (7), 883-886.

92. Hyun, J.; Lee, W.-K.; Nath, N.; Chilkoti, A.; Zauscher, S., Capture and Release of Proteins on the Nanoscale by Stimuli-Responsive Elastin-Like Polypeptide ₸Switches₮. *J. Am. Chem. Soc.* **2004,** 126, 7330-7335.

93. Wilson, D. L.; Martin, R.; Hong, S.; Cronin-Golomb, M.; Mirkin, C. A.; Kaplan, D. L., Surface organization and nanopatterning of collagen by dip-pen nanolithography. *Proc. Natl. Acad. Sci.* **2001,** 98, (24), 13660-13664.

94. Lim, J.-H.; Ginger, D. S.; Lee, K.-B.; Heo, J.; Nam, J.-M.; Mirkin, C. A., Direct-Write Dip-Pen Nanolithography of Proteins on Modified Silicon Oxide Surfaces. *Angew. Chem. Int. Ed.* **2003,** 42, 2309-2312.

95. Lee, K.-B.; Lim, J.-H.; Mirkin, C. A., Protein Nanostructures Formed via Direct-Write Dip-Pen Nanolithography. *J. Am. Chem. Soc.* **2003,** 125, 5588-5589.

96. Nam, J.-M.; Han, S. W.; Lee, K.-B.; Liu, X.; Ratner, M. A.; Mirkin, C. A., Bioactive Protein Nanoarrays on Nickel Oxide Surfaces Formed by Dip-Pen Nanolithography. *Angew. Chem. Int. Ed.* **2004,** 43, 1246-1248.

97. Li, Y.; Maynor, B. W.; Liu, J., Electrochemical AFM "Dip-Pen" Nanolithography. *J. Am. Chem. Soc.* **2001,** 123, 2105-2106.

98. Agarwal, G.; Naik, R. R.; Stone, M. O., Immobilization of histidine-tagged proteins on nickel by electrochemical dip pen nanolithography. *Journal Of The American Chemical Society* **2003,** 125, (24), 7408-7412.

99. Haynes, C. L.; Van Duyne, R. P., Nanosphere Lithography: A Versatile Nanofabrication Tool for Studies of Size-Dependent Nanoparticle Optics. *J. Phys. Chem. B* **2001,** 105, 5599-5611.

100. Frey, W.; Woods, C. K.; Chilkoti, A., Ultraflat nanosphere lithography: A new method to fabricate flat nanostructures. *Adv. Mater.* **2000,** 12, (20), 1515-1519.

101. Xia, Y. N.; Gates, B.; Yin, Y. D.; Lu, Y., Monodispersed colloidal spheres: Old materials with new applications *Adv. Mater.* **2000,** 12, 693-713.

102. Jiang, P.; Hwang, K. S.; Mittleman, D. M.; Bertone, J. F.; Colvin, V. L., Template-Directed Preparation of Macroporous Polymers with Oriented and Crystalline Arrays of Voids *J. Am. Chem. Soc.* **1999,** 121, (50), 11630-11637.

103. Denis, F. A.; Hanarp, P.; Surtherland, D. S.; Dufrene, Y. F., Nanoscale Chemical Patterns Fabricated by Using Colloidal Lithography and Self-Assembled Monolayers. *Langmuir* **2004,** 20, 9335-9339.

104. Michel, R.; Reviakine, I.; Sutherland, D.; Fokas, C.; Csucs, G.; Danuser, G.; Spencer, N. D.; Textor, M., A Novel Approach to Produce Biologically Relevant Chemical Patterns at the Nanometer Scale: Selective Molecular Assembly Patterning Combined with Colloidal Lithography. *Langmuir* **2002,** 18, 8580-8586.

105. Marquette, C. A.; Degiuli, A.; Imbert-Laurenceau, E.; Mallet, F.; Chaix, C.; Mandrand, B.; Blum, L. J., Latex bead immobilisation in PDMS matrix for the detection of p53 gene point mutation and anit-HIV-1 capsid protein antibodies. *Anal Bioanal Chem* **2005,** 381, 1019-1024.
106. MacBeath, G., Protein microarrays and proteomics. *Nature Genetics Supplement* **2002,** 32, 526-532.

107. Eggers, M.; Hogan, M.; Reich, R. K.; Lamture, J.; Ehrlich, D.; Hollis, M.; Kosicki, B.; Powdrill, T.; Beattie, K.; Smith, S.; Varma, R.; Gangadharan, R.; Mallik, A.; Burke, B.; Wallace, D., Microchip for quantitative detection of molecules utilizing luminescent and radioisotope reporter groups. *Biotechniques* **1994,** 17, 516.

108. Kunz, R. E., Miniature integrated optical modules for chemical and biochemical sensing. *Sensors Actuators B-Chemical* **1997,** 38, (1-3), 13-28.

109. Lee, K.-B.; Kim, E.-Y.; Mirkin, C. A.; Wolinsky, S. M., The Use of Nanoarrays for Highly Sensitive and Selective Detection of Human Immunodeficiency Virus Type 1 in Plasma. *Nano Lett.* **2004,** 4, (10), 1869-1872.

110. Wilson, D. S.; Nock, S., Functional protein microarrays *Current Opinion in Chemical Biology* **2002,** 6, (1), 81-85.

111. Templin, M. F.; Stoll, D.; Schrenk, M.; Traub, P. C.; Vohringer, C. F.; Joos, T. O., Protein microarray technology. *Trends Biotechnol.* **2002,** 20, (4), 160-166.

112. Schweitzer, B.; Kingsmore, S. F., Measuring proteins on microarrays *Current Opinion in Chemical Biotechnology* **2002,** 13, (1), 14-19.

113. Blawas, A. S.; Reichert, W. M., Protein patterning. *Biomaterials* **1998,** 19, 595-609.

114. Bergveld, P., The future of biosensors. *Sensors Actuators A-Physical* **1996,** 56, (1-2), 65-73.

115. Templin, M. F.; Stoll, D.; Schwenk, J. M.; Pötz, O.; Kramer, S.; Joos, T. O., Protein microarrays: Promising tools for proteomic research. *Proteomics* **2003,** 3, 2155-2166.

116. Walt, D. R., Miniature Analytical Methods for Medical Diagnostics. *Science* **2005,** 308, 217-219.

117. Chan, W., C. W.; Nie, S., Quantum Dot Bioconjugates for Ultrasensitive Nonisotopic Detection. *Science* **1998,** 281, 2016-2018.

118. Baselt, D. R.; Lee, G. U.; Colton, R. J., Biosensor based on force microscope technology. *J. Vac. Sci. Technol. B* **1996,** 14, (2), 789-793.

119. Wouters, D.; Schubert, U. S., Nanolithography and Nanochemistry: Probe-Related Patterning Techniques and Chemical Modification for Nanometer-Sized Devices. *Angew. Chem. Int. Ed.* **2004,** 43, 2480 - 2495.

120. Minne, S. C.; Flueckiger, P.; Soh, H. T.; Quate, C. F., Atomic force microscope lithography using amorphous silicon as a resist and advances in parallel operation. *J. Vac. Sci. Technol. B* **1995,** 13, (3), 1380-1385.

121. Minne, S. C.; Adams, J. D.; Yaralioglu, G.; Manalis, S. R.; Atalar, A.; Quate, C. F., Centimeter scale atomic force microscope imaging and lithography. *Appl. Phys. Lett.* **1998,** 73, (13), 1742-1744.

122. Minne, S. C.; Manalis, S. R.; Atalar, A.; Quate, C. F., Independent parallel lithography using the atomic force microscope. *J. Vac. Sci. Technol. B* **1996,** 14, (4), 2456-2461.

123. Chow, E. M.; Yaralioglu, G.; Quate, C. F.; Kenny, T. W., Characterization of a two-dimensional cantilever array with through-wafer electrical interconnects. *Appl. Phys. Lett.* **2002,** 80, (4), 664-666.

124. Chow, E. M.; Soh, H. T.; Lee, H. C.; Adams, J. D.; Minne, S. C.; Yaralioglu, G.; Atalar, A.; Quate, C. F.; Kenny, T. W., Integration of through-wafer interconnects with a two-dimensional cantilever array. *Sensors Actuators A-Physical* **2000,** 83, 118-123.

125. Sulchek, T.; Grow, R. J.; Yaralioglu, G.; Minne, S. C.; Quate, C. F., Parallel atomic force microscopy with optical interferometric detection. *Appl. Phys. Lett.* **2001,** 78, (12), 1787-1789.

126. Hafizovic, S.; Barrettino, D.; Volden, T.; Sedivy, J.; Kirstein, k.-U.; Brand, O.; Hierlemann, A., Single-chip mechatronic microsystem for surface imaging and force response studies. *Proc. Natl. Acad. Sci.* **2004,** 101, (49), 17011-17015.

127. Akiyama, T.; Staufer, U.; deRooij, N. F.; Lange, D.; Hagleitner, C.; Brand, O.; Baltes, H.; Tonin, A.; Hidber, H. R., Integrated atomic force microscopy array probe with metal-oxide-semiconductor field effect transistor stress sensor, thermal bimorph actuator, and on-chip complementary metal-oxide-semiconductor electronics. *J. Vac. Sci. Technol. B* **2000,** 18, (6), 2669-2675.

128. Volden, T.; Zimmerman, M.; Lange, D.; Brand, O.; Baltes, H., Dynamics of CMOS-based thermally actuated cantilever arrays for force microscopy. *Sensors Actuators A-Physical* **2004,** 115, 516-522.

129. Bullen, D.; Chung, S.-W.; Wang, X.; Zou, J.; Mirkin, C. A.; Liu, C., Parallel dip-pen nanolithography with arrays of individually addressable cantilevers. *Appl. Phys. Lett.* **2004,** 84, (5), 789-791.

130. Wang, X.; Bullen, D.; Zou, J.; Liu, C.; Mirkin, C. A., Thermally actuated probe array for parallel dip-pen nanolithography. *J. Vac. Sci. Technol. B* **2004,** 22, (6), 2563-2567.

131. Zou, J.; Bullen, D.; Wang, X.; Liu, C.; Mirkin, C. A., Conductivity-based contact sensing for probe arrays in dip-pen nanolithography. *Appl. Phys. Lett.* **2003,** 83, (3), 581-583.

132. Zhang, M.; Bullen, D.; Chung, S.-W.; Hong, S.; Ryu, K. S.; Fan, Z.; Mirkin, C. A.; Liu, C., A MEMS nanoplotter with high-density parallel dip-pen nanolithography probe arrays. *Nanotechnol.* **2002,** 13, 212-217.

133. Hong, S.; Mirkin, C. A., Multiple Ink Nanolithography: Toward a Multiple-Pen Nano-Plotter. *Science* **1999,** 286, 523-525.

134. Su, M.; Li, S.; Dravid, V. P., Miniaturized Chemical Multiplexed Sensor Array. *J. Am. Chem. Soc.* **2003,** 125, 9930-9931.

135. King, W. P.; Kenny, T. W.; Goodson, K. E.; Cross, G. L. W.; Despont, M.; Durig, U. T.; Rothuizen, H.; Binnig, G.; Vettiger, P., Design of Atomic Force Microscope Cantilevers for Combined Thermomechanical Writing and Thermal Reading in Array Operation. *J. Microelectricalmechanical Systems* **2002,** 11, (6), 765-774.

136. Lutwyche, M.; Andreoli, C.; Binnig, G.; Brugger, J.; Drechsler, U.; Haberle, W.; Rohrer, H.; Rothuizen, H.; Vettiger, P.; Yaralioglu, G.; Quate, C. F., 5 X 5 2D AFM cantilever arrays a first step towards Terabit storage device. *Sensors Actuators A-Physical* **1999,** 73, 89-94.

137. Vettiger, P.; Despont, M.; Drechsler, U.; Durig, U. T.; Haberle, W.; Lutwyche, M.; Rothuizen, H.; Stutz, R.; Widmer, R.; Binnig, G. K., The "Millipede" -- one thousand tips for future AFM data storage. *IBM J. Res. Develop.* **2000,** 44, (3), 323-340.

138. Xu, S.; Liu, G.-Y., Nanometer-scale fabrication by simultaneous nanoshaving and molecular self-assembly. *Langmuir* **1997,** 13, 127-129.

139. Price, W. P.; Kuo, P. K.; Lee, T. R.; Colorado, R. J.; Ying, Z. C.; Liu, G. Y., Probing the local structure and mechanical response of nanostructures using force modulation and nanofabrication. *Langmuir* **2005,** 21, 8422-8428.

140. Liu, J. F.; Cruchon-Dupeyrat, S.; Garno, J. C.; Frommer, J.; Liu, G.-Y., Three-dimensional nanostructure construction via nanografting: positive and negative pattern transfer. *Nano Lett.* **2002,** 2, 937-940.

141. Garno, J. C.; Zangmeister, C. D.; Batteas, J. D., Directed Electroless Growth of Metal Nanostructures on Patterned Self-Assembled Monolayers. *Langmuir* **2007,** 23, 7874-7879.

142. Wadu-Mesthrige, K.; Amro, N. A.; Liu, G.-Y., Immobilization of proteins on self-assembled monolayers. *Scanning* **2000,** 22, 380-388.

143. Wadu-Mesthrige, K.; Xu, S.; Amro, N. A.; Liu, G.-Y., Fabrication and imaging of nanometer-sized protein patterns. *Langmuir* **1999,** 15, (25), 8580-8583.

144. Roco, M. C.; Bainbridgem, W. S., Societal implications of nanoscience and nanotechnology: Maximizing human benefit. *J. Nanoparticle Res.* **2005,** 7, 1-13.

145. www.nano.gov Nanotechnology - Big Things from a Tiny World.

146. Ngunjiri, J. N.; Li, J.-R.; Garno, J. C., Nanolithography: Towards Fabrication of Nanodevices for Life Sciences. In *Nanotechnologies for the Life Sciences*, Kumar, C. S. S. R., Ed. Wiley-VCH Verlag GmbH & Co.: Weinheim, 2006; Vol. 4, pp 67-108.

147. Love, J. C.; Estroff, L. A.; Kriebel, J. K.; Nuzzo, R. G.; Whitesides, G. M., Self-assembled monolayers of thiolates on metals as a form of nanotechnology. *Chem. Rev.* **2005,** 105, (4), 1103-1169.

148. Hong, S.; Zhu, J.; Mirkin, C. A., Multiple ink nanolithography:toward a multiple-pen nano-plotter. *Science* **1999,** 286, 523-525.

149. Hong, S.; Zhu, J.; Mirkin, C. A., A new tool for studying the in situ growth processes for self-assembled monolayers under ambient conditions *Langmuir* **1999,** 15, 7897-7900.

150. Ginger, D.; Zhang, H.; Mirkin, C. A., The evolution of dip-pen nanolithography. *Angew. Chem. Int. Ed.* **2004,** 43, 30-45.

151. Kramer, S.; Fuierer, R. R.; Gorman, C. B., Scanning probe lithography using self-assembled monolayers. *Chem. Rev.* **2003,** 103, (11), 4367-4418.

152. Gorman, C. B.; Carroll, R. L.; He, Y. F.; Tian, F.; Fuierer, R., Chemically well-defined lithography using self-assembled monolayers and scanning tunneling microscopy in nonpolar organothiol solutions. *Langmuir* **2000,** 16, (15), 6312-6316.

153. Maoz, R.; Frydman, E.; Cohen, S. R.; Sagiv, J., "Constructive nanolithography": Inert monolayers as patternable templates for in-situ nanofabrication of metal-semiconductor-organic surface structures - A generic approach. *Adv. Mater.* **2000,** 12, (10), 725-731.

154. Peter, M.; Li, X. M.; Huskens, J.; Reinhoudt, D. N., Catalytic probe lithography: Catalyst-functionalized scanning probes as nanopens for nanofabrication on self-assembled monolayers. *J. Am. Chem. Soc.* **2004,** 126, (37), 11684-11690.

155. Garno, J. C.; Batteas, J. D., Nanofabrication with Self-Assembled Monolayers by Scanning Probe Lithography. In *Applied Scanning Probe Methods*, Bhushan, B.; Fuchs, H., Eds. Springer-Verlag: Berlin Heidelberg 2006; Vol. IV, pp 105-135.

156. Liu, G.-Y.; Xu, S.; Qian, Y., Nanofabrication of self-assembled monolayers using scanning probe lithography. *Acc. Chem. Res.* **2000,** 33, 457-466.

157. Garcia, R.; Martinez, R. V.; Martinez, J., Nano-chemistry and scanning probe nanolithographies. *Chem. Soc. Rev.* **2006,** 35, (1), 29-38.

158. Piner, R. D.; Hong, S.; Mirkin, C. A., Improved Imaging of Soft Materials with Modified AFM Tips. *Langmuir* **1999,** 15, 5457-5460.

159. Wei, Z. Q.; Wang, C.; Bai, C. L., Surface imaging of fragile materials with hydrophobic atomic force microscope tips. *Surf. Sci.* **2000,** 467, 185-190.

160. Knapp, H. F.; Stemmer, A., Preparation, comparison and performance of hydrophobic AFM tips. *Surf. Interface Anal.* **1999,** 27, 324-331.

161. Zhou, D.; Wang, X.; Birch, L.; Rayment, T.; Abell, C., AFM Study on Protein Immobilization on Charged Surfaces at the Nanoscale: Toward the Fabricaiton of Three-Dimensional Protein Nanostructures. *Langmuir* **2003,** 19, 10557-10562.

162. Kenseth, J. R.; Harnisch, J. A.; Jones, V. W.; Porter, M. D., Investigation of approaches for the fabrication of protein patterns by scanning probe lithography. *Langmuir* **2001,** 17, (13), 4105-4112.

163. Case, M. A.; McLendon, G. L.; Hu, Y.; Vanderlick, T. K.; Scoles, G., Using Nanografting to Achieve Directed Assembly of de novo Designed Metalloproteins on Gold. *Nano Lett.* **2003,** 3, 425-429.

164. Cheung, C. L.; Camarero, J. A.; Woods, B. W.; Lin, T.; Johnson, J. E.; DeYoreo, J. J., Fabrication of Assembled Virus Nanostructures on Templates of Chemoselective Linkers Formed by Scanning Probe Nanolithography. *J. Am. Chem. Soc.* **2003,** 125, 6848-6849.

165. Jang, C.-H.; Stevens, B. D.; Phillips, R.; Calter, M. A.; Ducker, W. A., A Strategy for the Sequential Patterning of Proteins: Catalytically Active Multiprotein Nanofabrication. *Nano Lett.* **2003,** 3, 691-694.

166. Wagner, P.; Zaugg, F.; Kernen, P.; Hegner, M.; Semenza, G., functionalized self-assembled monolayers chemisorbed on ultraflat Au(111) surfaces for biological scanning probe microscopy in aqueous buffers. *J. Vac. Sci. Technol. B* **1996,** 14, 1466-1471.

167. Hegner, M.; Wagner, P.; Semenza, G., Ultraflat atomically flat template-stripped Au surfaces for scanning probe microscopy. *Surf. Sci.* **1993,** 291, 39-46.

168. Neumeister, J. M.; Ducker, W. A., Lateral, Normal, and Longitudinal Spring Constants of Atomic-Force Microscopy Cantilevers. *Review of Scientific Instruments* **1994,** 65, (8), 2527-2531.

169. Hutter, J. L.; Bechhoefer, J., Calibration of Atomic-Force Microscope Tips. *Review of Scientific Instruments* **1993,** 64, (7), 1868-1873.

170. Sader, J. E.; Larson, I.; Mulvaney, P.; White, L. R., Method for the Calibration of Atomic-Force Microscope Cantilevers. *Review of Scientific Instruments* **1995,** 66, (7), 3789-3798.

171. Xu, S.; Laibinis, P. E.; Liu, G.-Y., Accelerating the kinetics of thiol self-assembly on gold - a spatial confinement effect. *J. Am. Chem. Soc.* **1998,** 120, (36), 9356-9361.

172. Xu, S.; Amro, N. A.; Liu, G.-Y., Characterization of AFM tips using nanografting. *Appl. Surf. Sci.* **2001,** 175-176, 649-655.

173. Brower, T. L.; Garno, J. C.; Ulman, A.; Liu, G.-Y.; Yan, C.; Golzhauser, A.; Grunze, M., Self-assembled multilayers of 4,4 '-dimercaptobiphenyl formed by Cu(II)-catalyzed oxidation. *Langmuir* **2002,** 18, (16), 6207-6216.

174. Yu, J.; Tan, Y. H.; Kuo, P. K.; Liu, G.-Y., A nanoengineering approach to regulate the lateral heterogeneity of self-assembled monolayers. *J. Am. Chem. Soc.* **2006,** 128, 11574-11581.

175. Kadalbajoo, M.; Park, J.; Opdahl, A.; Suda, H.; Kitchens, C. A.; Garno, J. C.; Batteas, J. D.; Tarlov, M. J.; DeShong, P., Synthesis and structural characterization of glucopyranosylamide films on gold. *Langmuir* **2007,** 23, (2), 700-707.

176. Hu, Y.; Das, A.; Hecht, M. H.; Scoles, G., Nanografting de novo proteins onto gold surfaces. *Langmuir* **2005,** 21, (20), 9103-9109.

177. Vettiger, P.; Despont, M.; Drechsler, U.; Durig, U.; Haberle, W.; Lutwyche, M. I.; Rothuizen, H. E.; Stutz, R.; Widmer, R.; Binnig, G. K., The "Millipede" - More than one thousand tips for future AFM data storage. *IBM Journal of Research and Development* **2000,** 44, (3), 323-340.

178. Salaita, K.; Wang, Y.; Fragala, J.; Vega, R. A.; Liu, C.; Mirkin, C. A., Massively Parallel Dip-Pen Nanolithography with 55000-Pen Two-Dimensional Arrays. *Angew. Chem. Int. Ed.* **2007,** 45, 7220-7223.

179. Childs, W. R.; Nuzzo, R. G., Large-area patterning of coinage-metal thin films using decal transfer lithography. *Langmuir* **2005,** 21, (1), 195-202.

180. Weimann, T.; Geyer, W.; Hinze, P.; Stadler, V.; Eck, W.; Golzhauser, A., Nanoscale patterning of self-assembled monolayers by e-beam lithography. *Microelectronic Engineering* **2001,** 57-8, 903-907.

181. Gorman, C. B.; Biebuyck, H. A.; Whitesides, G. M., Use of a Patterned Self-Assembled Monolayer to Control the Formation of a Liquid Resist Pattern on a Gold Surface. *Chemistry of Materials* **1995,** 7, (2), 252-254.

182. Sondaghuethorst, J. A. M.; Vanhelleputte, H. R. J.; Fokkink, L. G. J., Generation of Electrochemically Deposited Metal Patterns by Means of Electron-Beam (Nano)Lithography of Self-Assembled Monolayer Resists. *Applied Physics Letters* **1994,** 64, (3), 285-287.

183. Xia, Y.; Whitesides, G. M., Soft Lithography. *Angew. Chem. Int. Ed.* **1998,** 37, 550-575.
184. Schreiber, F., Self-assembled monolayers: from ''simple'' model systems to biofunctionalized interfaces. *J. Phys.: Condens. Matter* **2004,** 16, R881-R900.

185. Flink, S.; van Veggel, F.; Reinhoudt, D. N., Sensor functionalities in self-assembled monolayers. *Adv. Mater.* **2000,** 12, (18), 1315-1328.

186. Mrksich, M.; Whitesides, G. M., Patterning self-assembled monolayers using microcontact printing - a new technology for biosensors. *Trends Biotechnol.* **1995,** 13, (6), 228-235.

187. Pena, D. J.; Raphael, M. P.; Byers, J. M., "Dip-Pen" nanolithography in registry with photolithography for biosensor development. *Langmuir* **2003,** 19, (21), 9028-9032.

188. Crooks, R. M.; Ricco, A. J., New organic materials suitable for use in chemical sensor arrays. *Acc. Chem. Res.* **1998,** 31, (5), 219-227.

189. Chaki, N. K.; Vijayamohanan, K., Self-assembled monolayers as a tunable platform for biosensor applications. *Biosensors & Bioelectronics* **2002,** 17, (1-2), 1-12.
190. Love, J. C.; Estroff, L. A.; Kriebel, J. K.; Nuzzo, R. G.; Whitesides, G. M., Self-assembled monolayers of thiolates on metals as a form of nanotechnology. *Chemical Reviews* **2005,** 105, (4), 1103-1169.

191. Engelkes, V. B.; Beebe, J. M.; Frisbie, C. D., Length-Dependent Transport in Molecular Junctions Based on SAMs of Alkanethiols and Alkanedithiols: Effect of Metal Work Function and Applied Bias on Tunneling Efficiency and Contact Resistance. *J. Am. Chem. Soc.* **2004,** 126, (43), 14287-14296.

192. Tour, J. M.; Jones, L.; Pearson, D. L.; Lamba, J. J. S.; Burgin, T. P.; Whitesides, G. M.; Allara, D. L.; Parikh, A. N.; Atre, S. V., Self-Assembled Monolayers and Multilayers of Conjugated Thiols, Alpha,Omega-Dithiols, and Thioacetyl-Containing Adsorbates - Understanding Attachments between Potential Molecular Wires and Gold Surfaces. *Journal of the American Chemical Society* **1995,** 117, (37), 9529-9534.

193. Blum, A. S.; Yang, J. C.; Shashidhar, R.; Ratna, B., Comparing the conductivity of molecular wires with the scanning tunneling microscope. *Applied Physics Letters* **2003,** 82, (19), 3322-3324.

194. Adams, D. M.; Brus, L.; Chidsey, C. E. D.; Creager, S.; Creutz, C.; Kagan, C. R.; Kamat, P. V.; Lieberman, M.; Lindsay, S.; Marcus, R. A.; Metzger, R. M.; Michel-Beyerle, M. E.; Miller, J. R.; Newton, M. D.; Rolison, D. R.; Sankey, O.; Schanze, K. S.; Yardley, J.; Zhu,

X. Y., Charge transfer on the nanoscale: Current status. *Journal of Physical Chemistry B* **2003,** 107, (28), 6668-6697.

195. Vandamme, N.; Snauwaert, J.; Janssens, E.; Vandeweert, E.; Lievens, P.; Van Haesendonck, C., Visualization of gold clusters deposited on a dithiol self-assembled monolayer by tapping mode atomic force microscopy. *Surf. Sci.* **2004,** 558, (1-3), 57-64.

196. Yang, Y. C.; Yau, S. L.; Lee, Y. L., Electrodeposition of Au Monolayer on Pt(111) Mediated by Self-Assembled Monolayers. *J. Am. Chem. Soc.* **2006,** 128, (11), 3677-3682.

197. Noda, H.; Tai, Y.; Shaporenko, A.; Grunze, M.; Zharnikov, M., Electrochemical Characterizations of Nickel Deposition on Aromatic Dithiol Monolayers on Gold Electrodes. *J. Phys. Chem. B* **2005,** 109, (47), 22371-22376.

198. Sugawara, T., Functionalized gold nanoparticles chemisorbed by organic pi-ligands and their networked structures. *J. Synth. Org. Chem. Japan* **2004,** 62, 447-458.

199. Joseph, Y.; Besnard, I.; Rosenberger, M.; Guse, B.; Nothofer, H. G.; Wessels, J. M.; Wild, U.; Knop-Gericke, A.; Su, D. S.; Schlogl, R.; Yasuda, A.; Vossmeyer, T., Self-assembled gold nanoparticle/alkanedithiol films: Preparation, electron microscopy, XPS-analysis, charge transport, and vapor-sensing properties. *J. Phys. Chem. B* **2003,** 107, 7406-7413.

200. Fendler, J. H., Chemical self-assembly for electronic applications. *Chemistry of Materials* **2001,** 13, (10), 3196-3210.

201. Nakanishi, T.; Ohtani, B.; Uosaki, K., Fabrication and characterization of CdS-nanoparticle mono- and multilayers on a self-assembled monolayer of alkanedithiols on gold. *Journal of Physical Chemistry B* **1998,** 102, (9), 1571-1577.

202. Huang, W.; Masuda, G.; Maeda, S.; Tanaka, H.; Ogawa, T., Molecular junctions composed of oligothiophene dithiol-bridged gold nanoparticles exhibiting photoresponsive properties. *Chemistry-a European Journal* **2005,** 12, (2), 607-619.

203. Ulman, A., Formation and structure of self-assembled monolayers. *Chem. Rev.* **1996,** 96, (4), 1533-1554.

204. Xu, S.; Cruchon-Dupeyrat, S.; Garno, J. C.; Jennings, G. K.; Yong, T.-H.; Laibinis, P. E.; Liu, G.-Y., In-situ Studies of Thiol Self -Assembly on Gold from Solution using Atomic Force Microscopy. *J. Chem. Phys.* **1998,** 108, 5002-5012.

205. Schreiber, F., Structure and growth of self-assembling monolayers. *Prog. Surf. Sci.* **2000,** 65, 151-257.

206. Nuzzo, R. G.; Zegarski, B. R.; Dubois, L. H., Fundamental-Studies of the Chemisorption of Organosulfur Compounds on Au(111) - Implications for Molecular Self-Assembly on Gold Surfaces. *Journal of the American Chemical Society* **1987,** 109, (3), 733-740.

207. Ulman, A.; Evans, S. D.; Shnidman, Y.; Sharma, R.; Eilers, J. E., Mixed Alkanethiol Monolayers on Gold Surfaces - Wetting and Stability Studies. *Advances in Colloid and Interface Science* **1992,** 39, 175-224.

208. Bain, C. D.; Troughton, E. B.; Tao, Y. T.; Evall, J.; Whitesides, G. M.; Nuzzo, R. G., Formation of Monolayer Films by the Spontaneous Assembly of Organic Thiols from Solution onto Gold. *Journal of the American Chemical Society* **1989,** 111, (1), 321-335.

209. Laibinis, P. E.; Whitesides, G. M.; Allara, D. L.; Tao, Y. T.; Parikh, A. N.; Nuzzo, R. G., Comparison of the Structures and Wetting Properties of Self-Assembled Monolayers of Normal-Alkanethiols on the Coinage Metal-Surfaces, Cu, Ag, Au. *Journal of the American Chemical Society* **1991,** 113, (19), 7152-7167.

210. Ryu, S.; Schatz, G., Nanografting: modeling and simulation. *J. Am. Chem. Soc* **2006,** 128, (35), 11563-11573.

211. Leung, T. Y. B.; Gerstenberg, M. C.; Lavrich, D. J.; Scoles, G.; Schreiber, F.; Poirier, G. E., 1,6-Hexanedithiol Monolayers on Au(111): A Multitechnique Structural Study. *Langmuir* **2000,** 16, (2), 549-561.

212. Kobayashi, K.; Yamada, H.; Horiuchi, T.; Matsushige, K., UHV-STM studies on the structures of alkanedithiol self-assembled monolayers. *Applied Surface Science* **1999,** 145, 435-438.

213. Kobayashi, K.; Umemura, J.; Horiuchi, T.; Yamada, H.; Matsushige, K., Structural study on self-assembled monolayers of alkanedithiol molecules. *Japanese Journal of Applied Physics Part 2-Letters* **1998,** 37, (3A), L297-L299.

214. Porter, M. D.; Bright, T. B.; Allara, D. L.; Chidsey, C. E. D., Spontaneously Organized Molecular Assemblies .4. Structural Characterization of Normal-Alkyl Thiol Monolayers on Gold by Optical Ellipsometry, Infrared-Spectroscopy, and Electrochemistry. *Journal of the American Chemical Society* **1987,** 109, (12), 3559-3568.

215. Nuzzo, R. G.; Allara, D. L., Adsorption of Bifunctional Organic Disulfides on Gold Surfaces. *Journal of the American Chemical Society* **1983,** 105, (13), 4481-4483.

216. Nuzzo, R. G.; Fusco, F. A.; Allara, D. L., Spontaneously Organized Molecular Assemblies .3. Preparation and Properties of Solution Adsorbed Monolayers of Organic Disulfides on Gold Surfaces. *Journal of the American Chemical Society* **1987,** 109, (8), 2358-2368.

217. Fenter, P.; Eberhardt, A.; Liang, K. S.; Eisenberger, P., Epitaxy and chainlength dependent strain in self-assembled monolayers. *Journal of Chemical Physics* **1997,** 106, (4), 1600-1608.

218. Fenter, P.; Eisenberger, P.; Liang, K. S., Chain-Length Dependence of the Structures and Phases of Ch3(Ch2)N-1sh Self-Assembled on Au(111). *Physical Review Letters* **1993,** 70, (16), 2447-2450.

219. Nuzzo, R. G.; Dubois, L. H.; Allara, D. L., Fundamental-Studies of Microscopic Wetting on Organic-Surfaces .1. Formation and Structural Characterization of a Self- Consistent Series of Polyfunctional Organic Monolayers. *Journal of the American Chemical Society* **1990,** 112, (2), 558-569.

220. Nuzzo, R. G.; Korenic, E. M.; Dubois, L. H., Studies of the Temperature-Dependent Phase-Behavior of Long- Chain Normal-Alkyl Thiol Monolayers on Gold. *Journal of Chemical Physics* **1990,** 93, (1), 767-773.

221. Poirier, G. E.; Pylant, E. D., The Self-Assembly Mechanism of Alkanethiols on Au(111). *Science* **1996,** 272, 1145-1148.

222. Poirier, G. E., Characterization of organosulfur molecular monolayers on Au(111) using scanning tunneling microscopy. *Chem. Rev.* **1997,** 97, (4), 1117-1127.

223. Kohli, P.; Taylor, K. K.; Harris, J. J.; Blanchard, G. J., Assembly of Covalently-Coupled Disulfide Multilayers on Gold. *J. Am. Chem. Soc.* **1998,** 120, (46), 11962-11968.

224. Joo, S. W.; Han, S. W.; Kim, K., Multilayer formation of 1,2-ethanedithiol on gold: Surface-enhanced Raman scattering and ellipsometry study. *Langmuir* **2000,** 16, (12), 5391-5396.

225. Haiss, W.; vanZalinge, H.; Hobenreich, H.; Bethell, D.; Schiffrin, D. J.; Higgins, S. J.; Nichols, R. J., Molecular Wire Formation from Viologen Assemblies. *Langmuir* **2004,** 20, (18), 7694-7702.

226. Jiang, W.; Zhitenev, N.; Bao, Z.; Meng, H.; Abusch-Magder, D.; Tennant, D.; Garfunkel, E., Structure and Bonding Issues at the Interface between Gold and Self-Assembled Conjugated Dithiol Monolayers. *Langmuir* **2005,** 21, (19), 8751-8757.

227. Tai, Y.; Shaporenko, A.; Rong, H. T.; Buck, M.; Eck, W.; Grunze, M.; Zharnikov, M., Fabrication of thiol-terminated surfaces using aromatic self-assembled monolayers. *J. Phys. Chem. B* **2004,** 108, (43), 16806-16810.

228. Wei, H. A.; Masuda, G.; Maeda, S.; Tanaka, H.; Ogawa, T., Molecular junctions composed of oligothiophene dithiol-bridged gold nanoparticles exhibiting photoresponsive properties. *Chemistry-a European Journal* **2005,** 12, (2), 607-619.

229. Wakamatsu, S.; Nakada, J.; Fujii, S.; Akiba, U.; Fujihira, M., Self-assembled nanostructure of Au nanoparticles on a self-assembled monolayer. *Ultramicroscopy* **2005,** 105, (1-4), 26-31.

230. Niklewski, A.; Azzam, W.; Strunskus, T.; Fischer, R. A.; Woll, C., Fabrication of self-assembled monolayers exhibiting a thiol-terminated surface. *Langmuir* **2004,** 20, (20), 8620-8624.

231. de Boer, B.; Meng, H.; Perepichka, D. F.; Zheng, J.; Frank, M. M.; Chabal, Y. J.; Bao, Z., Synthesis and Characterization of Conjugated Mono- and Dithiol Oligomers and Characterization of Their Self-Assembled Monolayers. *Langmuir* **2003,** 19, (10), 4272-4284.

232. Walzer, K.; Marx, E.; Greenham, N. C.; Less, R. J.; Raithby, P. R.; Stokbro, K., Scanning Tunneling Microscopy of Self-Assembled Phenylene Ethynylene Oligomers on Au(111) Substrates. *J. Am. Chem. Soc.* **2004,** 126, (4), 1229-1234.

233. Tour, J. M.; Jones, L.; Pearson, D. L.; Lamba, J. J. S.; Burgin, T. P.; Whitesides, G. M.; Allara, D. L.; Parikh, A. N.; Atre, S., Self-Assembled Monolayers and Multilayers of Conjugated Thiols, .alpha.,.omega.-Dithiols, and Thioacetyl-Containing Adsorbates. Understanding Attachments between Potential Molecular Wires and Gold Surfaces. *J. Am. Chem. Soc.* **1995,** 117, (37), 9529-9534.

234. Esplandiu, M. J.; Carot, M. L.; Cometto, F. P.; Macagno, V. A.; Patrito, E. M., Electrochemical STM investigation of 1,8-octanedithiol monolayers on Au(111). Experimental and theoretical study. *Surf. Sci.* **2006,** 600, 155-172.

235. Xu, S.; Cruchon-Dupeyrat, S.; Garno, J. C.; Liu, G.-Y., In situ studies of thiol self-assembly on gold from solution using atomic force microscopy. *J. Chem. Phys.* **1998,** 108, 5002-5012.

236. Poirier, G. E.; Pylant, E. D., The self-assembly mechanism of alkanethiols on Au(111). *Science* **1996,** 272, (5265), 1145-1148.

237. Cretich, M.; Damin, F.; Pirri, G.; Chiari, M., Protein and peptide arrays: Recent trends and new directions. *Biomolec. Eng.* **2006,** 23, 77-88.

238. Mrksich, M.; Whitesides, G. M., Using self-assembled monolayers to understand the interactions of man-made surfaces with proteins and cells. *Annu. Rev. Biophys. Biomolec. Struct.* **1996,** 25, 55-78.

239. Roach, P.; Farrar, D.; Perry, C. C., Interpretation of protein adsorption: Surface-induced conformational changes. *J. Am. Chem. Soc.* **2005,** 127, (22), 8168-8173.

240. Wilson, D. S.; Nck, S., Functional protein arrays. *Curr. Opin. Chem. Biol.* **2001,** 6, 81-85.

241. Ostuni, E.; Yan, L.; Whitesides, G. M., The interaction of proteins and cells with self-assembled monolayers of alkanethiolates on gold and silver. *Colloids Surf., B* **1999,** 15, (1), 3-30.

242. Love, J. C.; Estroff, L. A.; Kriebel, J. K.; Nuzzo, R. G.; Whitesides, G. M., Self-assembled monolayers of thiolates on metals as a form of nanotechnology. *Chem. Rev.* **2005,** 105, 1103-1169.

243. Ulman, A., *An Introduction to Ultrathin Organic Films: From Langmuir–Blodgett to Self-Assembly*. Academic Press: Boston, MA, 1991.

244. Maeda, Y.; Yamamoto, H.; Hiromi, K., Self-Assembled Monolayers as Novel Biomembrane Mimetics 1. Characterization of Cytochrome *c* Bound to Self-Assembled Monolayers on Silver by Surface-Enhanced Resonance Raman Spectroscopy. *J. Phys. Chem* **1995,** 99, 4837-4841.

245. Sugimura, H.; Lee, S.-H.; Saito, N.; Takai, O., Reversible nanochemical conversion. *J. Vac. Sci. Technol. B* **2004,** 22, L44-L46.

246. Ostuni, E.; Grzybowski, B. A.; Mrksich, M.; Roberts, C. S.; Whitesides, G. M., Adsorption of proteins to hydrophobic sites on mixed self-assembled monolayers. *Langmuir* **2003,** 19, (5), 1861-1872.

247. Luk, Y. Y.; Kato, M.; Mrksich, M., Self-assembled monolayers of alkanethiolates presenting mannitol groups are inert to protein adsorption and cell attachment. *Langmuir* **2000,** 16, (24), 9604-9608.

248. Deng, L.; Mrksich, M.; Whitesides, G. M., Self-assembled monolayers of alkanethiolates presenting tri(propylene sulfoxide) groups resist the adsorption of protein. *J. Am. Chem. Soc.* **1996,** 118, (21), 5136-5137.

249. Schreiber, F., Self-assembled monolayers: from 'simple' model systems to biofunctionalized interfaces. *J. Phys. Condens. Matter* **2004,** 16, (28), R881-R900.

250. Herrwerth, S.; Eck, W.; Reinhardt, S.; Grunze, M., Factors that determine the protein resistance of oligoether self-assembled monolayers - Internal hydrophilicity, terminal hydrophilicity, and lateral packing density. *J. Am. Chem. Soc.* **2003,** 125, (31), 9359-9366.

251. Binnig, G.; Quate, C. F.; Gerber, C., Atomic Force Microscope. *Phys. Rev. Letts.* **1986,** 56, 930-933.

252. Wiesendanger, R., *Scanning probe microscopy and spectroscopy methods and applications*. Cambridge University Press: **1994**.

253. Bonnell, D., *Scanning Probe Microscopy and Spectroscopy: Theory, Techniques, and Applications* 2nd ed.; Wiley-VCH: New York, **2000**.

254. Gu, J. H.; Yam, C. M.; Li, S.; Cai, C. Z., Nanometric protein arrays on protein-resistant monolayers on silicon surfaces. *J. Am. Chem. Soc.* **2004,** 126, (26), 8098-8099.

255. Fuierer, R. R.; Carroll, R. L.; Feldheim, D. L.; Gorman, C. B., Patterning mesoscale gradient structures with self-assembled monolayers and scanning tunneling microscopy based replacement lithography. *Adv. Mater.* **2002,** 14, 154-157.

256. Piner, R. D.; Zhu, J.; Xu, F.; Hong, S. H.; Mirkin, C. A., "Dip-pen" nanolithography. *Science* **1999,** 283, (5402), 661-663.

257. Xu, S.; Miller, S.; Laibinis, P. E.; Liu, G. Y., Fabrication of nanometer scale patterns within self-assembled monolayers by nanografting. *Langmuir* **1999,** 15, (21), 7244-7251.

258. Ginger, D. S.; Zhang, H.; Mirkin, C. A., The evolution of dip-pen nanolithography. *Angew. Chem. Int. Ed.* **2004,** 43, 30-45.

259. Salaita, K.; Wang, Y. H.; Mirkin, C. A., Applications of dip-pen nanolithography. *Nat. Nanotech.* **2007,** 2, 145-155.

260. Lim, J. H.; Ginger, D. S.; Lee, K. B.; Heo, J.; Nam, J. M.; Mirkin, C. A., Direct-write dip-pen nanolithography of proteins on modified silicon oxide surfaces. *Angew. Chem. Int. Ed.* **2003,** 42, 2309-2312.

261. Lee, K. B.; Lim, J. H.; Mirkin, C. A., Protein nanostructures formed via direct-write dip-pen nanolithography. *J. Am. Chem. Soc.* **2003,** 125, 5588-5589.

262. Wilson, D. L.; Martin, R.; Hong, S.; Cronin-Golomb, M.; Mirkin, C. A., Surface organization and nanopatterning of collagen by dip-pen nanolithography. *Proc. Natl. Acad. Sci. U.S.A.* **13660-13664,** 98, 13660-13664.

263. Lee, K. B.; Park, S. J.; Mirkin, C. A.; Smith, J. C.; Mrksich, M., Protein nanoarrays generated by dip-pen nanolithography. *Science* **2002,** 295, 1702-1705.

264. Hyun, J.; Ahn, S. J.; Lee, W. K.; Chilkoti, A.; Zauscher, S., Molecular recognition-mediated fabrication of protein nanostructures by dip-pen lithography. *Nano Lett.* **2002,** 2, (11), 1203-1207.

265. Liu, G. Y.; Amro, N. A., Positioning protein molecules on surfaces: A nanoengineering approach to supramolecular chemistry. *Proc. Natl. Acad. Sci. U.S.A.* **2002,** 99, (8), 5165-5170.

266. Wong, S. S., *Chemistry of Protein Conjugation and Cross-linking*. CRC Press: Boca Raton, FL, 1991.

267. MacBeath, G.; Koehler, A. N.; Schreiber, S. L., Printing small molecules as microarrays and detecting protein-ligand interactions en masse. *J. Am. Chem. Soc.* **1999,** 121, (34), 7967-7968.

268. Wadu-Mesthrige, K.; Amro, N. A.; Garno, J. C.; Xu, S.; Liu, G. Y., Fabrication of nanometer-sized protein patterns using atomic force microscopy and selective immobilization. *Biophys. J.* **2001,** 80, (4), 1891-1899.

269. Wadu-Mesthrige, K.; Xu, S.; Amro, N.; Liu, G.-Y., *Langmuir* **1999,** 15, 8580-8583.

270. Zhou, D. J.; Wang, X. Z.; Birch, L.; Rayment, T.; Abell, C., AFM study on protein immobilization on charged surfaces at the nanoscale: Toward the fabrication of three-dimensional protein nanostructures. *Langmuir* **2003,** 19, (25), 10557-10562.

271. MacBeath, G., Protein microarrays and proteomics. *Nat. Genet.* **2002,** 32, 526-532.

272. Kodadek, T., Protein microarrays: prospects and problems. *Chem. Biol.* **2001,** 8, 105-115.

273. Petersso, B.; Sjoquist, J., Some Physicochemical Properties of Protein A from Staphylococcus-Aureus. *Eur. J. Biochem.* **1972,** 29, (3), 579.

274. Murata, M.; Arakawa, M.; Yoshida, T.; Hato, M., Binding of immunoglobulin molecules to preadsorbed protein A layers as observed by surface forces measurements. *Colloids Surf., B* **1998,** 12, (1), 35-47.

275. Grabarek, Z.; Gergely, J., Zero-Length Crosslinking Procedure With The Use Of Active Esters. *Anal. Biochem* **1990,** 185, (1), 131-135.

276. Cruchon-Dupeyrat, S.; Porthun, S.; Liu, G. Y., Nanofabrication using computer-assisted design and automated vector-scanning probe lithography. *Appl. Surf. Sci.* **2001,** 175-176, 636-642.

277. Drake, B.; Prater, C. B.; Weisenhorn, A. L.; Gould, S. A. C.; Albrecht, T. R.; Quate, C. F.; Cannell, D. S.; Hansma, H. G.; Hansma, P. K., Imaging Crystals, Polymers and Processes in Water with the Atomic Force Microscope. *Science* **1989,** 243, 1586-1589.

278. Weisenhorn, A. L.; Hansma, P. K.; Albrecht, T. R.; Quate, C. F., Forces in atomic force microscopy in air and water. *Appl. Phys. Lett.* **1989,** 54, 2651-2653.

279. Blattler, T.; Huwiler, C.; Ochsner, M.; Staedler, B.; Solak, H.; Voros, J.; Grandin, H. M., Nanopatterns with biological functions. *J. Nanosci. Technol.* **2006,** 6, (8), 2237-2264.

280. Yonson, C. R.; Stuart, D. A.; Zhang, X.; McFarland, A. D.; Haynes, C. L.; VanDuyne, R. P., Towards advanced chemical and biological nanosensors--An overview. *Talanta* **2005,** 67, 438-448.

281. Choi, D. G.; Jang, S. G.; Yu, H. K.; Yang, S. M., Two-dimensional polymer nanopattern by using particle-assisted soft lithography. *Chem. Mater.* **2004,** 16, (18), 3410-3413.

282. Han, S. B.; Briseno, A. L.; Shi, X. Y.; Mah, D. A.; Zhou, F. M., Polyelectrolyte-coated nanosphere lithographic patterning of surfaces: Fabrication and characterization of electropolymerized thin polyaniline honeycomb films. *J. Phys. Chem. B* **2002,** 106, (25), 6465-6472.

283. Yi, D. K.; Kim, D.-Y., Polymer nanosphere lithography: fabrication of an ordered trigonal polymeric nanostructure. *Chem. Comm.* **2003**, 982-983.

284. Sun, Z.; Li, Y.; Wang, Y.; Chen, X.; Zhang, J.; Zhang, K.; Wang, Z.; Bao, C.; Zeng, J.; Zhao, B.; Yang, B., Three-dimensional colloidal crystal-assisted lithography for two-dimensional patterned arrays. *Langmuir* **2007,** 23, 10725-10731.

285. Cai, Y.; Ocko, B. M., Large-Scale Fabrication of Protein Nanoarrays Based on Nanosphere Lithography. *Langmuir* **2005,** 21, (20), 9274-9279.

286. Valsesia, A.; Meziani, T.; Bretagnol, F.; Colpo, P.; Ceccone, G.; Rossi, F., Plasma assisted production of chemical nano-patterns by nano-sphere lithography: applicaiton to bio-interfaces. *J. Phys. D. Appl. Phys.* **2007,** 40, 2341-2347.

287. Garno, J. C.; Amro, N. A.; Wadu-Mesthrige, K.; Liu, G.-Y., Production of periodic arrays of protein nanostructures using particle lithography. *Langmuir* **2002,** 18, (21), 8186-8192.

288. Li, J.-R.; Henry, G. C.; Garno, J. C., Fabrication of nanopatterned films of bovine serum albumin and staphylococcal protein A using latex particle lithography. *Analyst* **2006,** 131, (2), 244-250.

289. Hulteen, J. C.; Treichel, D. A.; Smith, M. T.; Duval, M. L.; Jensen, T. R.; Van Duyne, R. P., Nanosphere lithography: Size-tunable silver nanoparticle and surface cluster arrays. *J. Phys. Chem. B* **1999,** 103, (19), 3854-3863.

290. Bullen, H. A.; Garrett, S. J., TiO_2 nanoparticle arrays prepared using a nanosphere lithography technique. *Nano Lett.* **2002,** 2, (7), 739-745.

291. Cheng, S. L.; Lu, S. W.; Wong, S. L.; Chang, C. C.; Chen, H., Fabrication of 2D ordered arrays of cobalt silicide nanodots on (001)Si substrates. *J. Crystal Growth* **2007,** 300, 473-477.

292. Zhang, G.; Wang, D.; Mohwald, H., Ordered binary arrays of Au nanoparticles derived from colloidal lithography. *Nano Lett.* **2007,** 7, (1), 127-132.

293. Liu, D. F.; Xiang, Y. J.; Liao, Q.; Zhang, J. P.; Wu, X. C.; Zhang, Z. X.; Liu, L. F.; Ma, W. J.; Shen, J.; Zhou, W. Y.; Xie, S. S., A simple route to scalable fabrication of perfectly ordered ZnO nanorod arrays. *Nanotechnology* **2007,** 18, 1-5.

294. Zin, M. T.; Leong, K.; Wong, N.-Y.; Ma, H.; Jen, A. K.-Y., Plasmon resonant structures with unique topographic characteristics and tunable optical properties for surface-enhanced Raman scattering. *Nanotechnology* **2007,** 455301, 1-6.

295. Li, Y.; Li, C.; Cho, S. O.; Duan, G.; Cai, W., Silver hierarchical bowl-like array: synthesis, superhydrophobicity, and optical properties. *Langmuir* **2007,** 23, 9802-9807.

296. Weekes, S. M.; Ogrin, F. Y.; Murray, W. A.; Keatley, P. S., Macroscopic arrays of magnetic nanostructures from self-assembled nanosphere templates. *Langmuir* **2007,** 23, 1057-1060.

297. Ctistis, G.; Patoka, P.; Wang, X.; Kempa, K.; Giersig, M., Optical transmission through hexagonal arrays of subwavelength holes in thin metal films. *Nano Lett.* **2007,** 7, (9), 2926-2930.

298. Wang, X. D.; Summers, C. J.; Wang, Z. L., Large-scale hexagonal-patterned growth of aligned ZnO nanorods for nano-optoelectronics and nanosensor arrays. *Nano Lett.* **2004,** 4, (3), 423-426.

299. Wu, W.; Katsnelson, A.; Memis, O. G.; Mohseni, H., A deep sub-wavelength process for the formation of highly uniform arrays of nanoholes and nanopillars. *Nanotechnology* **2007,** 8, 1-4.

300. Ryu, K. M.; Badmaev, A.; Gomez, L.; Ishikawa, F.; Lei, B.; Zhou, C. W., Synthesis of aligned single-walled nanotubes using catalysts defined by nanosphere lithography. *J. Am. Chem. Soc.* **2007,** 129, (33), 10104.

301. Ryu, K. S.; Wang, X.; Shaikh, K.; Bullen, D.; Goluch, E.; Zou, j.; Liu, C., Integrated microfluidic linking chip for scanning probe nanolithography. *Appl. Phys. Letts.* **2004,** 85, 136-138.

302. McLellan, J. M.; Geissler, M.; Xia, Y. N., Edge spreading lithography and its application to the fabrication of mesoscopic gold and silver rings. *J. Am. Chem. Soc.* **2004,** 126, (35), 10830-10831.

303. Geissler, M.; McLellan, J. M.; Chen, J. Y.; Xia, Y. N., Side-by-side patterning of multiple alkanethiolate monolayers on gold by edge-spreading lithography. *Angew. Chem. Int. Ed.* **2005,** 44, (23), 3596-3600.

304. Nakamura, H.; Karube, I., Current research activity in biosensors. *Anal. Bioanal. Chem.* **2003,** 377, 446-468.

305. Agheli, H.; Malmstrom, J.; Larsson, E. M.; Textor, M.; Sutherland, D. S., Large Area Protein Nanopatterning for Biological Applications. *Nano Lett.* **2006,** 6, (6), 1165-1171.

306. Lueking, A.; Horn, M.; Eickhoff, H.; Bussow, K.; Lehrach, H.; Walter, G., Protein microarrays for gene expression and antibody screening. *Anal. Biochem.* **1999,** 270, (1), 103-111.

307. Saviranta, P.; Okon, R.; Brinker, A.; Warashina, M.; Eppinger, J.; Geierstager, B., Evaluating Sandwich Immunoassays in Microarray Format in Terms of the Ambient Analyte Regime. *Clinical Chem.* **2004,** 50, (10), 1907-1920.

308. Zhu, H.; Bilgin, M.; Bangham, R.; Hall, D.; Casamayor, A.; Bertone, P.; Lan, N.; Jansen, R.; Bidlingmaier, S.; Houfek, T.; Mitchell, T.; Miller, P.; Dean, R. A.; Gerstein, M.; Snyder, M., Global analysis of protein activities using proteome chips. *Science* **2001,** 293, (5537), 2101-2105.

309. Robinson, W. H.; DiGennaro, C.; Hueber, W.; Haab, B. B.; Kamachi, M.; Dean, E. J.; Fournel, S.; Fong, D.; Genovese, M. C.; deVegvar, H. E. N.; Skriner, K.; Hirschberg, D. L.; Morris, R. I.; Muller, S.; Pruijn, G. J.; vanVenrooij, W. J.; Smolen, J. S.; Brown, P. O.; Steinman, L.; Utz, P. J., Autoantigen microarrays for multiplex characterization of autoantibody responses. *Nat. Med.* **2001,** 8, (3), 295-301.

310. Huff, J. L.; Lynch, M. P.; Nettikadan, S.; Johnson, J. C.; Vengasandra, S.; Henderson, E., Label-free protein and pathogen detection using the atomic force microscope. Journal of Biomolecular Screening. *J. Biomol. Screening* **2004,** 9, (6), 491-2004.

311. Allen, S.; Chen, X.; Davies, J.; Davies, M.; Dawkes, A. C.; Edwards, J. C.; Roberts, C. J.; Sefton, J.; Tendler, S. J. B.; Williams, P. M., Detection of antigen-antibody binding events with the atomic force microscope. *Biochem.* **1997,** 36, 7457-7463.

312. Haab, B. B., Applications of antibody array platforms. *Curr. Opin. Biotech.* **2006,** 17, 415-421.

313. Hegner, M.; Wagner, P.; Semenza, G., Ultralarge Atomically Flat Template-Stripped Au Surfaces for Scanning Probe Microscopy. *Surf. Sci.* **1993,** 291, (1-2), 39-46.

314. Cowley, J. M.; Janney, D. E.; Gerkin, R. C.; Buseck, P. R., The structure of ferritin cores determined by electron nanodiffraction. *J. Struct. Biol.* **2000,** 131, (3), 210-216.

315. Theil, E. C.; Matzapetakis, M.; Liu, X., Ferritins: iron/oxygen biominerals in protein nanocages. *J. Biol. Inorg. Chem.* **2006,** 11, 803-810.

316. Peters, T.; Feldhoff, R. C., Fragments of bovine serum-albumin produced by limited proteolysis - Isolation and characterization of tryptic fragments. *Biochemistry* **1975,** 14, (15), 3384-3391.

317. Saphire, E. O.; Parren, P.; Pantophlet, R.; Zwick, M. B.; Morris, G. M.; Rudd, P. M.; Dwek, R. A.; Stanfield, R. L.; Burton, D. R.; Wilson, I. A., Crystal structure of a neutralizing human IgG against HIV-1: A template for vaccine design. *Science* **2001,** 293, (5532), 1155-1159.

318. Pereira, A. S.; Small, W.; Krebs, C.; Tavares, P.; Edmondson, D. E.; Theil, E. C.; Huynh, B. H., Direct spectroscopic and kinetic evidence for the involvement of a peroxodiferric

intermediate during the ferroxidase reaction in fast ferritin mineralization. *Biochem.* **1998,** 37, (28), 9871-9876.

319. Harrison, P. M.; Theil, E. C., The ferritins: molecular properties, iron storage function and cellular regulation. *Biochim. Biophys. Acta* **1996,** 1275, (3), 161-203.

320. Roginsky, V. A.; Barsukova, T. K.; Bruchelt, G.; Stegmann, H. B., Iron bound to ferritin catalyzes ascorbate oxidation: effects of chelating agents. *Biochim. Biophys. Acta* **1997,** 1335, 33-39.

321. Dechakiatkrai, C.; Chen, C.; Lynam, C.; Shin, K. M.; Kim, S. J.; Phanichphant, S.; Wallace, G. G., Direct Ascorbic Acid Detection with Ferritin Immobilized on Single-Walled Carbon Nanotubes. *Electrochem Solid St* **2008,** 11, (1), K4-K6.

322. Yu, Q.; Qin, G.; Li, H.; Xia, Z.; Nian, Y.; Pei, S.-S., Mechanism of horizontally aligned growth of single-wall carbon nanotubes on R-plane sapphire. *J. Phys. Chem. B* **2006,** 110, 22676-22680.

323. Lopez, A.; Gutierrez, L.; Lazaro, F. J., The role of dipolar interaction in the quantitative determination of particulate magnetic carriers in biological tissues. *Phys. Med. Biol.* **2007,** 52, 5043-5056.

324. Guertin, R. P.; Harrison, N.; Zhou, Z. X.; McCall, S.; Drymiotis, F., Very high field magnetization and AC susceptibility of native horse spleen ferritin. *J. Magn. Magn. Mater.* **2007,** 308, 97-100.

325. Clemente-Leon, M.; Coronado, E.; Soriano-Portillo, A.; Colacio, E.; Dominguez-Vera, J. M.; Galvez, N.; Madueno, R.; Martin-Romero, M. T., Magnetic Langmuir-Blodgett films of Ferritin with Different Iron Contents. *Langmuir* **2006,** 22, 6993-7000.

326. Xu, D. G.; Watt, G. D.; Harb, J. N.; Davis, R. C., Electrical conductivity of ferritin proteins by conductive AFM. *Nano Lett.* **2005,** 5, (4), 571-577.

327. Liu, G.; Debnath, S.; Paul, K. W.; Han, W.; Hausner, D. B.; Hosein, H.-A.; Michel, F. M.; Parise, J. B.; Sparks, D. L.; Stongin, D. R., Characterization and surface reactivity of ferrihydrite nanoparticles assembled in ferritin. *Langmuir* **2006,** 22, 9313-9321.

328. Klem, M. T.; Resnick, D. A.; Gilmore, K.; Young, M.; Idzerda, Y. U.; Douglas, T., Synthetic Control over Magnetic Moment and Exchange Bias in All-Oxide Materials Encapsulated within a Spherical Protein Cage. *J. Am. Chem. Soc.* **2007,** 129, (1), 197-201.

329. Takagi, H.; Shi, D. S.; Ha; Allewell, N. M.; Theil, E. C., Localized unfolding at the junction of three ferritin subunits - A mechanism for iron release? *J. Biol. Chem.* **1998,** 273, (301), 18685-18688.

330. Muller, D. J.; Amrein, M.; Engel, A., Adsorption of Biological Molecules to a Solid Support for Scanning Probe Microscopy. *J. Struct. Biol.* **1997,** 119, 172-188.

331. Nielsen, U. B.; Geierstanger, B. H., Multiplexed sandwich assays in microarray format. *J. Immunol. Methods* **2004,** 290, 107-120.

332. Lynch, M.; Mosher, C.; Huff, J.; Nettikadan, S.; Johnson, J.; Henderson, E., Functional protein nanoarrays for biomarker profiling. *Proteomics* **2004,** 4, (6), 1695-1702.

333. Silverton, E. W. N., M. A.; Davies, D. R. PNAS 1977, 74, 5140-5144, 3-Dimensional structure of an intact human immunoglobulin. *Proc. Nat. Acad. Sci. USA* **1977,** 74, (11), 5140-5144.

334. Sarma, V. R. S., E. W.; Davies, D. R.; Terry, W. D. J. Biol. Chem. 1971, 246, 3753-3759, 3-Dimensional structure at 6 A resolution of a human gamma GL immunoglobulin molecule. *J. Biol. Chem.* **1971,** 246, (11), 3753-3759.

335. Sugio, S.; Kashima, A.; Mochizuki, S.; Noda, M.; Kobayashi, K., Crystal structure of human serum albumin at 2.5 angstrom resolution. *Prot. Eng.* **1999,** 12, (6), 439-446.

336. Peters, T., *All about albumin*. Academic Press: San Diego, 1996.

337. Rosenoer, V. M.; Oratz, M.; Rothschilde, M. A., *Albumin Structure and Function*. Pergamon Press: New York, 1977.

338. Ngunjiri, J. N.; Kelley, A. T.; Lejeune, Z. M.; Li, J.-R.; Lewandowski, B. R.; Serem, W. K.; Daniels, S. L.; Lusker, K., Achieving Precision and Reproducibility for Writing Patterns of n-alkanethiol Self-assembled Monolayers with Automated Nanografting. *Scanning* **2008,** 30, (1).

339. Ngunjiri, J. N.; Garno, J. C., AFM-Based Lithography for Nanoscale Protein assays. *Analytical Chemistry* **2008,** 80, (1), 1361-1369.

340. Yu, J.-J.; Ngunjiri, J. N.; Kelley, A. T.; Garno, J. C., Solution Self-Assembly of α,ω-Alkanedithiols on Au(111). *Langmuir* **2008**, (*Submitted*).

341. Ngunjiri, J. N.; Li, J.-R.; Garno, J. C., *Chapter 3, Nanodevices for the Life Sciences*. Wiley-VCH: Weinheim, **2006**.

342. Garno, J. C.; Yang, Y. Y.; Amro, N. A.; Cruchon-Dupeyrat, S.; Chen, S. W.; Liu, G. Y., Precise positioning of nanoparticles on surfaces using scanning probe lithography. *Nano Letters* **2003,** 3, (3), 389-395.

343. Ngunjiri, J. N.; Daniels, S. L.; Li, J.-R.; Serem, W. K.; Garno, J. C., Controlling the surface coverage and arrangement of proteins using particle lithography. *Nanomedicine* **2008**, *submitted*.

APPENDIX A. LITHOGRAPHY SCRIPT FOR WRITING AN ARRAY OF FILLED SQUARE PATTERNS

Computer codes can be defined by the user to write different geometries using AFM-based lithography. The script commands enable users to assign designed parameters for writing such as writing speed (ss), applied force (wzdac), tip movement (pr), tip lift (pu), tip down (pd), define the z scale (szs), and counter functions (jnz) to repeat designs. Once an IP address has been created with XPMPro software, the scripts can be executed to control the tip motion and force as desired by the user. The control can then be returned to the imaging program to enable imaging.

An example script is detailed for writing a 4 x 4 array of square nanopatterns (100 x 100 nm^2). A topograph is presented showing 11-MUA squares written within an ODT matrix at a force of 3 nN.

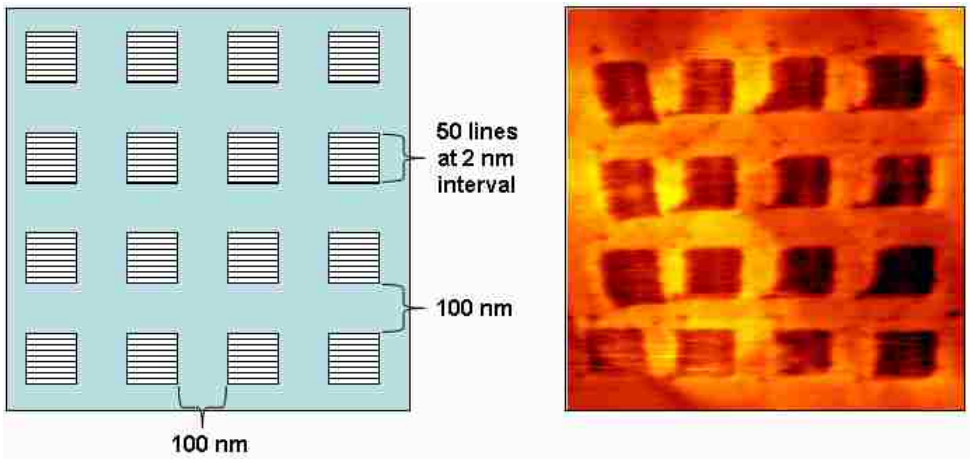

Figure A1. An example scripts and image for writing an array of sixteen squares each 100 x 100 nm^2. [Left] the AFM tip raster over each square fifty times at a line interval of 2 nm; [Right] AFM topograph of the 11-MUA patterns (dark contrast) written within ODT SAM.

```
# squares4x4.lth
# Array of 4x4 filled squares (100nm)
# optimized for SPM100 AFM
# takes about 5 minutes for this script

1.0 szs
1.0e-10 pushs
250.0 zss
0.0 sza
0.0 wzdac
pu
5000.0 ss

# equilibration square
-8000.0 0.0 pr
0.0 -8000.0 pr
#
8 diotake
8 dioset
20
1.0 wzdac pd
-1 +
-30 jnz
# lift pen and move to next pattern
0.0 500.0 pr
10.0 0.0 pr
0.0 -500.0 pr
10.0 0.0 pr
-1 +
-30 jnz

0.0 3000.0 pr
8 dioclr
0 diotake

# begin arrays from left to right
8 diotake
8 dioset
4
4
# box
50
1.0 wzdac pd
0.0 1000.0 pr
10.0 0.0 pr
0.0 -1000.0 pr
10.0 0.0 pr

0.0 wzdac pu
-1000.0 0.0 pr
0.0 1500.0 pr
-1 +
-52 jnz

1500.0 0.0 pr
0.0 -6000.0 pr
-1 +
-70 jnz
0.0 wzdac pu
8 dioclr
0 diotake

1.0 szs
pops
rlb
exit
```

APPENDIX B. LITHOGRAPHY SCRIPT FOR WRITING A COMPLEX ARRAY OF CIRCLE PATTERNS

A script for writing a 2 × 2 array of ring patterns consisting of circle designs is presented. Four circles are arranged with a common focal point. For this script the "arcr" command describes the circular arc trajectory of the tip and designates the diameter of the circles. A counter index function directs the tip to trace each circle five times with the C-based command "jnz" or "jump not zero."

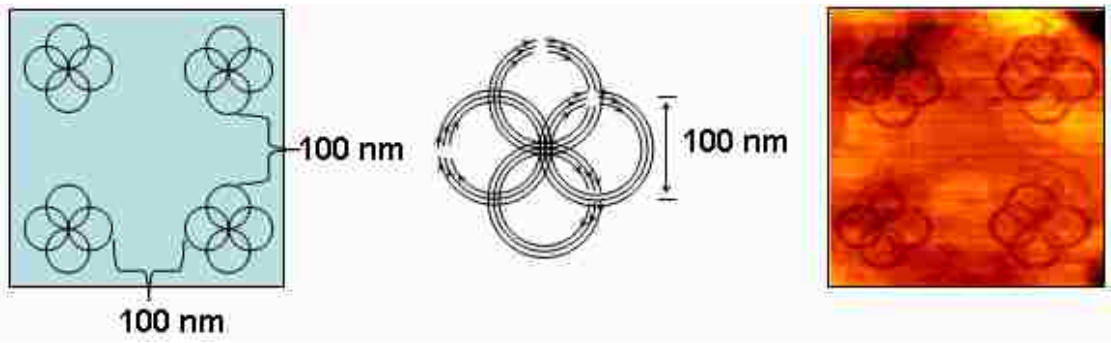

Figure B1. Writing complex patterns of SAMs. [Left] drawings showing the path of an AFM tip in writing a combination of four circles to generate each pattern; [Center] each circle is traced three times; [Right] an AFM topograph showing patterns of 11-MUA nanografted within ODT matrix.

```
# circlefun-1v.lth
# patterned circle shapes (100 nm
diameter)
# optimized for SPM100 AFM
# takes about 2 minutes for this script

1.0 szs
1.0e-10 pushs
250.0 zss
0.0 sza
0.0 wzdac pu
5000.0 ss

# equilibration square
-8000.0 0.0 pr
0.0 -8000.0 pr
#
8 diotake
8 dioset
20
0.8 wzdac pd
0.0 200.0 pr
10.0 0.0 pr
0.0 -200.0 pr
10.0 0.0 pr
-1 +
-30 jnz
0.0 1500.0 pr
1500.0 0.0 pr
# circle patterns
4
4
0.8 wzdac pd
5
360.0 400.0 0.0 arcr
-1 +
```

```
-13 jnz

5
360.0 -400.0 0.0 arcr
-1 +
-13 jnz

5
360.0 0.0 400.0 arcr
-1 +
-13 jnz

5
360.0 0.0 -400.0 arcr
-1 +
-13 jnz

0.0 wzdac pu
0.0 2200.0 pr
-1 +
-79 jnz

2200.0 0.0 pr
0.0 -8800.0 pr
-1 +
-97 jnz

8 dioclr
0 diotake

1.0 szs
pops
rlb
exit
```

APPENDIX C: PEN TABLET AND INTERACTIVE PEN DISPLAY FOR GRAPHIC TRANSFER

Sophisticated artwork can be created by hand for AFM-based lithography using the Graphire pen tablet. The pen tablet is interfaced to the AFM computer (USB device) to generate AFM tip designs. Scrapbook lithography scripts are written by tracing designs with the pen/mouse device. The tablet is equipped with a 6 x 8 sq. in. active area which is a mapped representation of the drawing area in the PicoLith window. To commence writing, the pen needs to be within 5 mm (0.20 inch) of the tablet surface.

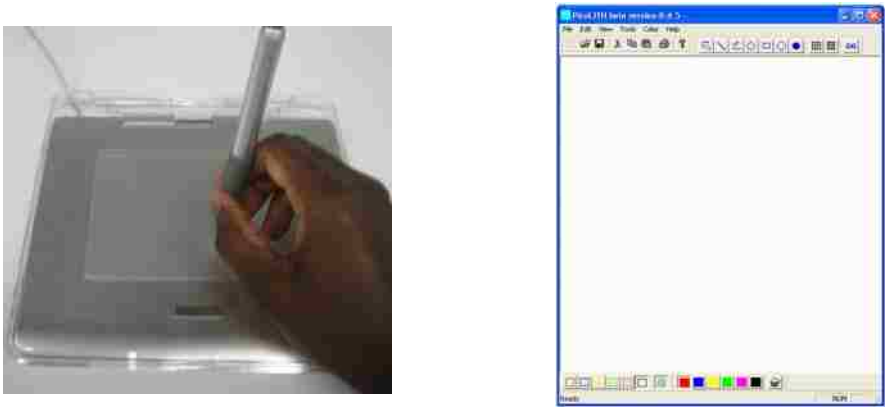

Figure C1. The Graphire tablet, pen and PicoLith window used for free-hand design of patterns

1. Connect the Graphire tablet to the computer using a USB interface.
2. Place the pen about 5 mm above the tablet; the green indicator on the tablet shows the pen is in range.

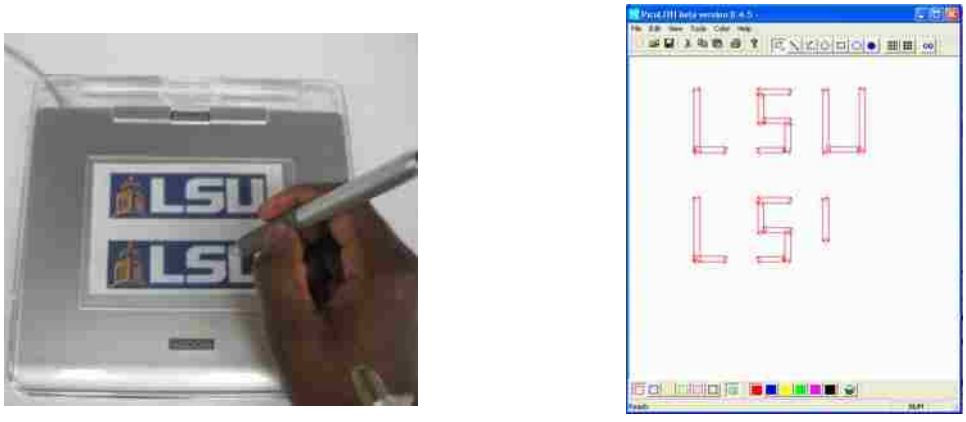

Figure C2. Tracing the "LSU" logos using a combination Graphire tablet, pen and PicoLith window

3. Open the dialog window for the Picolith browser, and select the line trace function.
4. Trace the letters or drawing on the active area of the tablet with the pen.
5. A replica drawing is formed in the Picolith window.
6. Lithographic parameters of a drawing such as writing speed, applied force, and bias pulse duration are then assigned as desired by user by selecting and assigning color codes with the color palette of the Picolith dialog window.
7. The density of lines for writing filled patterns is achieved by assigning a scale of 1 to 10 where 1 is the most closely spaced. Different items of an array can be assigned different line densities for raster filling of patterns.
8. When the Picolith script is activated to write, the relative motion of the tip on the surface is graphically presented on the Picolith window. One can track the progress of writing by observing the drawing lines changing from continuous to dotted markers.
9. The display size of the Picolith window directly scales to the actual size of the image frame chosen when running script. Therefore, the script will produce patterns of different sizes according to the selected image size of the Picoscan program.

APPENDIX D: LETTERS OF PERMISSION

PERMISSION REQUEST

Date: 01/24/2008

To: Bettina Loycke
Copyright & Licensing Manager
Wiley-VCH Verlag GmbH & Co. KGaA
Boschstr. 12 69469 Weinheim Germany

From: Johnpeter Ngunjiri
232 Choppin Hall
Louisiana State University
Baton Rouge, LA 70803
jngunj1@lsu.edu
Phone: (225) 578-8853
Fax: (225) 578-3458

Request for Permission to Reproduce

I am preparing my dissertation entitled "**Designing Surface Chemistries for in Situ AFM Investigations of Biomolecular Reactions with Proteins at the Nanoscale**" and would like to request your permission to use Chapter 3 of the publication listed below in my dissertation to be submitted to Louisiana State University.

Book title: Nanodevices for the Life Sciences
Editor: Kumar. Challa
Edition: 1
Publisher: Wiley-VCH | Publish Date 09/06 | Copyright 2006
Volume: 4
Chapter 3 : Nanolithography : towards fabrication of nanodevices for life sciences
Johnpeter Ndiangui Ngunjiri, Jie-Ren Li, Jayne Carol Garno
ISBN-10: 3-527-31384-2

Thank you

Sincerely

Johnpeter Ngunjiri
232 Choppin Hall
Louisiana State University
Baton Rouge, LA 70803
jngunj1@lsu.edu
Phone: (225) 578-8853
Fax: (225) 578-3458

We hereby grant permission for the requested use expected that due credit is given to the original source.

WILEY-VCH, STM-Copyright & Licenses

Weinheim, Jan. 29, 2008

Please note that we only grant rights for a printed version, but not the rights for an electronic/online/web/microfiche publication

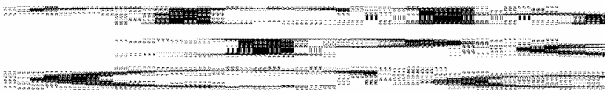

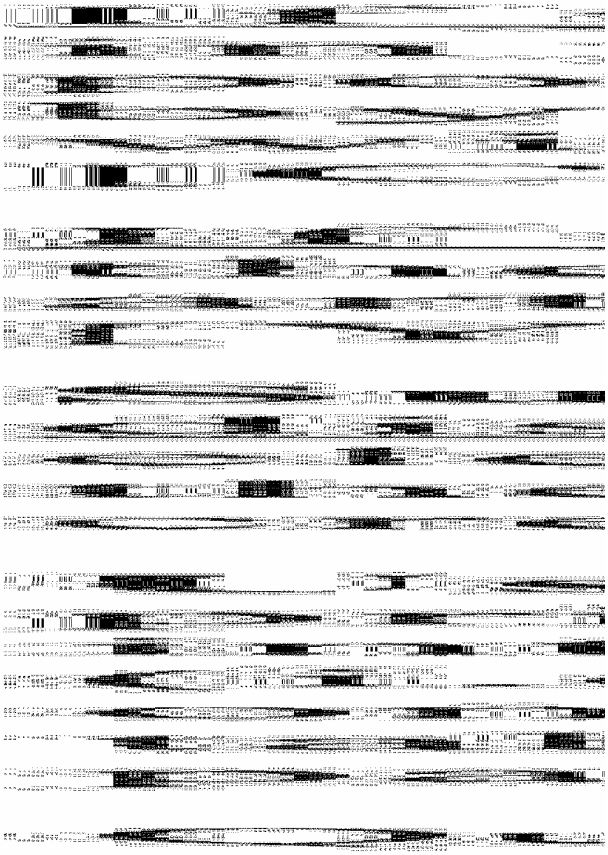

VITA

Johnpeter Ndiang'ui Ngunjiri was born in Nyeri, Kenya, and is a graduate of Madaraka Primary School and Ngumo High School. He received bachelor's and master's degrees in chemistry from Moi University, Kenya. In 2003 he enrolled in the doctoral program at Louisiana State University to pursue a doctorate degree in chemistry. He is a candidate for the Degree of Philosophy during the Spring Commencement 2008.

During studies at LSU, Ngunjiri submitted four first author journal articles. One of these articles was featured on journal covers (*Analytical Chemistry*). A collaborative manuscript for *Journal of Applied Physics* resulted from with research with Dr. Philip Adams of the LSU Physics Department. Ngunjiri participated in regional, national and international conferences, where he has presented ten first author presentations and five shared presentations. To attend these meetings, Ngunjiri applied and was awarded three travel awards including an LSU Graduate Travel stipend, a Rohm & Haas Graduate Travel Award (2006) and a Coates Graduate Award (2007). Ngunjiri earned a best student poster award in the Colloids & Surfaces Symposium of the American Chemical Society 231st National meeting (Atlanta, GA 2006). During the same year, he won a best student poster award at the Society of Applied Spectroscopy of the Federation of Analytical Chemistry and Spectroscopy Societies National Meeting (Orlando, FL 2006). Also, he won a best poster award at the Biointerfaces Symposium of the American Vacuum Society 53rd International Symposium (San Francisco, CA 2006). The Center for Biomodular MultiScale Systems awarded Ngunjiri an honorable mention during a local research symposium at Louisiana State University (Baton Rouge, LA 2006).